Capstone Design Project I

Field Development Plan

Offshore Volve Field in Norway

Final Report

Team A

Student Name	Student ID
Tengiz Abilkairov	202024889
Yelnur Abdualiyev	202064398
Adiya Muratkhozhina	202079544
Alibek Suyumkul	202068627
Karina Zhumagali	201922334

Table of Contents

List of Figures

List of Tables

Chapter I

1.1. Introduction

Company name - “WellBorn”

Company Services: WellBorn is a well known oil and gas company specialized in comprehensive field development services, especially for offshore operations. WellBorn is the company to be relied on for the Volve field development in terms of the engineering aspect, the environmental assessment and the production optimization respectively. We propose a geological and reservoir study, deep-water drilling techniques, and environmental-friendly production processes customized for offshore settings. WellBorn's working style is built around the principles of safety, and environment and productivity which is why they work towards making sure that the Volve field development is efficient in production and is in compliance with industry requirements along with environmental regulations for responsible energy extraction.

1.1.1. Team Members

Tengiz Abilkairov - Team leader:

- Role: Drilling & Completion Engineer, Basic Reservoir Engineer
- Responsibilities: Responsibilities include assessing the reservoir's potential, estimating recoverable reserves, and selecting the optimal development strategy. Also choosing and designing well placement, drilling schedules, and completion techniques. As a reservoir engineer and static model creator, it will be required to analyze the drive mechanisms, reservoir characterization and create the static model or the reservoir using specific softwares.

Yelnur Abdualiyev:

- Role: Economist & HSE
- Responsibilities: Include creating and refining reservoir models to optimize production, forecasting reservoir behavior, and ensuring accurate simulations. Analyze project feasibility, profitability, and market conditions. Ensures compliance with safety and environmental regulations, mitigating risks during field operations.

Adiya Muratkhozhina:

- Role: Reservoir and Simulation Engineer
- Responsibilities: As a reservoir engineer, the main role is to provide a comprehensive analysis of the reservoir's characteristics, evaluate production strategies, and recommend techniques for maximizing recovery while mitigating risks. It includes outlining the reservoir description, modeling, drive mechanisms, well design, production forecasts, reservoir management strategy, and key risks involved in the field development plan. Moreover, it involves creation of reservoir models, testing on sensitivity analysis to create the most efficient recovery scenario.

Alibek Suyumkul:

- Role: Production engineer
- Responsibilities: ML implementation, production forecasting, IPR&TPR (Vogel and Fetkovich comparison), flow assurance problem statement and overcoming, Surface well testing, facility design.

Karina Zhumagali:

- Role: Geologist & Petrophysicist
- Responsibilities: Search about the geology of the Volve field. To analyze and interpret the geological data and geological characteristics of the field. To create seismic interpretation. To construct and interpret the logs. To make the PVT analysis.

1.1.2. Background information on the Oil and Gas Industry in Kazakhstan

Kazakhstan is a global player with a critical role in the world oil market. Location of a country is important, occupying a place worthy of attention in the global energy sector, particularly for its oil and gas. Its broad petroleum resources place it amongst the world's leading producers and exporters of energy. The oil and gas industry has been a cornerstone of Kazakhstan's economy, shaping its policies and interactions both at home and abroad.

Exploration of oil in Kazakhstan began at the break of the 20th century, and the first commercial well was drilled as early as 1911 (Figure 1) in the Emba region. It was only after Kazakhstan received its independence in 1991 that the complete potentiality of its energy resources began to be recognized. With its declaration of independence from the Soviet Union, Kazakhstan started to attract foreign investments that partnered with international energy companies for the development of oil and gas reserves in the country. Indeed, this was a very important step for the beginning of fast development processes in its energy sector.

Figure 1. First oil well in Kazakhstan, Dossor field, Atyrau [3].

The rich oil and gas reserves of the Republic of Kazakhstan are concentrated basically in three areas: Caspian Sea basin, Mangistau region, and North Ustyurt Basin. The country holds a

big share of the world's largest oil fields: Tengiz, Karachaganak, and Kashagan. These fields possess the majority of the energy potential of Kazakhstan.

Kashagan Field: Discovered on 30th June of 2000, Kashagan (see Figure 2) is in the north of the Caspian Sea, 80 kilometers from the city Atyrau. At the same moment, Kashagan is the fifth largest oil field in the world regarding reserves and first in Kazakhstan. It has potential reserves as high as 70 billion barrels of crude oil, with recoverable volume of 7-13 billion barrels. Currently, the field is being developed by a group of partners that includes KazMunayGas with 16.88%, Shell at 16.81%, ExxonMobil at 16.81%, Total at 16.81%, Eni at 16.81%, CNPC at 8.3%, and INPEX at 7.56%. After early setbacks and technical hitches, production finally started in 2016; over the longer term, Kashagan is expected to make an important contribution to Kazakhstan's energy security.

Figure 2. Kashagan field [1].

Tengiz Field: Discovered in 1979, Tengiz is one of the deepest and largest oil fields in the world. This oilfield is located 350 kilometers to the south-east of Atyrau city. Tengiz belongs to the Peri-Caspian oil and gas province. It is operated by Tengizchevroil (TCO) consortium, a joint venture between Chevron (50%), ExxonMobil (25%), KazMunayGas (20%) and LukArco

(5%). The recoverable oil reserves of the field are estimated as 750 million to 1.125 billion tons of oil. Tengiz (see Figure 3) ranked as the second biggest oilfield in Kazakhstan.

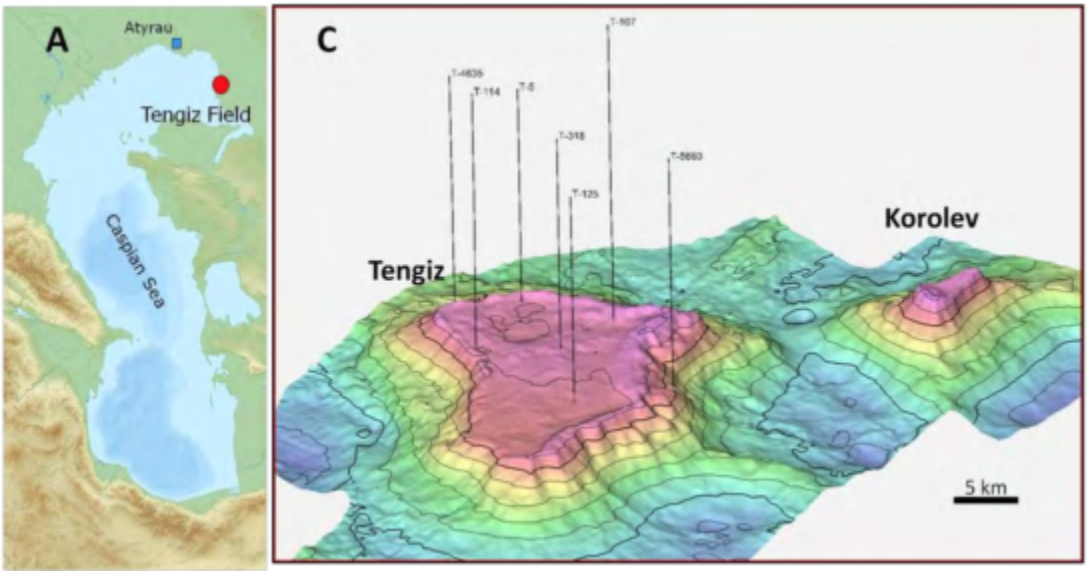

Figure 3. Location and geological structure of Tengiz field [4].

Karachaganak Field: Located in north-west Kazakhstan (see Figure 4.), Karachaganak is one of the largest oil and gas condensate fields in the world. It holds 13.6 billion barrels of hydrocarbons as oil and 59.4 trillion cubic feet of gas initially in place. It is operated by a consortium that includes Eni (29.25%), Shell (29.25%), Chevron (18%), Lukoil (13.5%) and KazMunayGas (10%). This field is important for both oil and gas production, with much of its gas being exported to Russia.

Figure 4. Location of Karachaganak field [5].

Kazakhstan ranks among the top 15 oil producers worldwide, with daily oil production averaging about 1.8 million barrels. Its natural gas production is also growing, with over 55 billion cubic meters of gas produced annually. Most of Kazakhstan's oil is exported to Europe and China, making the country a vital player in the regional energy market.

Kazakhstan's main oil export route is through the Caspian Pipeline Consortium (CPC) (Figure 5), which connects the Tengiz field to the Russian Black Sea port of Novorossiysk. Kazakhstan is working to expand its pipeline network to reduce its reliance on Russian routes, while China has become an increasingly important destination for Kazakh oil and gas, thanks to new pipelines linking Kazakh fields to Chinese refineries.

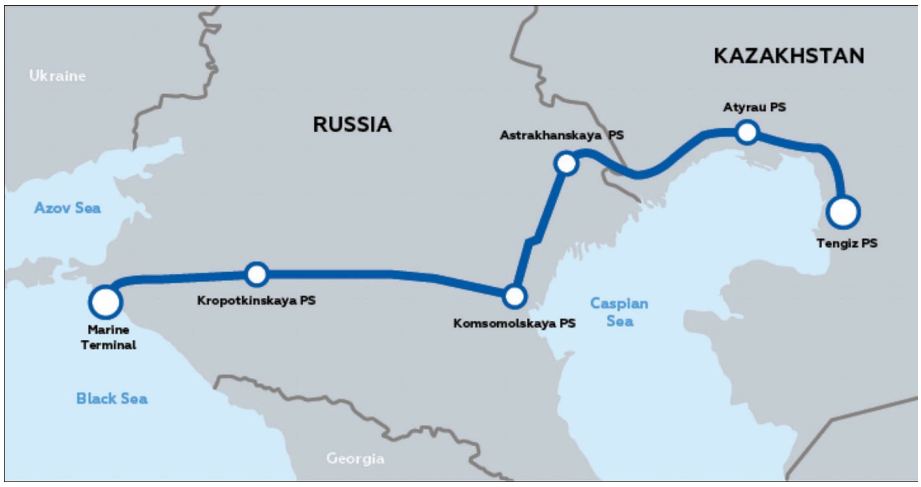

Figure 5. Caspian Pipeline Consortium (CPC) [5].

Foreign investment has been a key factor in Kazakhstan's oil and gas success. International companies have provided the funding, technology, and expertise needed to tap into the country's massive resources. In exchange, Kazakhstan has created a welcoming environment for investors, while ensuring that KazMunayGas retains control over strategic assets. This balance between foreign investment and state control has been essential in building Kazakhstan's energy industry into the powerhouse it is today.

1.2. Introduction to the Study

In the oil and gas industry, the development of petroleum fields is a critical process that involves comprehensive planning, technical expertise, and large financial investment. A successful Field Development Plan (FDP) tends to be essential for ensuring that a field is optimally developed in a way that minimizes risks, maximizes economic and resources value, aligns with both corporate objectives and governmental regulations [5].

The exploration phase is the beginning of the whole process, where the wells are drilled to assess the presence of hydrocarbons. Upon the discovery of the commercially viable reservoir, the focus shifts to understanding and evaluating the subsurface risks, field size, and general viability of the whole project for development. The FDP is then drafted to provide a comprehensive strategy and comprehensive design that addresses all technical, environmental, and economic aspects of the field. This plan includes the well design, infrastructure development, reservoir management, and the economic forecast for production costs and revenues [6]. Approval of the FDP tends to be a crucial regulatory step since it shows the government's consent for the company to proceed with field development and ensures that the proposed plan aligns with national interests. A well-structured FDP considers various factors such as geophysics, geology, reservoir engineering, surface facilities, and economics, aiming for the safe and sustainable extraction of oil and gas. The provided figure visually represents and summarizes the major disciplines involved in the FDP.

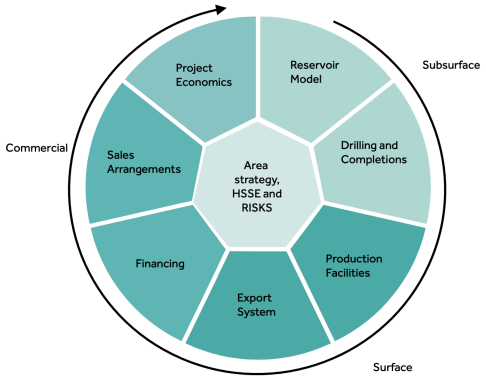

Figure 6. Major disciplines included in the Field Development Plan [8].

The following report presents the Field Development Plan (FDP) for the Volve field. Volve is an offshore oil field located in Block 15/9 in the southern part of the Norwegian North Sea, at a water depth of approximately 80 meters [14]. It is situated approximately 200 km west of Stavanger and 8 km from Sleipner gas fields. It lies at a depth of 2700 to 3100 meters and produces from sandstone reservoirs of the Middle Jurassic Hugin sandstone formations with the western part of the structure being heavily faulted. Recoverable reserves are estimated at 78.6 million barrels of oil and 1.5 billion cubic meters of gas, with a daily production of 56,000 barrels of oil a day. Development of the Volve oil field commenced in 2024 [12]. The project involves drilling 8-10 oil, gas and water injection wells. Water produced from the field is planned to be then reinjected into the formation in order to stabilize the reservoir pressure and increase oil recovery.

The Volve field is chosen for our research because Kazakhstan's oil industry is looking to adopt best practices from fields worldwide. The technologies and production strategies used in the North Sea are often at the forefront of innovation. Learning from the successful application of gas and water injection in Volve could help optimize production in Kazakh fields facing challenges like high residual oil saturation, pressure decline, and the need for the novel enhanced recovery methods. Kazakhstan’s fields, including Karachaganak, Tengiz, Uzen fields, like Volve, are also characterized by good-quality reservoir properties in certain zones, and the focus on sustainable production practices is becoming a common, major goal for both regions [8].

Another important factor is that in Kazakhstan, there are no publicly available resources that provide comprehensive information on oil and gas fields, including essential data on reservoir properties, well logging, seismic geological studies, and more. All such information is strictly private and restricted from public access. Given these limitations, we opted to explore foreign fields with accessible data and identified the Volve field in the Norwegian Sea. Norway mandates open publication of resource extraction data under its transparency laws, making detailed reports on the Volve field freely available. This accessibility has allowed us to select the Volve field as the focus of our capstone project, enabling in-depth analysis and study of its reservoir characteristics and production history.

That is why, due to availability of the data and the similarities in reservoir characteristics, shared production strategies, the Volve field can be considered as a relevant subject for our research on Kazakhstan's oil fields.

1.3. Problem Statement

Developing oil and gas fields such as the Volve offshore field, comes with many challenges, including technical, environmental, economic, and regulatory issues. Kazakhstan, ranked 12th in global oil and gas production (Jusan Analytics, 2022), has great potential, but unlocking this potential needs a well-designed Field Development Plan (FDP). Without a good plan, extracting resources can become inefficient, operations can be risky, and profits might not meet expectations.

One big challenge is finding the right balance between extracting hydrocarbons efficiently and maintaining the reservoir's long-term productivity. Over-extraction can damage the reservoir and reduce how much oil or gas can be recovered later. Creating a solid strategy for understanding the subsurface, planning wells, and using advanced technologies is also critical to ensure smooth and reliable operations. Oil and gas activities can affect the environment and local communities, so it is important to minimize these impacts and follow environmental laws. At the same time, meeting national regulations and safety standards is crucial to get the necessary approvals.

From a financial point of view, it is significant to balance spending on development and operations to stay profitable and get good returns. Managing risks, like unexpected geological issues, technical failures, or changes in the market, is also key. Finally, it is necessary to plan for the entire life of the field—from production to closing it down—to ensure everything runs sustainably and the assets remain in good condition.

This project will address these challenges by creating a detailed FDP for the Volve field. The goal is to recover as much resources as possible, maintain technical and environmental sustainability, meet regulations, and achieve good economic results, while keeping all stakeholders involved.

1.4. Objectives of the FDP

- To develop a strategy to efficiently extract the maximum possible hydrocarbons from the field, focusing on reservoir management, production rates, and recovery factor targets.
- To design a technically sound approach for all phases, including subsurface evaluation, well planning, and production infrastructure that leverages available technology and engineering solutions.
- To address environmental protection and minimize the impact on local communities, ensuring that development activities comply with environmental regulations and social responsibilities.
- To ensure that the field development plan meets national policies, legal frameworks, and regulatory standards for safe and sustainable resource extraction.
- To develop a financially viable project by analyzing capital expenditure (CAPEX), operational expenditure (OPEX), and overall project economics to ensure profitability and a positive return on investment.
- To identify, assess, and mitigate potential risks throughout the project lifecycle, including subsurface uncertainties, operational challenges, and market fluctuations.
- To create a comprehensive project execution plan, including a timeline for key milestones, well drilling schedules, facility development, and production start-up, while ensuring smooth project operations.
- To plan for the entire lifecycle of the field, from production start-up to decommissioning, ensuring sustainable operations and asset integrity over the long term.
- To ensure the plan can adapt to changes in reservoir performance, market conditions, or other unforeseen circumstances, allowing the project to remain viable throughout its lifecycle.

1.5. Objectives for Fall and Spring semesters

It is essential to understand the objectives and tasks for the Field Development Plan completion of the Volve field. Therefore, the below presented table summarizes the main stages and tasks as an action plan for the Fall and Spring semesters with exact dates.

Table 1. Action Plan for Fall and Spring semesters.

№	Stage	Actions	Due date
1	Online research	Searching for the available oil and gas fields around the world	01/09/2024 - Sunday
2		Discovering both onshore and offshore fields and their unique features	
3		Looking for the literature and papers about the chosen fields	
4	Data gathering	Searching for any data, datafiles and theoretical information concerning the chosen field	01/09/2024 - Sunday
5		Detailed seismic surveys, geological modeling, and reservoir simulations. Using existing data to assess the size, location, and behavior of the Volve field reservoirs	
6		Reviewing historical data from existing wells, including production rates, pressure, and any issues encountered	
7	Work with software	Exploring the available software to work with	08/09/2024 - Sunday
8		Choosing suitable software to work with	
9		Opening data files using software and starting creating 3D model of the reservoir	
10	Data interpretation	Analyzing log data of the field	08/09/2024 - Sunday
11		Analyzing production data of the field	

12		Analyzing drilling procedure of the wells	
13		Analyzing completion procedure of the wells	
14		Analyzing geological data of the field	
15	Writing report	Writing first draft report	15/09/2024 - Sunday
16		Editing first draft report based on the recommendations received	
17		Checking the report for the plagiarism and AI use, editing where necessary	
18	Simulation modeling	Static model - Petrel. Well log analysis + creation	14/03/2025 - Friday
		Dynamic models - ResInsight, Eclipse. Reservoir simulation	
		Sensitivity analysis to simulate and check different scenarios for the most efficient recovery operations	
		Recommend the best recovery strategy + design	
19	Final project design	Making final operation and production decisions	11/04/2025 - Friday
		Recommendations on enhanced oil recovery methods	
20	Submission and Presentation	Finishing the report and presentation	25/04/2025 - Friday

Chapter II

2.1. Geology

Geology is applied to interpret the subsurface properties and resource potential of any reservoir. Its primary goals are to identify and interpret rock bodies, structures, and fluid reservoirs, which are essential for efficient field development. Geology reveals the spatial distribution of reservoir rock properties such as porosity and permeability and helps in identifying the most effective drilling methods. It is important in understanding geological history, stratigraphy, and tectonics, which all directly impact reservoir quality and fluid migration. This knowledge is fundamental to maximize exploration, extraction, and resource management processes.

2.1.1. Geological Setting

The Volve Field is situated close to the intersection of three major geological structures in the North Sea: the South Viking Graben, the Horda Platform, and the Norwegian-Danish Basin (Figure 7) [18].

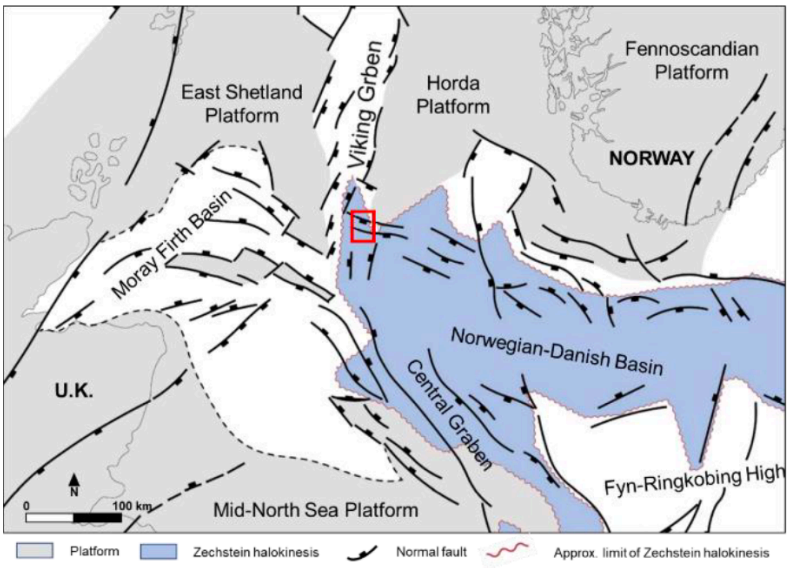

Figure 7. The structural elements map of the North Sea shows the Volve Field (highlighted in a red rectangle) positioned at the intersection of the Viking Graben, Utsira High, and the Norwegian-Danish Basin [18].

The Volve Field contains structural traps that hold hydrocarbons within the Jurassic Hugin Formation [29]. The reservoir presents complexity on two main levels. The first is tectonic in nature, involving a history of normal faulting along with episodes of reverse fault reactivation. Additionally, tectonic activity related to salt movement and dissolution has influenced both Triassic and Jurassic formations. The second level of complexity arises from the rapid lateral changes in reservoir thickness, which are caused by syndepositional faulting, rotations of fault blocks, and intervals of erosion and non-deposition.

According to Sun et al. (2021), the Hugin Formation is composed of sandstones that range widely in grain size from fine to coarse and vary in sorting from well to poorly sorted. Despite this variability, the formation generally exhibits excellent reservoir properties. The Hugin Formation, spanning the Jurassic and Triassic periods, includes deposits from shallow marine shoreface environments, coastal lagoons, channels, and possibly mouth bars. Beneath this, the underlying formation is characterized by low permeability due to significant cementation by kaolinite and dolomite.

2.1.2. Tectonic History and Geological Stratigraphy

The Volve field's geology stratigraphy is a duplicate of the Norwegian area in the northern part of the South Viking Graben of the North Sea. The tectono-stratigraphic evolution in the South Viking Graben is as follows: the Graben evolved under processes of crustal extension, where the Graben Boundary Fault Zone evolved to the west side of the principal basin structure. Extension and fault-controlled basin subsidence began during Early to Late Permian. The Rotliegendes Group, which is a Lower Permian unit, consists of interbedded red sandstones and breccia, indicating a fluvial-lacustrine to terrestrial environment. Furthermore, dolomite-cemented sandstone interbedded with red silty shale in some areas indicates more basinward facies [18].

The Volve Field also experienced localized tectonic activity driven by salt movement from the Late Permian during the Triassic and Jurassic periods. This activity significantly influenced the area's geological structure and sedimentation patterns. Notable structural features resulting from this include dome structures, minibasins, fault systems, and variations in sedimentary facies. During the Triassic, the movement of the Zechstein Supergroup's salt led to the formation of several minibasins. Later, in the Jurassic, additional secondary minibasins developed due to the collapse of underlying salt walls. These minibasins are enclosed by salt-cored structural highs. The salt bodies exhibit shapes ranging from sub-circular to elongated, leading to the development of complex subaerial topography and a corresponding submarine bathymetry along the southwestern margin of the Utsira High. Changes in the shape of the salt bodies may be attributed to partial dissolution, differential erosion of salt walls and nearby Triassic-filled minibasins, or remobilization of salt triggered by extension or sediment loading. The early phase of salt movement was dominated by non-marine units such as the Smith Bank shale and Skagerrak sand units. Salt mobility caused thickness variations and low-relief pillow-like structures to form [18].

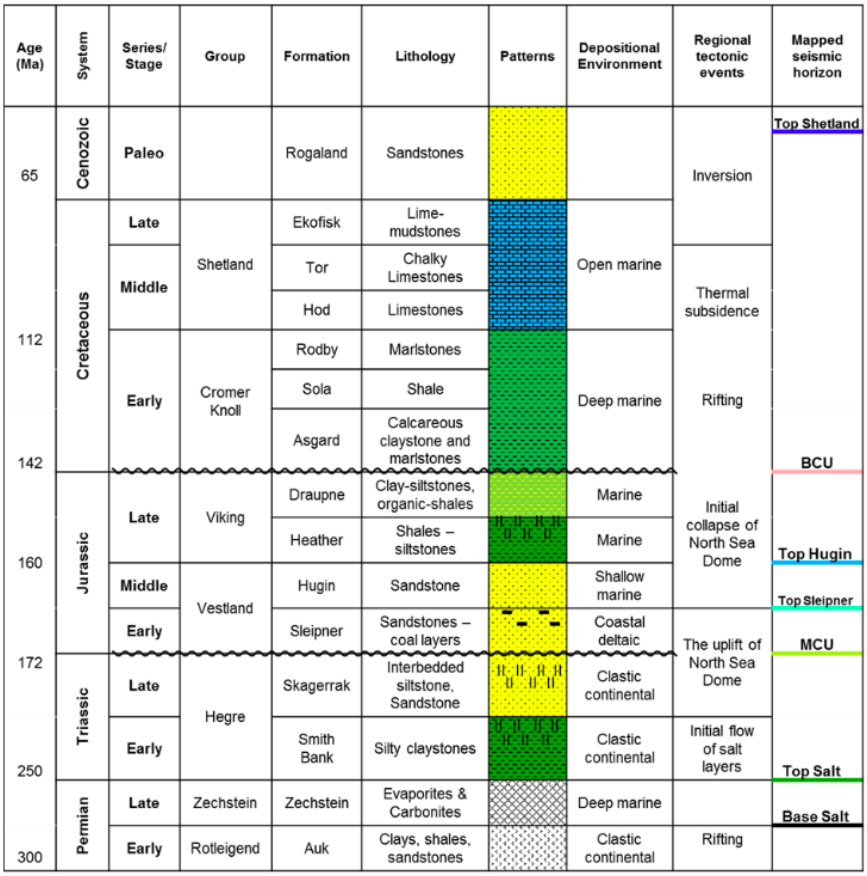

Figure 8. The tectono-stratigraphic column for the study area [31]

In the Early Jurassic, uplift and erosion of the South Viking Graben were caused by the development of the Mid-North Sea Dome. Therefore, the Middle Jurassic succession is split by a mid-Cimmerian unconformity. The first deposited facies above the unconformity are the Sleipner formation delta plain deposits, Late Bajocian to Late Bathonian. The Graben Boundary Fault Zone was reactivated during Middle Jurassic time through the collapse of the Mid-North Sea Dome. The effect was rapid subsidence and a marine transgression in the South Viking Graben. The initial rifting phase within the region contained shallow marine facies. Hugin formation Early to Middle Callovian was deposited at that time, following the Sleipner formation. Oxfordian to Volgian was the main period of extension and subsidence, where the eustatic increase in sea level led to the deposition of the Heather formation shelf mudstones and Draupne formation deep marine mudstones. The final phase of extension and subsidence occurred in the Ryazanian to Late Volgian, whereby some inversion structures formed in zones of the basin.

Post-rift deposition began in the Early Cretaceous during an inversion period after rifting and salt movement had ended. Sediment deposited during the period was mainly marine shale, marl, and siltstone. Upper Cretaceous sediments were mainly made up of chalk. Marine deposition continued in the region in the Cenozoic to Quaternary [18].

2.1.3. Lithology Characterization

For lithology characterization 3 different softwares were used which are Petrel, Techlog and Machine Learning on Python.

Applying Techlog, NPHI vs. bulk density RHOB crossplot was plotted using the NPHI and RHOB logs. In this plot, the green line represents the sandstone trend, the blue line corresponds to limestone, and the pink line marks the dolomite trend. On Techlog, using the data of 2 wells which are 15/9-F-12 and 15/9-F-14, the main types of lithologies were identified.

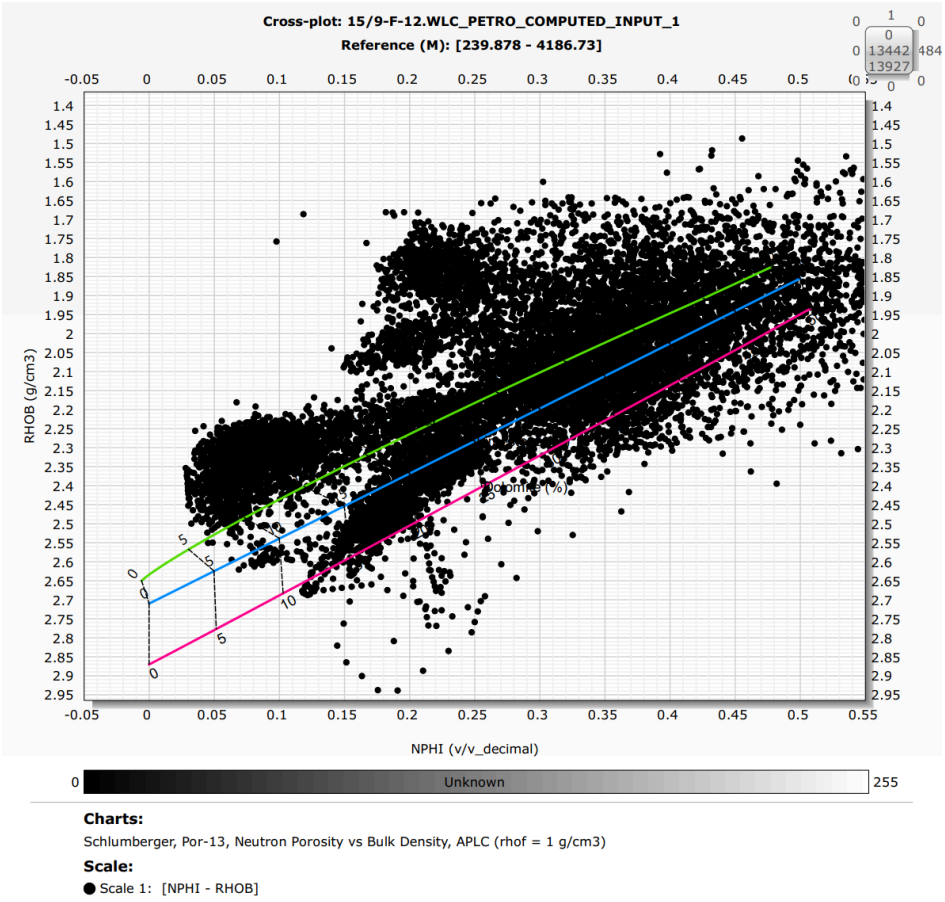

Figure 9. NPHI vs RHOB crossplot for 15/9-F-12 well.

Sandstones typically have a lower bulk density (~2.65 g/cm³) with neutron porosity values that increase with decreasing grain density, and data points along this trend indicate a sandstone presence in the formation. The limestone trend, with a higher bulk density (~2.71 g/cm³) and lower neutron porosity, suggests limestone zones in the reservoir. Dolomite, characterized by an even higher bulk density (~2.85 g/cm³) and lower neutron porosity, is indicated by data points following the dolomite trend. The data distribution suggests a mixed lithology, predominantly sandstone with interbedded limestone and some dolomitic zones. Scatter in the data points indicates varying porosity due to diagenetic effects, cementation, or grain size variations. The presence of gas could shift points leftward due to reduced neutron porosity, while shale content could increase neutron porosity due to bound water effects. Overall, the reservoir appears to be mainly composed of sandstone with some limestone and minor dolomite presence.

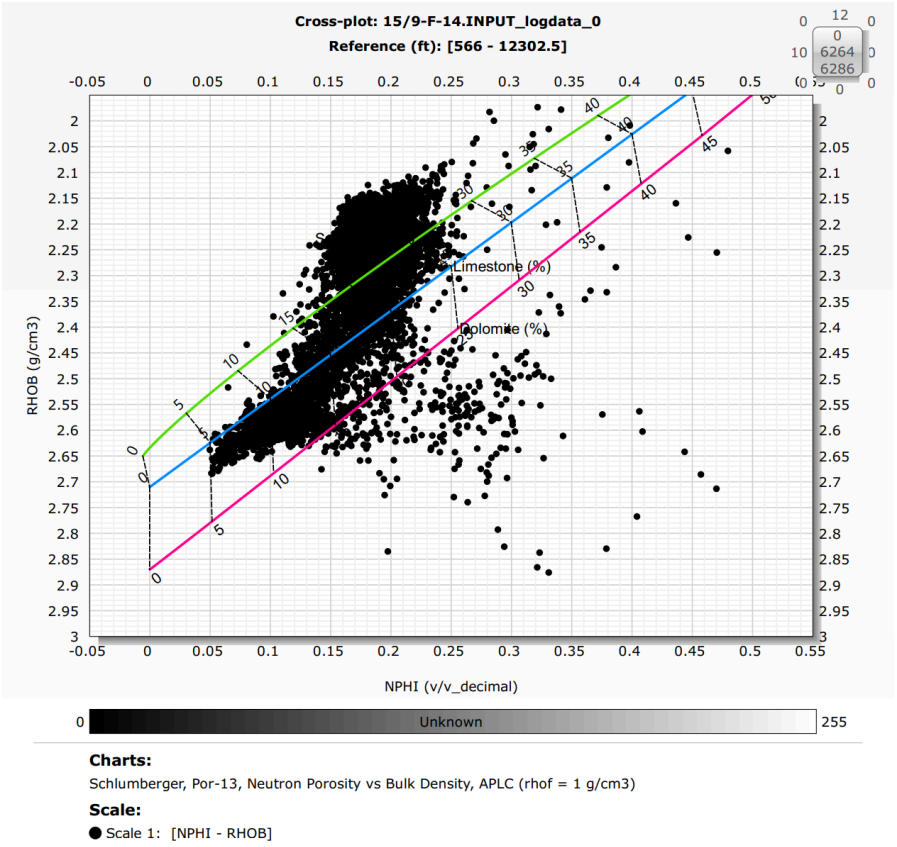

Figure 10. NPHI vs RHOB cross-plot for 15/9-F-14 well.

For the 15/9-F-14 well most points are between the limestone and dolomite lines, meaning the formation is mainly composed of these two rocks. Some points fall below the dolomite line, possibly indicating denser rocks like anhydrite or tight dolomite. Other points shift to the right, showing higher porosity, which may indicate gas or shale influence. The diagonal lines represent porosity percentages, with data moving to the right indicating higher porosity. If data points cross below the limestone or dolomite trend, they may represent mixed lithologies or gas zones. The formation mainly contains limestone and dolomite, with some sandstone. Porosity varies, meaning certain zones may store fluids like oil or gas. The spread of data may also indicate shale or gas effects.

Moreover, Machine Learning with Python was used to identify lithology. However, in this case, the goal was to identify sandstone as the major rock type in the dataset. Hence, the LAS data of 4 wells (P-F-11B, P-F-12, P-F-14, P-F-15C) were used. The results are presented as bar charts.

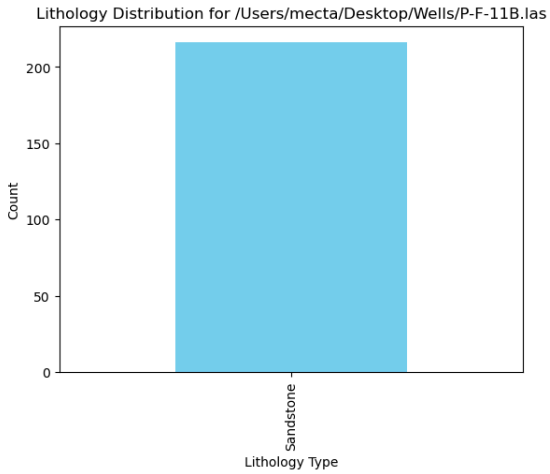

Figure 11. Identification of major lithology for well P-F-11B.

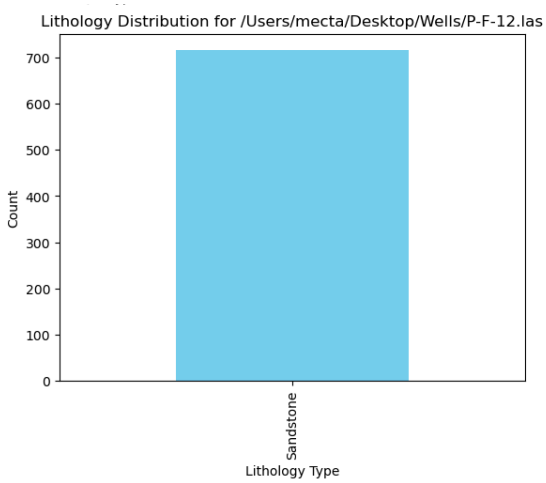

Figure 12. Identification of major lithology for well P-F-12.

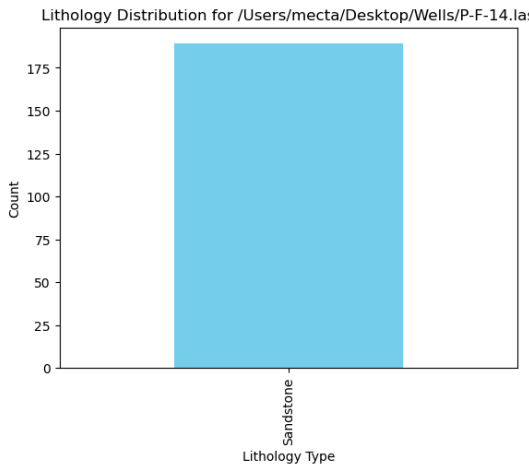

Figure 13. Identification of major lithology for well P-F-14.

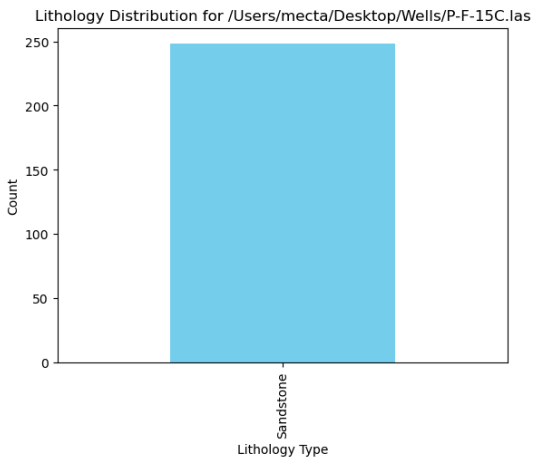

Figure 14. Identification of major lithology for well P-F-15C.

From the bar charts, it is seen that sandstone is the major rock type in the well logs regardless of other lithologies such as shale, limestone, and dolomite. Furthermore, for accuracy were applied Random Forest Classifier, Support Vector Machine (SVM) and Logistic Regression. The results shown in the tables.

Table 2. Lithology prediction and performance metrics.

Well	**Predicted major lithology**	**Lithology count**
P-F-11B	Sandstone	216
P-F-12	Sandstone	715
P-F-14	Sandstone	189
P-F-15C	Sandstone	248

Table 3. Random Forest Classifier.

Class	**Precision**	**Recall**	**F1-Score**	**Support**

Sandstone	0.99	0.99	0.99	201
Shale	0.83	0.79	0.81	90
Limestone	0.74	0.83	0.79	66
Dolomite	0.33	0.20	0.25	10
Accuracy	0.89			

Table 4. Support Vector Machine (SVM).

Class	**Precision**	**Recall**	**F1-Score**	**Support**
Sandstone	0.98	1.00	0.99	201
Shale	0.85	0.77	0.81	90
Limestone	0.73	0.91	0.81	66
Dolomite	0.00	0.00	0.00	10
Accuracy	**0.90**			

Table 5. Logistic Regression.

Class	**Precision**	**Recall**	**F1-Score**	**Support**
Sandstone	0.93	1.00	0.96	201
Shale	0.81	0.68	0.74	90
Limestone	0.76	0.88	0.82	66
Dolomite	0.00	0.00	0.00	10
Accuracy	**0.87**			

From the tables above, it can be stated that the machine learning results show that the model is highly effective at identifying sandstone as the dominant lithology which aligns with the focus on Sandstone as the major rock type in the dataset. The high precision, recall, and F1-score for sandstone across all classifiers (Random Forest, SVM, Logistic Regression) indicate that the model is very accurate in predicting this lithology. The precision values demonstrate the model's accuracy in predicting Sandstone, while the recall of 1.00 for SVM suggests that it successfully captures nearly all instances of Sandstone, with very few false negatives. However, the lower F1-scores for Shale, Limestone, and Dolomite, especially the 0.00 recall and precision for Dolomite in SVM and Logistic Regression, reflect the class imbalance in the training data. These lithologies are underrepresented, leading the model to focus primarily on Sandstone, which is the majority class. The accuracy values (around 0.89, 0.90, and 0.87) are high, but the model's performance is driven mainly by its ability to predict Sandstone, with poor performance on the minority classes. The results indicate that the class imbalance is a key factor in these outcomes, as the model tends to favor Sandstone, which is the most frequent class.

Petrel was also applied to identify the lithology by log interpretation. This lithology identification by logs can be found in the chapter "Petrophysical evaluation".

2.1.4. Seismic Evaluation

For the seismic evaluation, Petrel software was used. The data such as wells, well tops, and seismic data (time) were applied. Followingly, 2D and 3D views of 5 formations' surface maps with wells, RMS Amplitude, Relative Acoustic Impedance and Faults Interpretations were constructed.

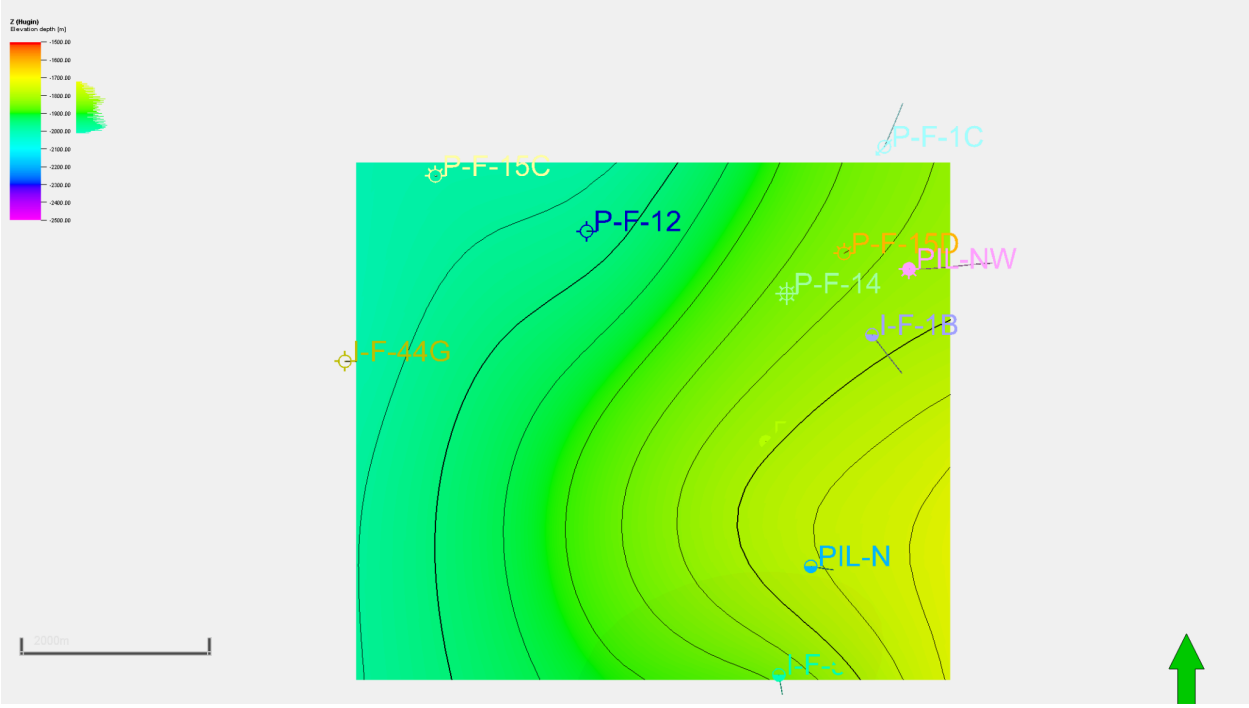

Figure 15. 2D view of Hugin formation.

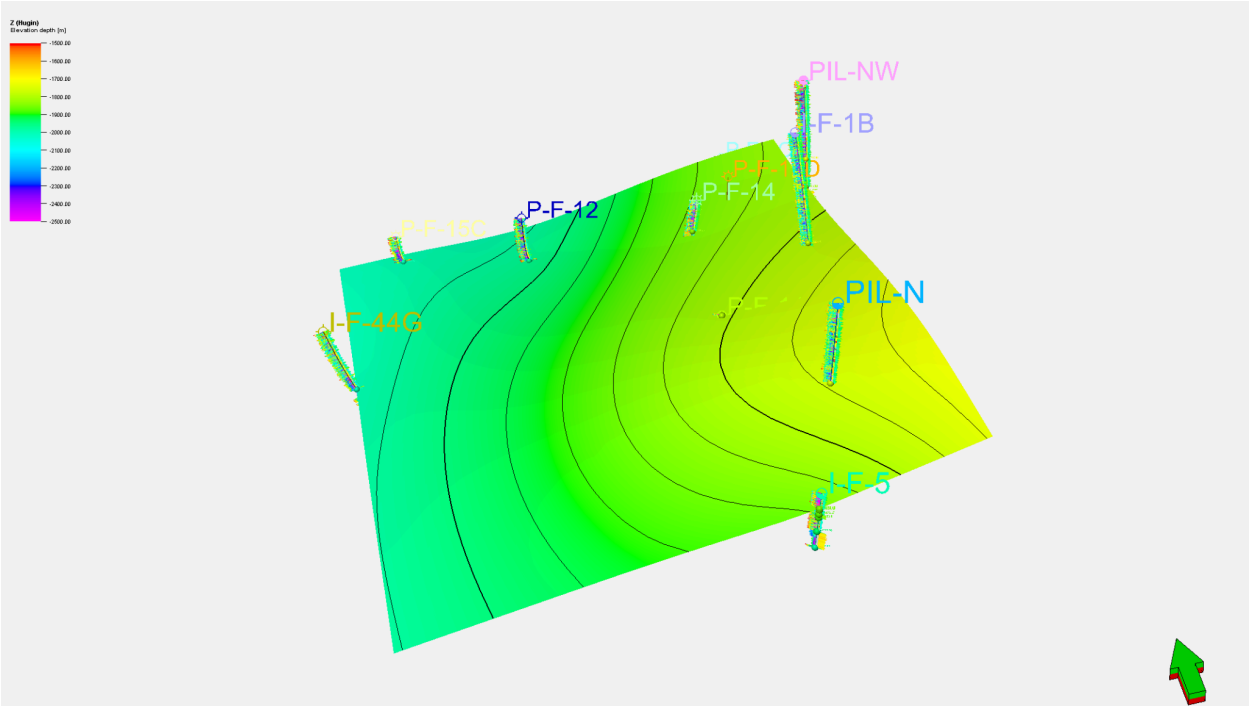

Figure 16. 3D view of Hugin formation.

The contours in the map indicate depth variations of the subsurface rock layers, ranging

from shallow to deeper regions. The colors represent depth in meters, with green and yellow zones indicating shallower depths, while blue represents deeper sections. The formation appears to be relatively gentle, with smooth contours suggesting minimal structural disruption or faulting. It shows that the Hugin Formation might have been subjected to relatively less tectonic activity compared to more complex structures that exhibit sharp bends or steep gradients. The well labeled P-F-12 appears to be positioned at a relatively shallow depth on the formation, as indicated by the green and yellow zones. It gives that it could be targeting a reservoir that is easier to access compared to deeper formations. The shallow depth may also imply that the hydrocarbons in this zone have migrated upward from deeper source rocks and are likely to be present in permeable reservoir rocks, such as sandstones. P-F-14 is located slightly deeper than P-F-12, within the yellow zone. The deeper position indicates that this well might be targeting hydrocarbons that have migrated from even deeper source rocks, possibly from the Middle or Lower Hugin formations. The layer around P-F-14 could potentially be a trap zone, with hydrocarbons accumulating due to structural features like subtle folds or fault-related traps. P-F-15C is located at a similar depth to P-F-12, but its proximity to a blue zone suggests that this well might be intersecting a deeper section of the formation. It could show that it is targeting either deeper parts of the reservoir or potential migration pathways for hydrocarbons that have moved up through faults or fractures. The wells labeled PIL-N and PIL-NW appear to be located on the shallower regions, likely representing wells placed on top of structural highs or near the crest of anticlines. This placement shows that the hydrocarbon trapping potential could be higher here, especially if the impermeable seal rocks have effectively trapped hydrocarbons in the permeable layers beneath. The PIL-N well, in particular, could be drilling into a promising reservoir rock where hydrocarbons have accumulated. I-F-5 is located in the deeper, blue-colored zones of the map, suggesting that it is targeting a deeper layer of the formation. This well might be exploring potential source rock areas that have undergone significant maturation, making it a possible target for both oil and gas. The deeper zones could be reservoirs formed under higher pressure, with hydrocarbon migration influenced by the structure and faulting present in this part of the formation.

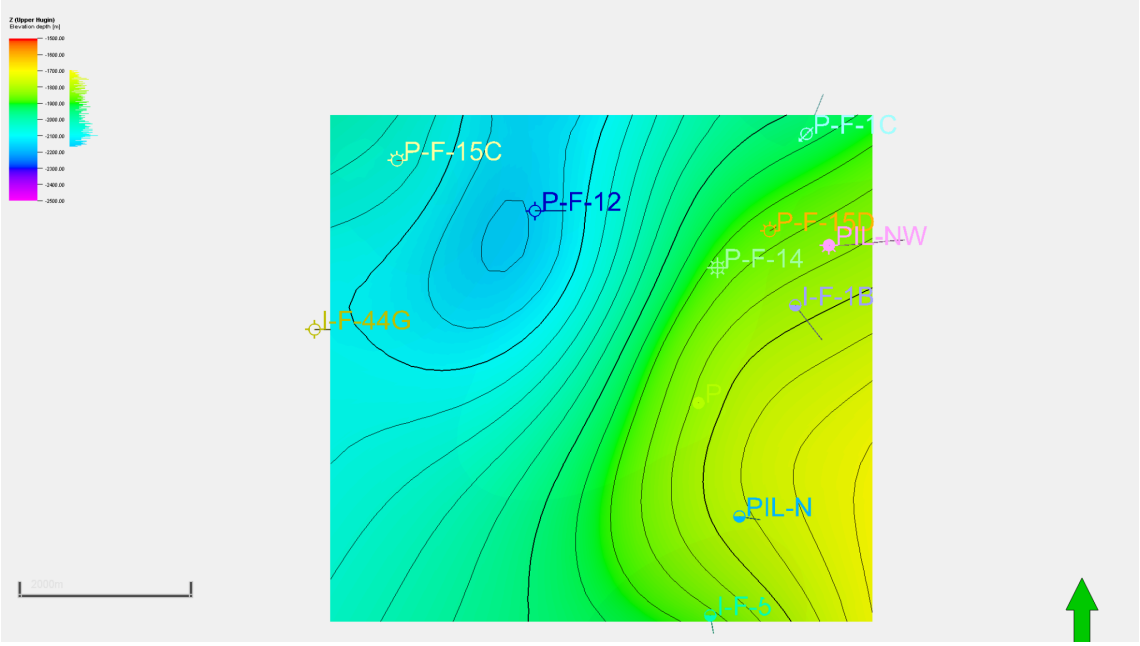

Figure 17. 2D view of Upper Hugin formation.

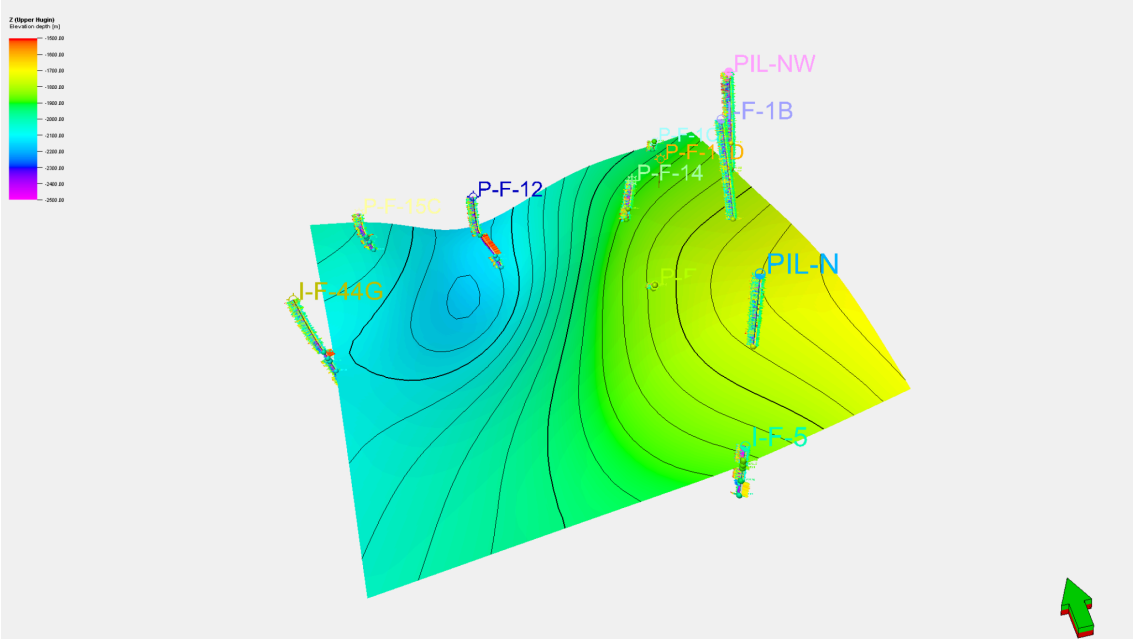

Figure 18. 3D view of Upper Hugin formation.

The Upper Hugin Formation is characterized by relatively shallow depths compared to the other layers. It could show a relatively uniform depositional environment, which may be conducive to the accumulation of hydrocarbons. The shallower depth implies that this formation could be more accessible for exploration and drilling. The consistent contour lines also suggest a

lower degree of faulting or tectonic disruption in this area, which might lead to a more predictable reservoir structure for hydrocarbon extraction.

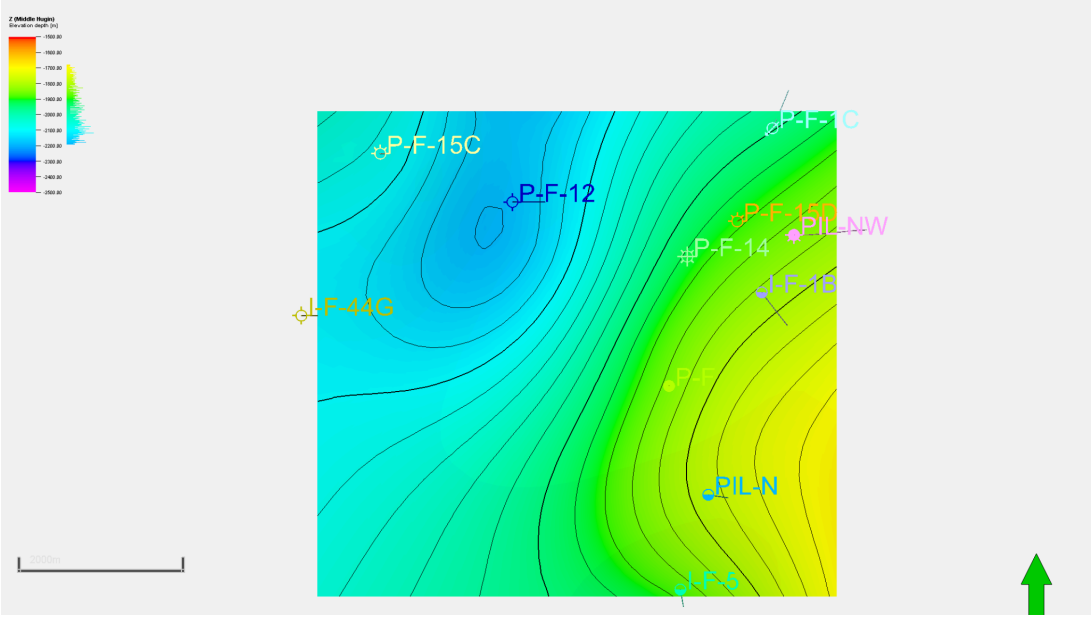

Figure 19. 2D view of Middle Hugin formation.

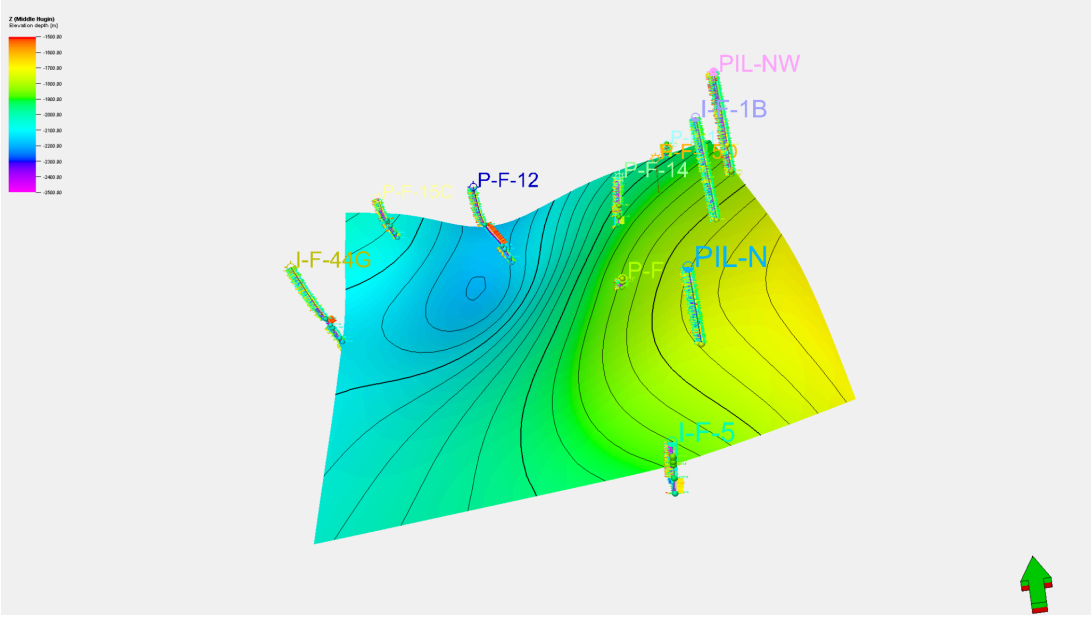

Figure 20. 3D view of Middle Hugin formation.

In contrast, the Middle Hugin Formation appears to be situated at slightly deeper depths. The contour lines in this layer show more curvature, potentially indicating the presence of

structural features like folds or slight anticlines. It can show a more complex geological environment with potential for hydrocarbons to migrate and accumulate, especially where the formation experiences pressure or faulting that could create traps. The deeper nature of this formation suggests that any hydrocarbons within it may have migrated from the Upper Hugin Formation or other deeper sources and been trapped in this layer due to impermeable barriers or structural folds.

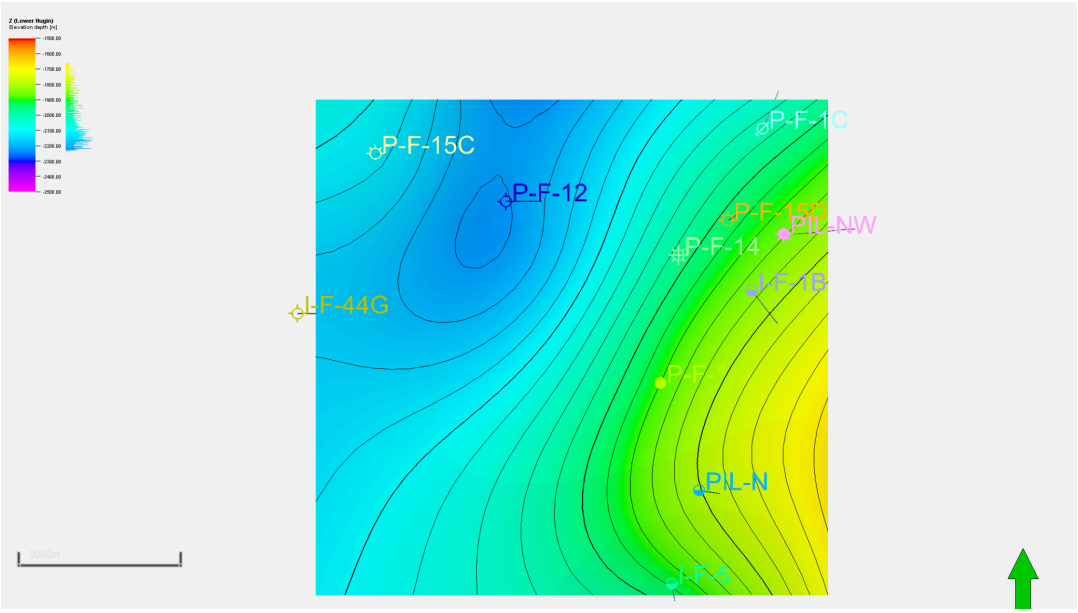

Figure 21. 2D view of Lower Hugin formation.

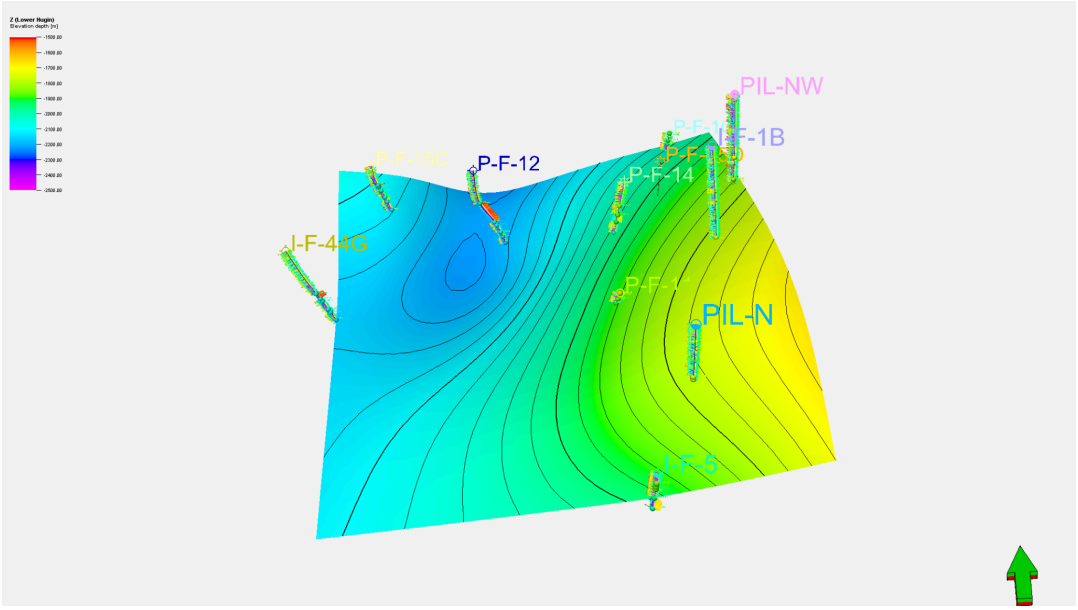

Figure 22. 3D view of Lower Hugin formation.

Lower Hugin Formation, although still deep, lies above Sleipner and shows gentler contours. These smoother contours suggest less tectonic complexity compared to Sleipner, which could mean that the Lower Hugin Formation is more uniform and less disturbed by faulting. The Lower Hugin may still contain hydrocarbon reservoirs, but its relatively more stable structure may not have as many opportunities for the creation of large, fault-controlled traps as seen in Sleipner.

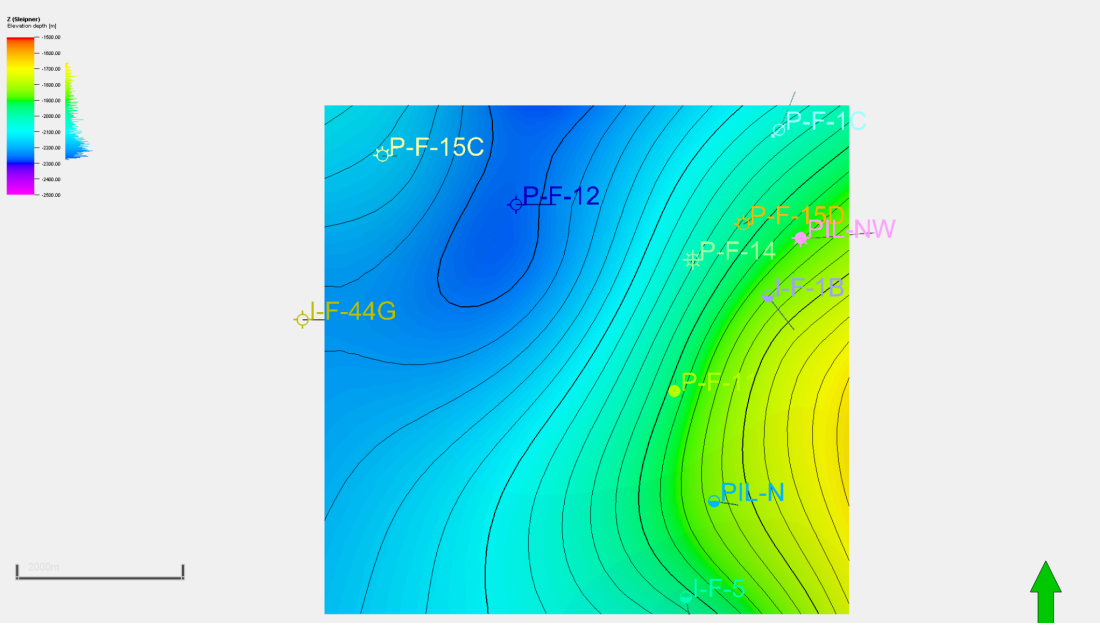

Figure 23. 2D view of Sleipner formation.

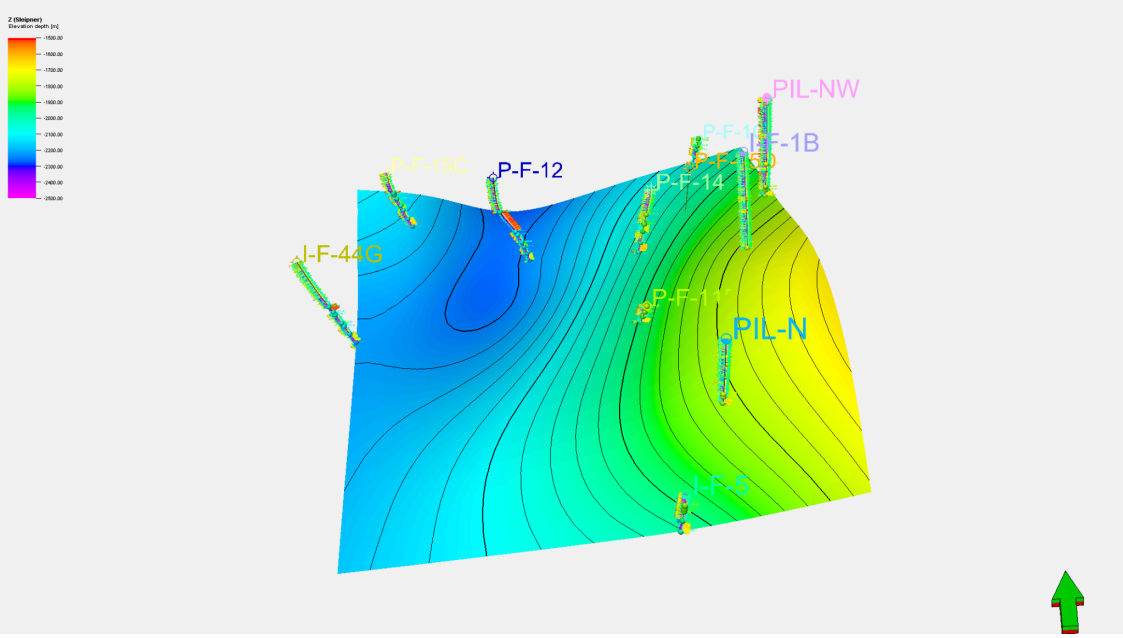

Figure 24. 3D view of Sleipner formation.

The Sleipner Formation is located at a deeper depth compared to the Lower Hugin, as indicated by the more pronounced contours in the Sleipner Formation, which reflect a greater depth. The contours of Sleipner show more complexity, showing that this formation has experienced significant tectonic activity, such as faulting or compression, which could result in the creation of hydrocarbon traps. Given its depth, Sleipner could potentially serve as both a source rock and a reservoir for hydrocarbons. The presence of faults and the irregular shape observed in Sleipner might create smaller traps or migration pathways, where hydrocarbons can accumulate in pockets, influenced by the structural disruptions within the formation.

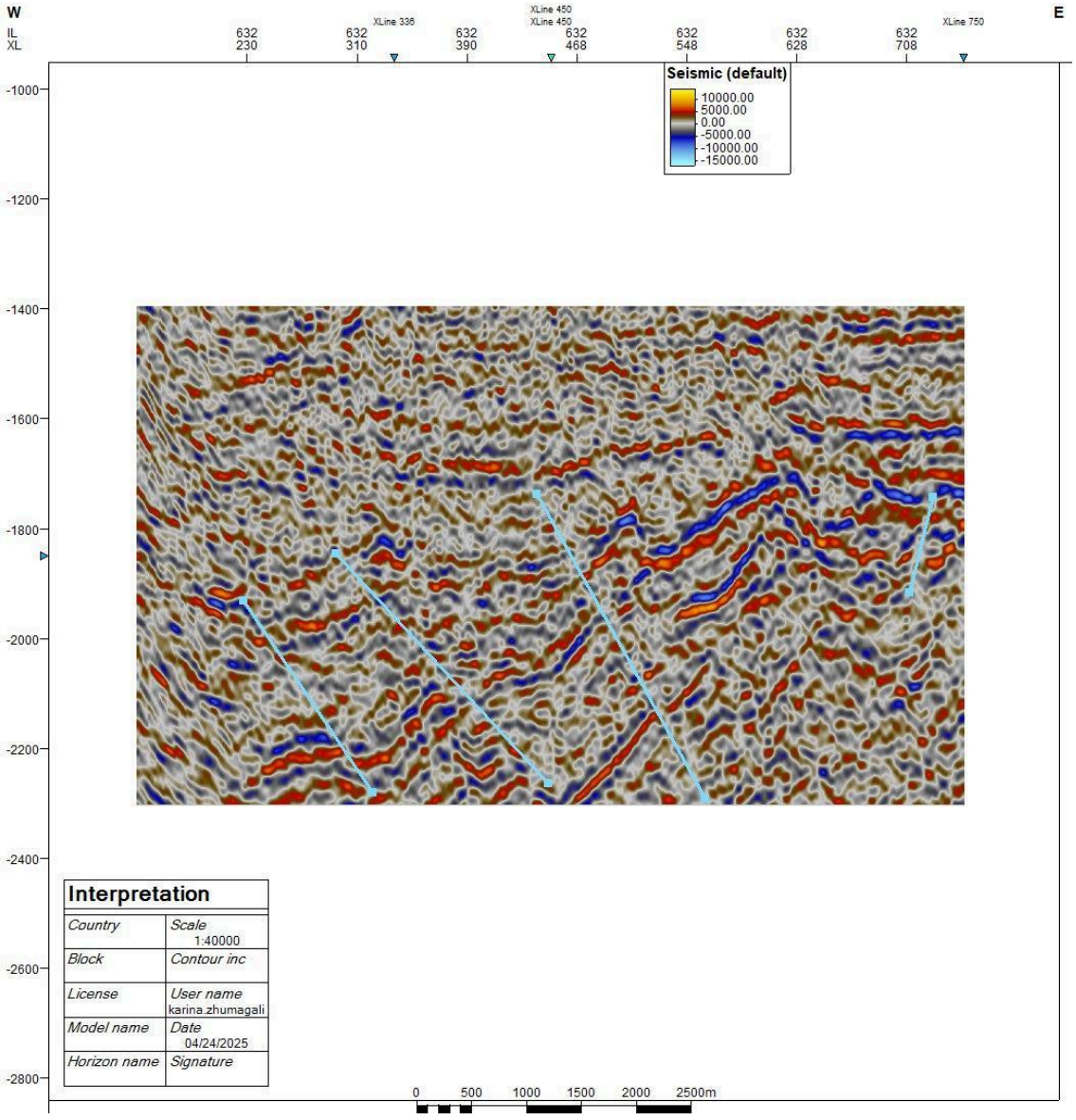

Figure 25. Fault interpretation of F-12 well's area.

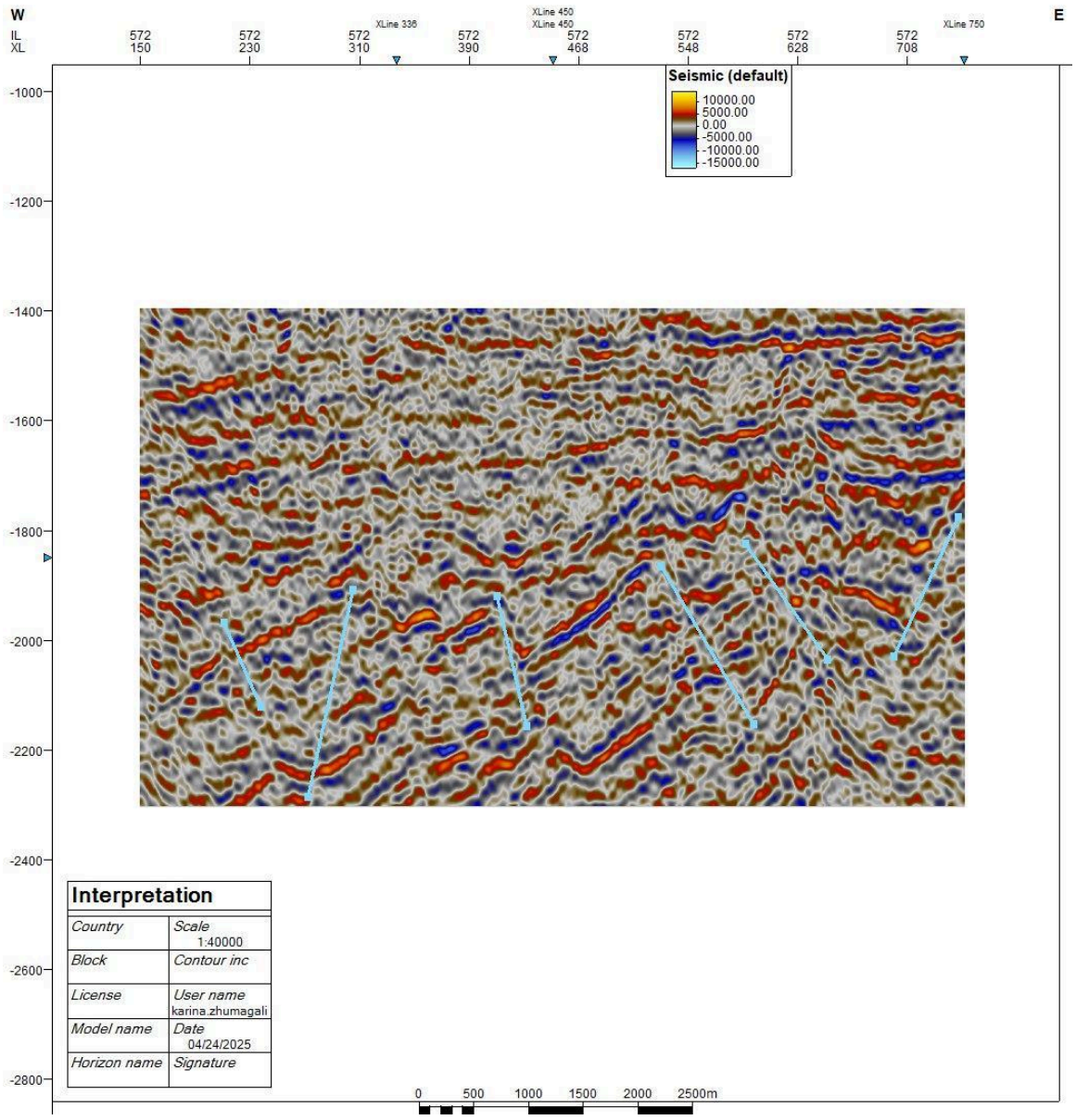
W
E
IL
XL
572 150
572 230
572 310
572 390
572 468
572 548
572 628
572 708
XLine 336
XLine 450
XLine 450
XLine 750
Seismic (default)
10000.00
5000.00
0.00
-5000.00
-10000.00
-15000.00
-1000
-1200
-1400
-1600
-1800
-2000
-2200
-2400
-2600
-2800
Interpretation
Country
Scale 1:40000
Block
Contour inc
License
User name karina.zhumagali
Model name
Date 04/24/2025
Horizon name
Signature
0 500 1000 1500 2000 2500m

Figure 26. Fault interpretation of F-14 well's area.

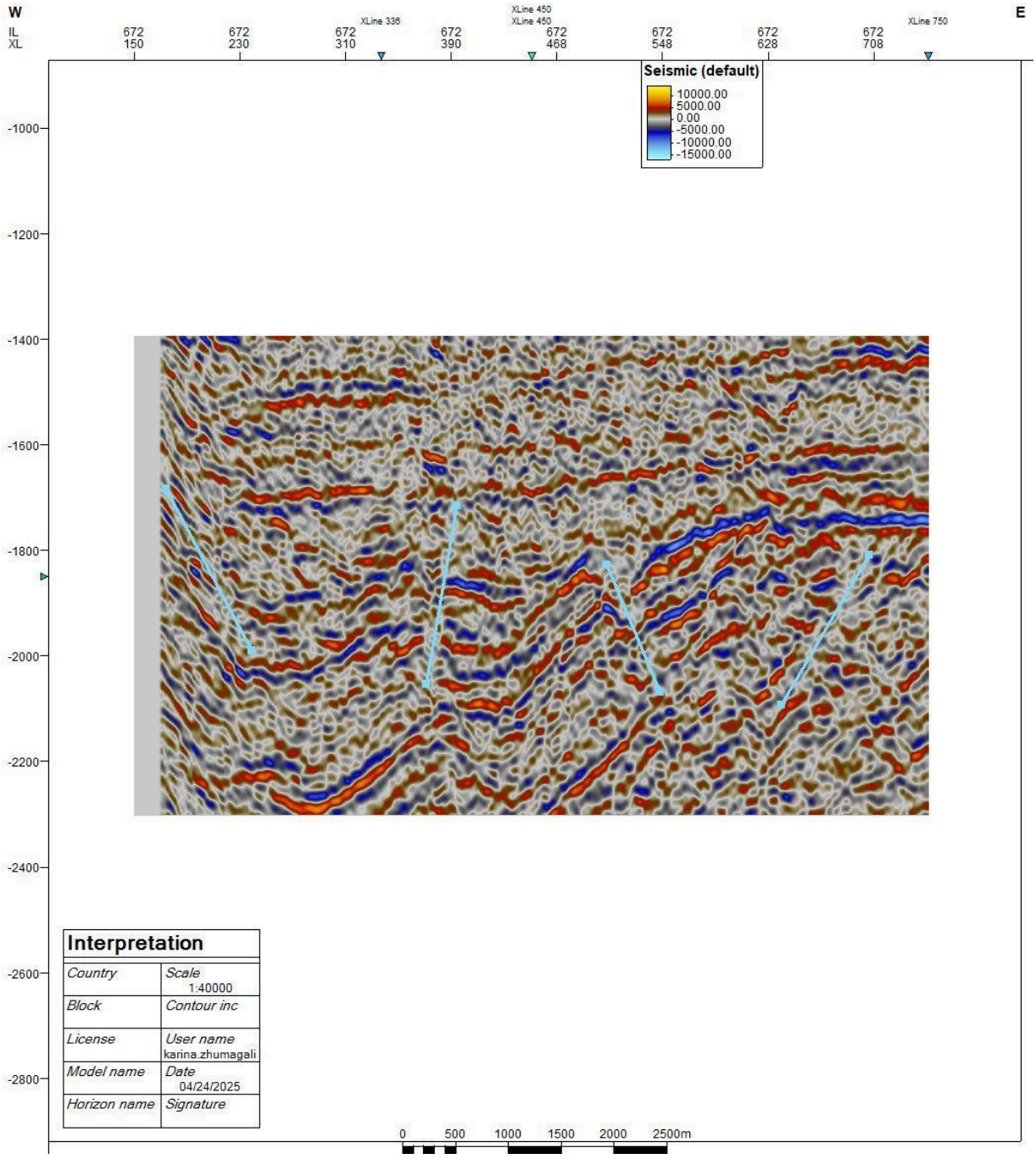

Figure 27. Fault interpretation of F-15C well's area.

Figures 25-27 show seismic images of fault interpretations of the area where 3 wells are located which represent strong geological structures controlling hydrocarbon migration, traps,

and accumulation beneath the surface. Blue lines in each image indicate faults that characterize discontinuities in the geological layers. Sealing faults have the potential to trap hydrocarbons within reservoir rocks and form traps, while non-sealing faults might allow hydrocarbons to exit through them. The presence of faults and the folds that they create are important to understand how hydrocarbons may be trapped in structural traps. The structures are formed by anticlines, the topographic highs where hydrocarbons may accumulate if capped by impermeable covers such as shale. Hydrocarbons migrate upward due to their buoyancy through permeable rock units, such as sandstone or limestone, until they are stopped by impermeable seals such as shales or tight carbonates. The seismic data suggest hydrocarbon migration along the faulted zones demonstrated in the Figures 25-27, which might be a source of migration to higher reservoir levels or lead to accumulation in structural traps at the junctions of faults. The migration routes rely on the depth variation data discussed for each well, where lower layers are the source rocks for hydrocarbons and the upper layers are reservoirs. The area where the given 3 wells share similar properties, and in each of them, folding structures are implied, which are apparently anticlines. Faults encountered in this area provide migration channels and act as barriers. Apart from that, the three seismic sections all reflect changes in stratigraphy, and with alternating positive and negative amplitudes indicating differences in permeable layers. Such changes suggest that there are reservoir rocks with hydrocarbons, with red and yellow areas indicating permeable zones and blue more impermeable layers. The variations among the 3 figures are in the fault geometry, the reservoir depth, and the efficiency of the seals. Some of the faults tend to be more discrete and create more distinct structural traps, whereas others could accommodate more intricate migration patterns. The layer depths are different, which affects the migration pathways and opportunities for hydrocarbon accumulation at varied subsurface levels.

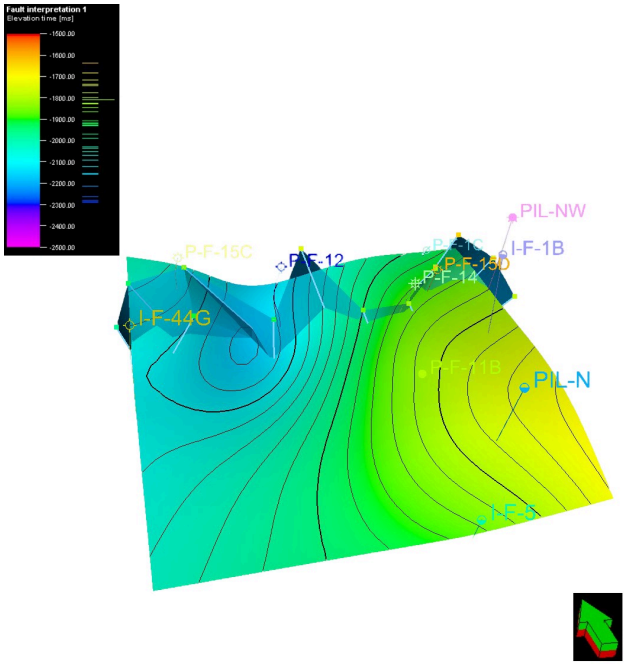

Figure 28. 3D view of fault interpretation.

The above 3 fault interpretations can be seen also in 3D in Figure 28.

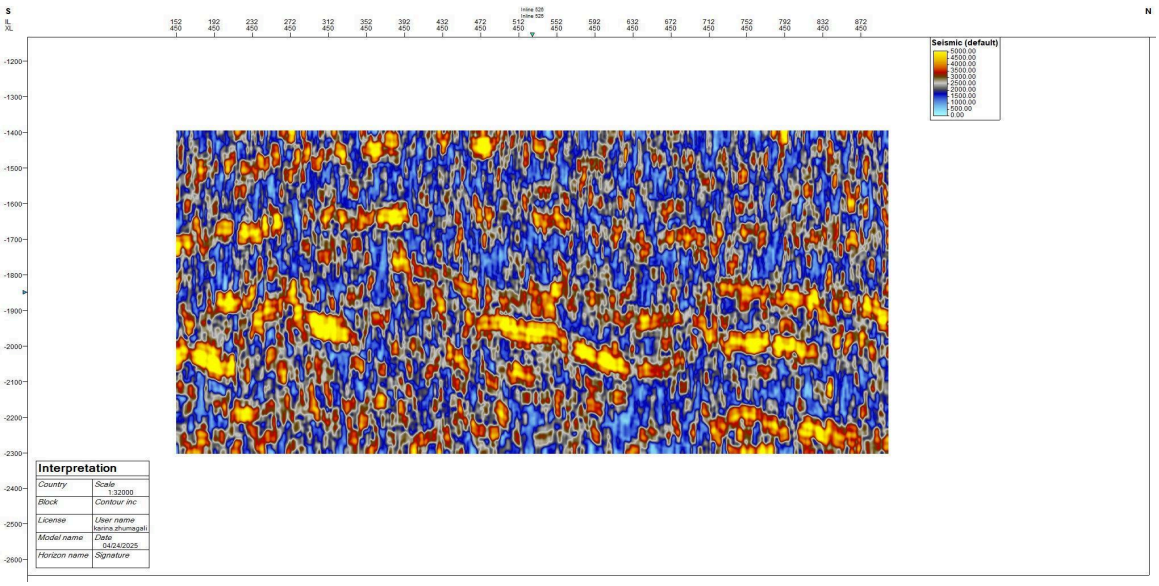

Figure 29. RMS Amplitude interpretation.

The interpretation of RMS amplitude displays a number of large features of the subsurface. The regions of high amplitude, emphasized by warm colors such as yellow and red,

are high seismic energy areas and may be interpreted as having high-porosity or hydrocarbon-bearing rock. Low amplitude areas, emphasized by cool colors such as blue and gray, are low seismic energy areas and may be representing denser or less porous rock that is not creating strong seismic reflection. Linearities, particularly where there is high and low amplitude difference, may be portraying fault zones or fractures because the break in amplitude signifies fault displacements or geologic boundaries. Moreover, anomalous blob-like shapes within high amplitude zones may indicate subsurface targets such as gas pockets, fluid migration channels, or even salt domes, which all tend to occur with high RMS amplitudes due to the influence that they have upon seismic waves. Transition zones where high-amplitude areas change into lower amplitude areas likely represent stratigraphic boundaries, such as between different rock units such as shales and sandstones. The mottled, mosaic-type texture throughout the image indicates a heterogeneous subsurface with alternating lithologies and varying reservoir properties. These variations may indicate more productive regions for hydrocarbon accumulation in some parts of the formation.

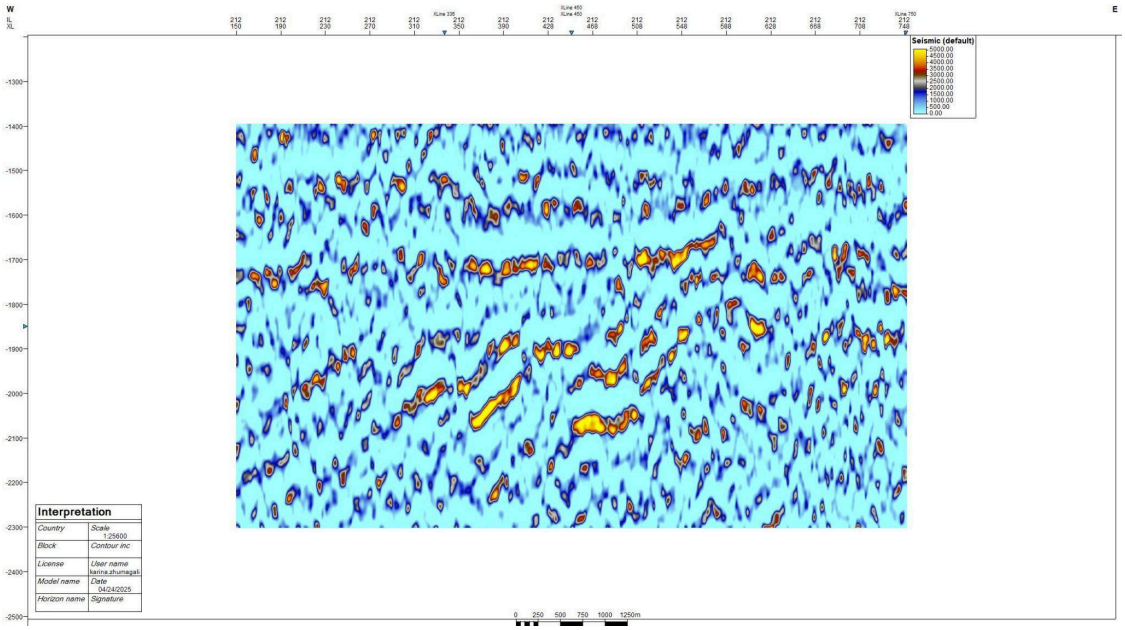

Figure 30. Relative acoustic impedance interpretation.

Figure 30, using a color gradient from blue to red, primarily shows variations in seismic amplitude. The high impedance areas which are red and yellow reflect more acoustic energy, typically associated with denser or harder rock formations, while the lower impedance areas which are blue represent softer or more porous formations. This figure exhibits distinct linear patterns, suggesting the presence of faults or fractures that influence how seismic waves interact with the subsurface, creating sharp contrasts in impedance values. These transitions between higher and lower impedance areas may indicate boundaries between different rock types or stratigraphic layers. It highlights a heterogeneous geological structure with faults or fractures, potentially important for identifying reservoir zones or barriers.

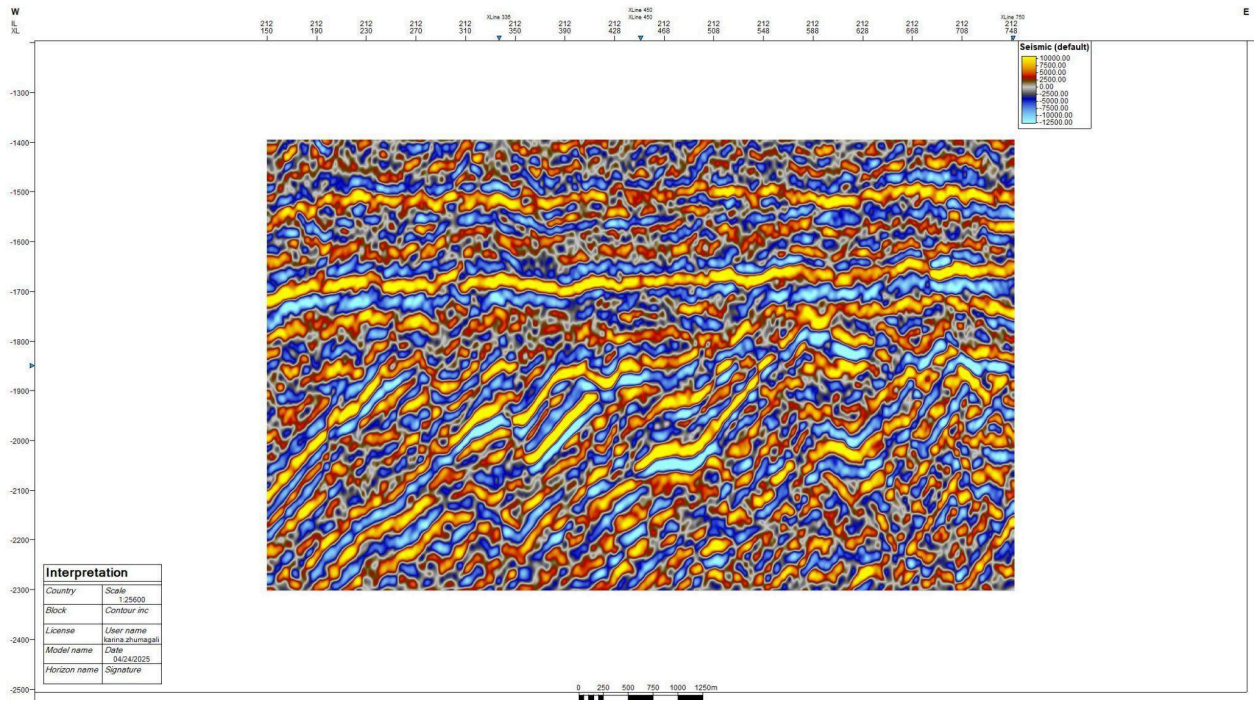

Figure 31. Relative acoustic impedance interpretation.

Figure 31 uses a broader color scale ranging from blue to yellow, representing even more variation in impedance values. Here, the higher amplitude values (yellow and red) correlate with denser rock formations, while the blues indicate softer formations or fluid-rich areas. Unlike the figure X, this map shows more continuous and elongated features, which could represent stratigraphic layers or structural folds. The impedance contrasts suggest transitions between layers of varying lithologies such as sandstone, shale, or limestone, influencing fluid migration

and reservoir formation. This map represents a broader, more continuous subsurface region with identifiable trends in impedance distribution.

The first figure focuses on amplitude variations, useful for identifying faults, fractures, and localized structural anomalies, while the second figure emphasizes acoustic impedance, providing insight into lithological properties and stratigraphy.

2.2. Petrophysical Evaluation

Petrophysical evaluation is a key part of reservoir characterization as it provides a complete picture about the subsurface rock and fluid properties. The main goal in petrophysical analysis is to identify the rock's ability to store and transmit fluids, and it has direct implications on the productivity of the reservoir. This process involves analyzing key petrophysical parameters such as porosity, permeability, and water saturation that hydrocarbon in place and the efficiency of fluid flow through the reservoir. Petrophysical analysis is interested in finding out the physical properties of the rock in order to facilitate the building of realistic models for reservoir simulation, optimization of well placement, and making proper decisions on reservoir management and production strategies. It is essential to identify the most productive areas of a reservoir and predict future performance, as it is an integral part of field development and exploitation.

The data were acquired from open source data of Equinor. The data in total contains 19 wells with different logs in the formats of LAS, DLIS, and ASCII. All the data were checked for its availability and further use. Therefore, it was summarized in Table 6.

Table 6. Summary of the well logs that are available.

Well	Log curves						Computer Processed Interpretation (CPI)						Well header	Deviation survey
	GR	*CALI*	*RHO*	*NEU*	*DTC*	*DTS*	*VSH*	*VCL*	*PHIT*	*SWT*	*PHIE*	*SWE*		
15/9-19A	Yes	Yes	Yes	Yes	Yes	Yes	Yes	**No**	Yes	Yes	Yes	Yes	**No**	Yes
15/9-19BT2	Yes	**No**	Yes	Yes	Yes	Yes	Yes	**No**	Yes	Yes	Yes	Yes	**No**	Yes
15/9-19SR	Yes	Yes	Yes	Yes	Yes	Yes	Yes	**No**	Yes	Yes	Yes	Yes	**No**	Yes
15/9-F1	Yes	Yes	Yes	Yes	Yes	Yes	Yes	**No**	Yes	Yes	Yes	Yes	**No**	Yes
15/9-F1A	Yes	Yes	Yes	Yes	Yes	Yes	Yes	**No**	Yes	Yes	Yes	Yes	**No**	Yes
15/9-F1C	Yes	Yes	Yes	Yes	**No**	**No**	Yes	**No**	Yes	Yes	**No**	**No**	**No**	Yes
15/9-F4	Yes	Yes	Yes	Yes	Yes	Yes	Yes	**No**	Yes	Yes	**No**	**No**	**No**	Yes
15/9-F5	Yes	Yes	Yes	Yes	Yes	**Yes**	Yes	**No**	Yes	Yes	**No**	**No**	**No**	Yes
15/9-F10	Yes	Yes	Yes	Yes	Yes	Yes	Yes	**No**	Yes	Yes	**No**	**No**	**No**	Yes
15/9-F11	**No**	**No**	**No**	**No**	**No**	**No**	**No**	**No**	**No**	**No**	**No**	**No**	**No**	Yes
15/9-F11A	Yes	Yes	Yes	Yes	Yes	Yes	Yes	**No**	Yes	Yes	**No**	**No**	**No**	Yes
15/9-F11B	Yes	Yes	Yes	Yes	**No**	**No**	Yes	**No**	Yes	Yes	**No**	**No**	**No**	Yes
15/9-F11T2	Yes	Yes	Yes	Yes	Yes	Yes	Yes	**No**	Yes	Yes	**No**	**No**	**No**	Yes
15/9-F12	Yes	Yes	Yes	Yes	Yes	Yes	Yes	**No**	Yes	Yes	Yes	Yes	Yes	Yes
15/9-F14	Yes	Yes	Yes	Yes	Yes	Yes	Yes	**No**	Yes	Yes	Yes	Yes	Yes	Yes
15/9-F15A	Yes	Yes	Yes	Yes	Yes	**No**	Yes	**No**	Yes	Yes	**No**	**No**	**No**	Yes
15/9-F15B	Yes	Yes	Yes	Yes	Yes	**No**	Yes	**No**	Yes	Yes	**No**	**No**	**No**	Yes
15/9-F15C	Yes	Yes	Yes	Yes	Yes	**No**	Yes	**No**	Yes	Yes	**No**	**No**	**No**	Yes
15/9-F15D	Yes	Yes	Yes	Yes	**No**	**No**	Yes	**No**	Yes	Yes	**No**	**No**	**No**	Yes

For the further detailed analysis of logs, two wells were selected which are 15/9-F12 and 15/9-F14.

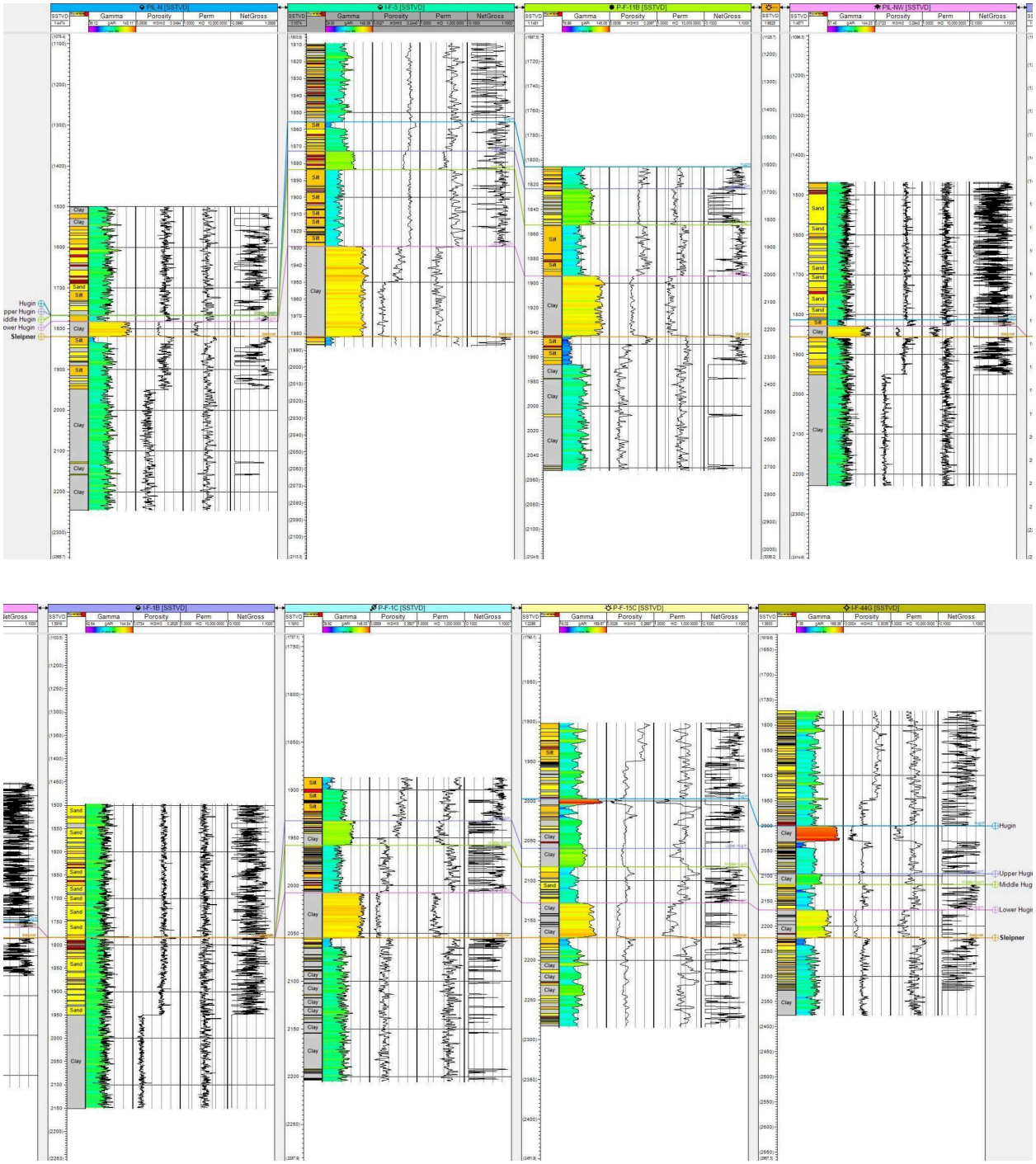

Figure 32. Log interpretation.

Figure 32 shows the log interpretations of 8 wells excluding 15/9-F-12 and 15/9-F-14 wells. The given log shows gamma, porosity, permeability and netgross logs. It also shows fluvial facies which can give the lithology characterization. From the log, it can be seen that the

lithology is as follows: clay, silt, and sandstone. Excluded two wells (15/9-F-12 and 15/9-F-14) selected separately as it has more variety of logs and further would be used for reservoir simulation and production. Hence, detailed petrophysical analysis were conducted for 15/9-F-12 and 15/9-F-14, and were chosen for further petrophysical analysis.

Firstly, the logs were constructed for two wells.

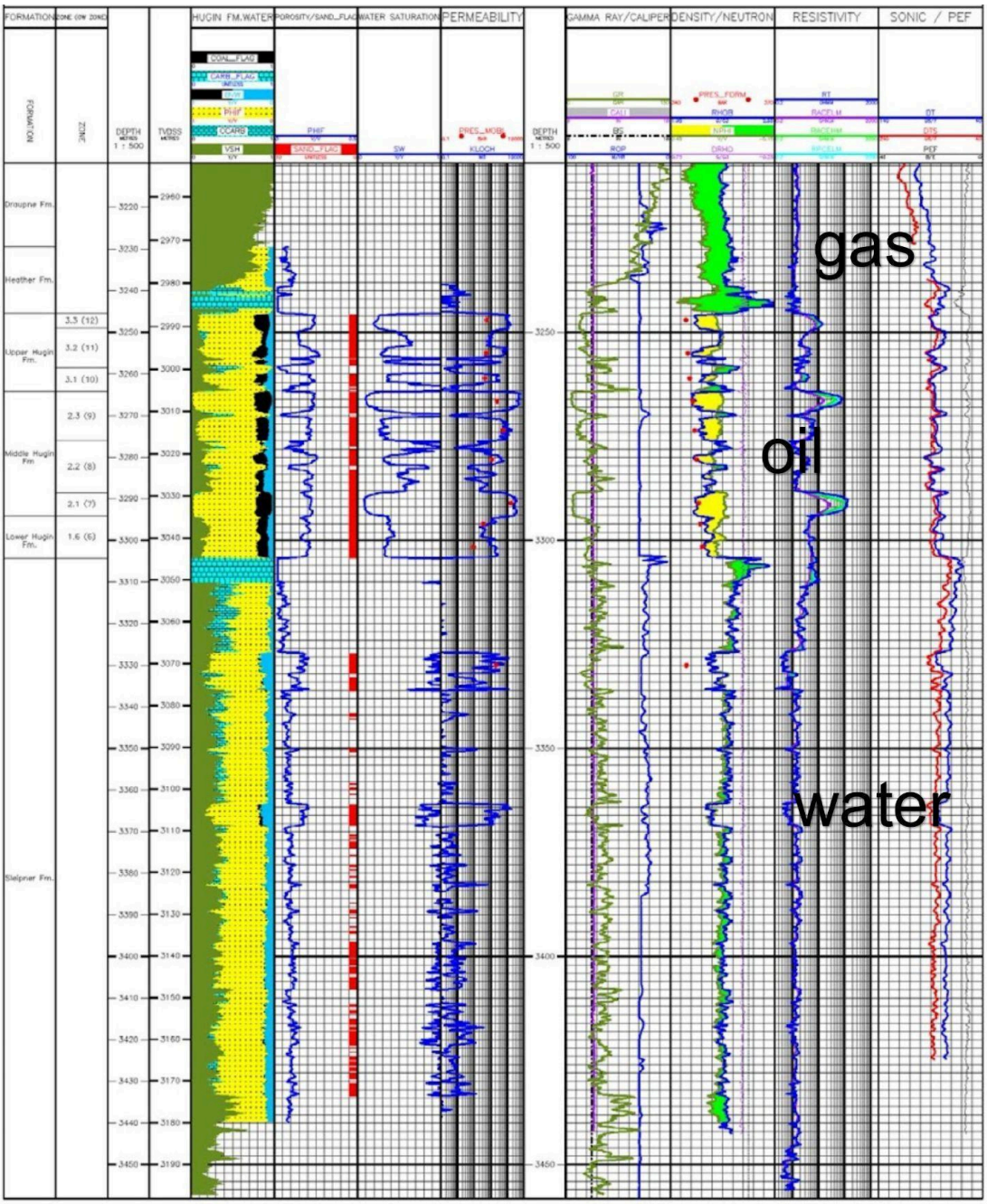

Figure 33. 15/9-F-12 log interpretation.

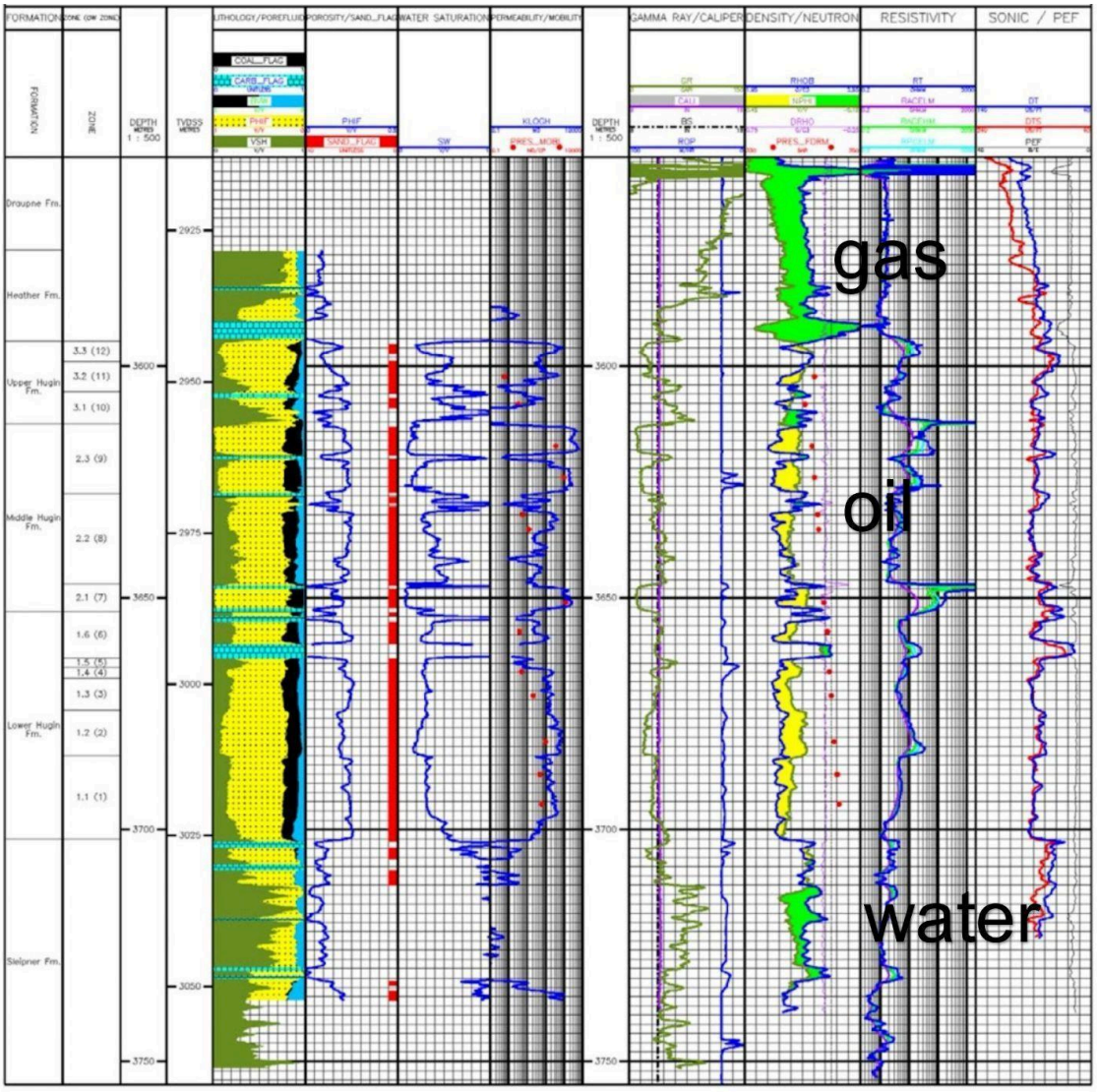

Figure 34. 15/9-F-14 well log interpretation.

From the above 2 log interpretations it can be concluded that gas, oil, water are present which were identified by the difference between RHOB and NPHI and using the resistivity logs. The big difference between RHOB and NPHI with the largest resistivity highlights the gas effect identifying the presence of gas. The lowest difference between RHOB and NPHI with the lowest resistivity shows the water zone. The difference between RHOB and NPHI which is smaller than the gas effect, but bigger than the water zone is oil. Oil's resistivity shows lower values than gas but higher than the water's one. High gamma ray values show the presence of shale, while lower

gamma ray values indicate the non-shale reservoir rocks. Hence, the volume of shales varies from 0 to 1. Caliper logs show no washout which suggest that there is no hole enlargement. Moreover, it can be said that the wellbore is stable as there are no swellings or carvings by caliper logs.

Finally, using the formulas 1-3, the exact values of porosity, water saturation and permeability were calculated for 2 wells. The results are shown in Tables 7-8.

Used formulas:

1. Porosity:

$$\phi_d = \frac{\rho_{ma} - \rho_b}{\rho_{ma} - \rho_f} \quad (1)$$

where:

- ϕ_d - density porosity, fraction.
- ρ_b - bulk density from the log (g/cm^3)
- ρ_{ma} - matrix density (g/cm^3) which depends on the lithology:
    - Sandstone: 2.65 g/cm^3
    - Limestone: 2.71 g/cm^3
    - Dolomite: 2.87 g/cm^3
- ρ_f - fluid density (g/cm^3)

2. Water saturation:

$$S_w = \left(\frac{a * R_w}{\phi^m * R_t}\right)^{\frac{1}{n}} \quad (2)$$

- S_w - water saturation, fraction
- a - Archie's lithology constant.
- R_w - formation water resistivity, Ω·m
- R_t - true formation resistivity, Ω·m
- ϕ - porosity, fraction

- m - cementation exponent
- n - saturation exponent

3. Permeability:

$$k = 10^{(a+b*log\phi-c*logS_{wir})} \quad (3)$$

- k - permeability, mD
- ϕ - porosity, fraction
- S_{wir} - irreducible water saturation, fraction
- a, b, c - Empirical constants

Table 7. Summary of petrophysical parameters of formations (F-12).

Formation	**PHIF (fraction)**	**Sw (fraction)**	**Permeability (mD)**
Hugin	0.20	0.36	864
Upper Hugin	0.19	0.41	416
Middle Hugin	0.21	0.33	1380
Lower Hugin	0.19	0.37	154
Sleipner	0.13	0.94	63

Table 8. Summary of petrophysical parameters of formations (F-14).

Formation	**PHIF**	**Sw**	**Permeability (mD)**
Hugin	0.21	0.32	513
Upper Hugin	0.17	0.44	121
Middle Hugin	0.21	0.29	1024
Lower Hugin	0.22	0.32	201
Sleipner	0.14	0.86	87

Chapter III

3.1. Reservoir Engineering

Reservoir analysis and characterization is the most crucial step at preparing a comprehensive description of the FDP, as well as designing the project itself. Reservoir engineering combines data from a variety of disciplines including geology, petrophysics, geochemistry, petroleum engineering, etc.

For the reservoir characterization itself, all the essential geological and petrophysical properties are mentioned in the previous section. The following part mostly focuses on the reservoir fluid properties, well test data analysis, as well the main reservoir driving mechanisms essential for the reservoir performance, reserves estimates, reservoir modeling, and future management strategies.

3.1.1. Reservoir Rock and Fluid Properties

Reservoir rock and fluid properties are collected during the early exploration processes and production tests. The major averaged data can be summarized in Table 1 and 2.

Table 9. Reservoir fluid properties.

Property [unit]	**The numeric value**	**Additional notes**
Saturation pressure [bar]	340	Measured at boiling point
API gravity of oil	$27 - 30^{\circ}$	Medium oil (Light oil)
Oil viscosity [cp]	$0.55 - 0.79$	- Measured at boiling point - Low viscosity oil
Formation volume factor	$1.39 - 1.5$	- Measured at boiling point

$[m^3/Sm^3]$		- Indicates slight expansion of the oil volume from reservoir to surface conditions
Gas - oil ratio $[sm^3/sm^3]$	$111.8 - 159.1$	Indicates the presence of associated gas
Water salinity $[ppm]$	35 000	- Indicates moderate to high water salinity due to the presence of aquifer - Potentially shows the need for water treatment during production
CO_2 $[mol\,\%]$	$1.6 - 4.9$	- Indicates moderate range - Potentially may require some considerations for CO_2 removal, corrosion control, or reinjection to minimize emissions

Table 10. Reservoir rock properties.

Property [unit]	**The numeric value**	**Additional notes**
Lithology	Sandstone	- Primarily sandstone but contains some interbedded shales - Clean sand with small amount of clay
Porosity [%]	21	- Quite good porosity
Permeability [mD]	1000	- High permeability, great fluid flow - Some variations in permeability due to

		local shale barriers and cementation
Net-to-gross ratio [%]	93	A significant portion of the reservoir rock is of good quality for hydrocarbon storage and flow
Water saturation [%]	20 - 30	Indicates high oil saturation
Reservoir depth [m]	3210	Measured below the sea level

3.1.2. PVT Analysis and Hydrocarbon Composition

The Volve field is distinguished from other North Sea oil fields by its unique hydrocarbon composition. It contains undersaturated oil with an API gravity ranging between 27° and 29°, classifying it as light to medium oil. The gas-oil ratio in the field varies between 111 and 159 Sm^3/Sm^3.

One notable characteristic of the Volve oil is its high aromatic content and low sulfur percentage. Investigations show that C10+ aromatics can constitute up to 52% of the oil composition, while sulfur content remains below 2%. However, no traces of hydrogen sulfide (H2S) have been detected in the field, simplifying the production process by eliminating the need for H2S treatment.

All the below-mentioned graphs represent the results of PVT analysis (made using CMG WinProp software) that confirmed hydrocarbon composition of the oil. First of all, the percentage composition demonstrated in the following figure, as well as the bar chart exhibited high content of methane in reservoir fluid which is a necessary point in indicating that it is light to medium oil.

Component	Reservoir Mole %	Stock Tank Gas Mole%		Stock Tank Oil Mole%	
		Lab	Sim	Lab	Sim
Nitrogen	0.41	0.69	0.69	0.00	0.00
Carbon dioxide	3.80	6.39	6.31	0.00	0.09
Hydrogen Sulphide	0.00	0.00	0.00	0.00	0.00
Methane	39.90	67.04	66.71	0.10	0.31
Ethane	6.07	10.03	9.97	0.26	0.32
Propane	5.45	8.38	8.41	1.15	1.07
iso-Butane	0.77	1.03	1.05	0.39	0.36
n-Butane	2.82	3.34	3.52	2.05	1.78
Neopentane	0.00	0.00	0.00	0.00	0.00
iso-Pentane	1.05	0.81	0.91	1.40	1.26
n-Pentane	1.70	1.06	1.21	2.63	2.42
Hexanes	2.34	0.62	0.46	4.87	5.12
Heptanes	3.59	0.45	0.56	8.19	8.06
Octanes	3.43	0.15	0.16	8.24	8.25
Nonanes	2.59	0.02	0.04	6.35	6.36
Decanes	2.21	0.00	0.01	5.44	5.45
Undecanes	1.89	0.00	0.00	4.66	4.68
Dodecanes	1.67	0.00	0.00	4.12	4.14
Tridecanes	1.59	0.00	0.00	3.91	3.93
Tetradecanes	1.44	0.00	0.00	3.56	3.57
Pentadecanes	1.37	0.00	0.00	3.37	3.38
Hexadecanes	1.03	0.00	0.00	2.55	2.56
Heptadecanes	1.05	0.00	0.00	2.58	2.59
Octadecanes	0.91	0.00	0.00	2.24	2.25
Nonadecanes	0.95	0.00	0.00	2.34	2.35
Eicosanes	0.74	0.00	0.00	1.82	1.83
C21	0.67	0.00	0.00	1.65	1.65
C22	0.62	0.00	0.00	1.53	1.54
C23	0.56	0.00	0.00	1.38	1.39
C24	0.52	0.00	0.00	1.27	1.28
C25	0.47	0.00	0.00	1.17	1.17
C26	0.46	0.00	0.00	1.14	1.14
C27	0.43	0.00	0.00	1.07	1.07
C28	0.42	0.00	0.00	1.04	1.04
C29	0.42	0.00	0.00	1.04	1.05
C30	0.42	0.00	0.00	1.03	1.04
C31	0.40	0.00	0.00	0.99	1.00
C32	0.36	0.00	0.00	0.89	0.90
C31	0.31	0.00	0.00	0.77	0.77
C34	0.29	0.00	0.00	0.70	0.71
C35	0.27	0.00	0.00	0.66	0.67
C36	4.64	0.00	0.00	11.45	11.50
	MW	25.46	25.70	241.1	241.6
	Density	1.099	1.093	879.0	886.0

Figure 35. The hydrocarbon composition of live oil.

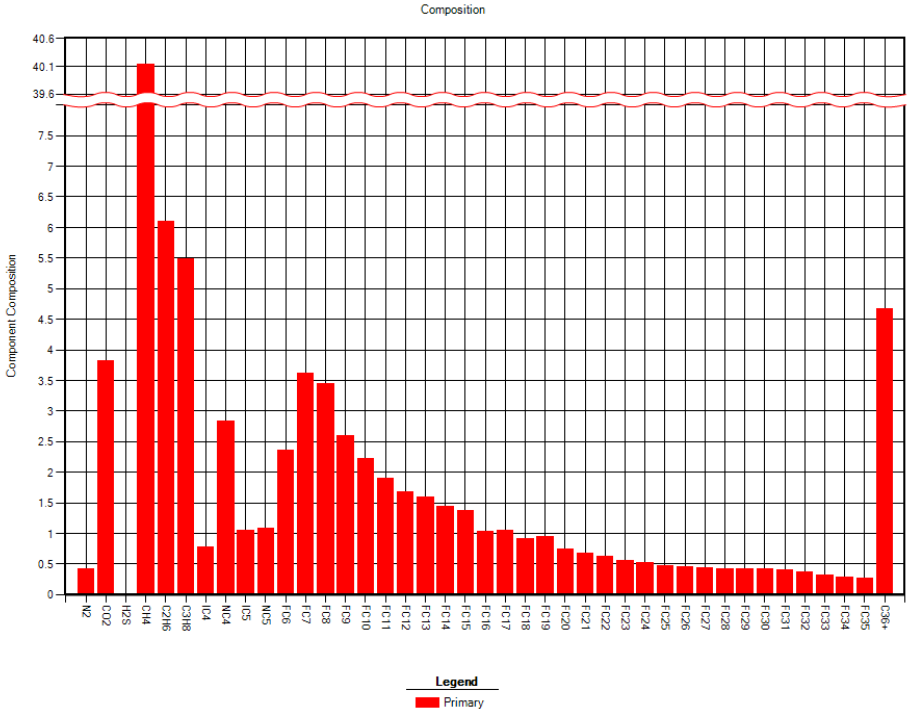

Figure 36. Column hydrocarbon composition.

Three graphs were obtained with respect to the molecular weight of the composition and are shown below:

- Capillary pressure vs. Molecular weight
- Critical temperature vs. Molecular weight
- Acentric factor vs. Molecular weight

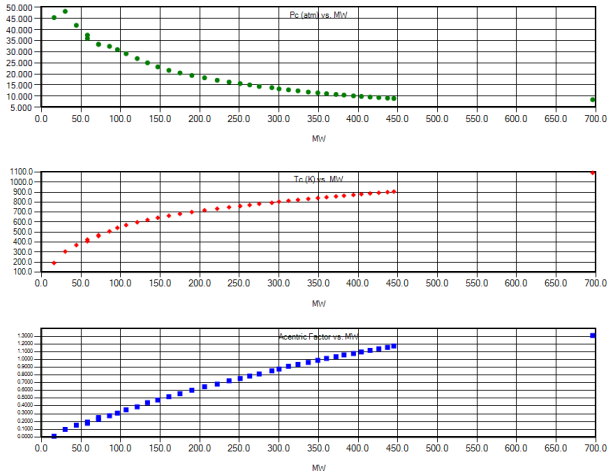

Figure 37. Capillary pressure, Critical temperature, and Acentric factor vs. Molecular weight.

The first graph shows that as molecular weight increases, the capillary pressure decreases due to the decreasing trend. This is useful to understand fluid behavior in the reservoir. The second graph demonstrates an increasing trend which implies that high critical temperatures belong to components with higher molecular weight. The third graph of an increasing trend suggests that heavy molecules have higher acentric factor values which can be used in the equation of state computations for the non-ideal behavior of the gas in the composition.

The two figures presented below show the generated graphs of phase behavior. This is crucial to identify the bubble point pressure and temperature, critical point and dew point components. It is obvious that inside the curve, both gas and liquid states coexist and the critical point to have a point of a maximum such a coexistence. It is approximately at 900F and 3000 psia according to the WinProp model.

The first graph illustrates a decreasing trend, indicating that as molecular weight increases, capillary pressure decreases. This relationship is essential for understanding fluid behavior within the reservoir. The second graph exhibits an increasing trend, suggesting that components with higher molecular weights correspond to higher critical temperatures. Similarly, the third graph follows an upward trend, implying that heavier molecules possess higher acentric factor values.

The two figures below present the generated phase behavior graphs, which are critical for identifying key phase equilibrium properties such as bubble point pressure and temperature, the critical point, and dew point components. Within the phase envelope, both gas and liquid phases coexist, with the critical point representing the maximum extent of this coexistence. According to the WinProp model, this occurs at approximately 900°F and 3000 psia.

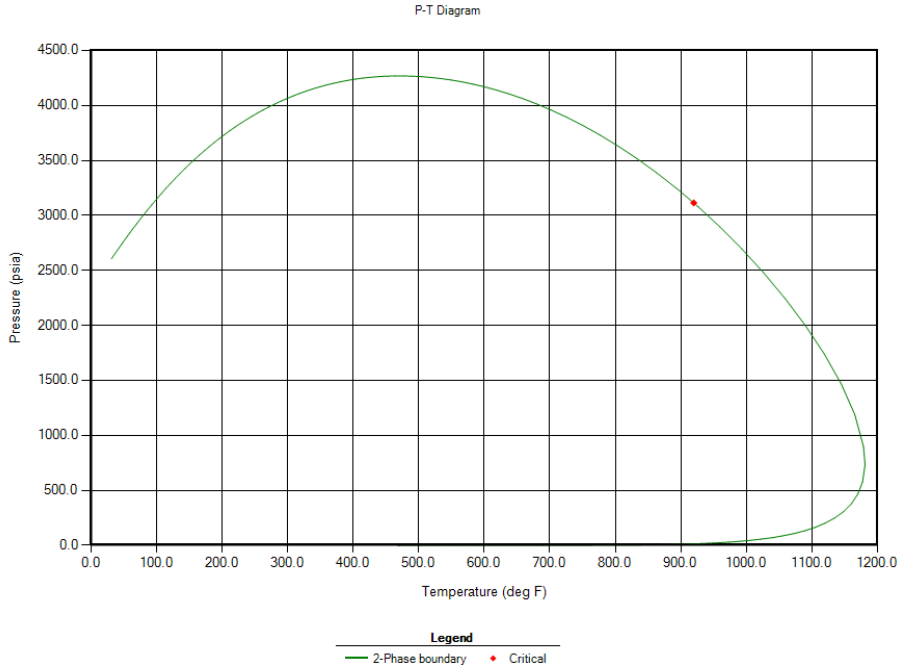

Figure 38. Phase envelope generated in the WinProp software.

The bubble point pressure is approximately 4250 psia (~293 bar) and the temperature is about 450 F which represents the condition when the first bubble from liquid appears.

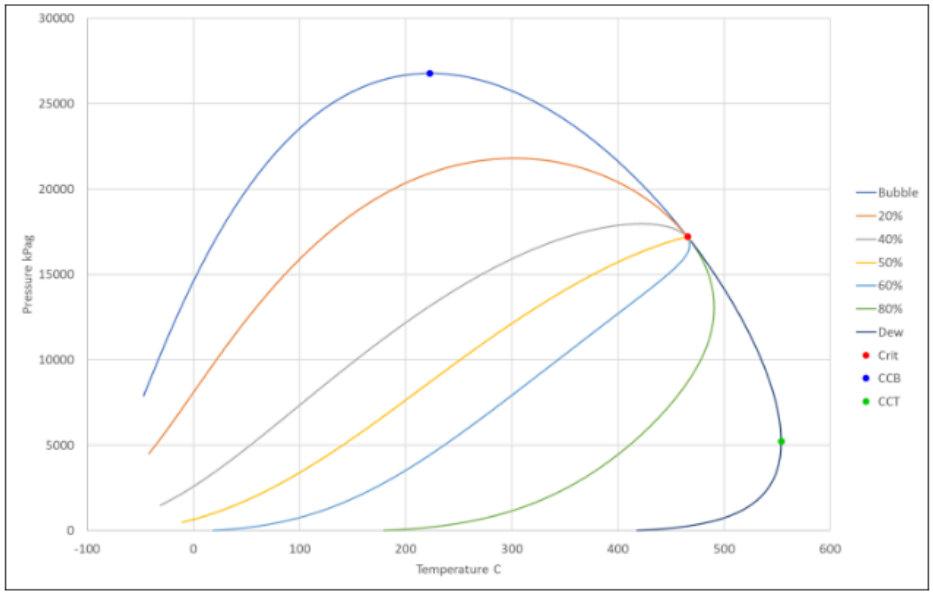

Figure 39. Phase envelope from the source.

Knowing the exact HC composition and constructing phase envelope graph allows us to identify phase transitions and properly classify the reservoir fluid which can further be applied in the reservoir simulation stage.

3.1.3. Reservoir Drive Mechanism

Studying reservoir drive mechanisms tends to be essential in maximizing hydrocarbon recovery by understanding how oil and gas reserves naturally move within the reservoir, which helps optimize recovery strategies. Additionally, identifying and evaluating these mechanisms allows for proper management of reservoir pressure, preventing issues such as early production decline or unwanted water/gas breakthrough.

The Volve oil field exhibits a combination of two drive mechanisms which are water drive and solution gas drive. Major initial production is supported by water drive originating from the aquifer pushing oil towards the producing wells, while solution gas drive involves dissolved gas expanding as pressure drops, helping mobilize the oil.

As a secondary recovery method water injection is implemented. The water injectors are strategically placed in the most productive area with production wells being drilled higher on the structure to delay water breakthrough. Even though the Volve field initially utilized water injection for pressure maintenance, still there is a potential for applying EOR methods like WAG injection or surfactant-polymer flooding as well.

Generally, in order to design the effective EOR project for the Volve field, several important factors such as reservoir characteristics, hydrocarbon composition, injection design, as well as previous successful implementation cases should be studied. In terms of earlier implementation cases, the following table shows the previous experience with EOR design for several neighboring fields in the North Sea with varying degrees of success.

Table 11. EOR methods used in the analogous fields.

Field	EOR method used	Result	Additional Notes
Ekofisk	Water - Alternating	Partially	Initially faced challenges with injectivity

	- Gas (WAG) Injection	successful	and reservoir heterogeneities that affected the effectiveness of recovery.
Snorre	Foam - Assisted WAG (FAWAG) Injection	Successful	Improved sweep efficiency and incremental oil recovery. However, experienced issues with injectivity and injection system monitoring.
Magnus, Statfjord	Miscible Gas Injection	Successful	Successfully increased oil recovery, demonstrating the effectiveness of WAG in certain reservoir conditions. Additional CO_2 injection is considered for further improvement.
Gullfaks, Oseberg	WAG Injection	Successful	Increased oil recovery. Ongoing evaluations for further EOR applications.

Based on the analyzed information, several comments and recommendations can be applied. Firstly, water-alternating-gas (WAG) injection has shown success in fields like Gullfaks and Oseberg. However, challenges in fields such as Ekofisk highlight the need for careful assessment of reservoir conditions. Secondly, foam-assisted WAG (FAWAG) injection demonstrated success in the Snorre field, improving sweep efficiency by mitigating gas channeling issues. The next one is miscible gas injection which was successfully applied in the Magnus and Statfjord fields. This involved injecting gas that mixes with the oil, reducing its viscosity and enhancing recovery.

Given the Volve field's parameters such as its heterogeneous sandstone reservoir in the Hugin Formation at depths of 2700 to 3200 meters, implementing WAG injection could be a viable EOR strategy. WAG involves a cyclic injection of alternating water followed by gas. The

main purpose of WAG injection is to improve both macroscopic and microscopic sweep efficiency, thereby mobilizing residual oil from the pores. The sandstone composition of the reservoir, as well as depth are quite conducive to WAG, as these methods are often effective in similar geological settings. Moreover, this method helps maintain nearly initial high pressure, and slow down the water/gas breakthrough.

There are several recommendations that can be considered when designing EOR. First of all, a comprehensive assessment should be conducted to evaluate the technical and economic viability of WAG in the Volve field, considering factors like injection costs, injection infrastructure, and potential recovery rates. Additionally, a pilot project should be implemented first to monitor the performance of this method under actual reservoir conditions, allowing for adjustments and optimization before full-scale implementation.

In conclusion, while the Volve field has not previously employed EOR methods, the application of WAG presents a promising opportunity to enhance oil recovery. Analyzing previous experiences of nearby fields can help selecting and implementing the most suitable EOR techniques for Volve.

3.1.4. Well Test Analysis. Pressure Buildup Analysis. Well performance

Well testing is another critical part in evaluating the dynamic characteristics of the Volve field's reservoir. This section covers the analysis of pressure data obtained from well tests, including pressure buildup and drawdown tests.

Pressure transient analysis was conducted to understand reservoir behavior and to estimate reservoir properties including permeability, skin factor, and reservoir boundaries. A series of pressure drawdown and buildup tests were conducted after completing the initial wells. Pressure data was collected from the downhole gauges, and the analysis was performed using PTA software such as Saphir or KAPPA [3]. These tests confirmed high permeability in the Hugin Formation, aligning with well productivity and fluid flow characteristics. The average permeability was determined to be 1000 millidarcies, indicating good flow properties in most parts of the reservoir, however, showing some insignificant variations due to local shale barriers. Moreover, the tests were performed to measure reservoir pressure and evaluate the way

formation responds after shutting in the well [2]. Reservoir pressure measurements indicated that the initial pressure was about 340 bar, and it dropped progressively during production, confirming the significance of using pressure maintenance methods such as water injection [6]. Additionally, the tests indicated strong fluid inflow performance, with some tests showing quite high flow rates reaching up to 10 000 bbl/day under favorable reservoir conditions. The skin factor showed comparatively low value, meaning that the wells experienced minimal damage during drilling and completion, allowing them to produce efficiently.

There were conducted one drill-stem test in the Sleipner and Hugin formations through the well 15/9-19A as well as DST as a set of 3 tests:

- Test 1 - Zone 1 - Water test - Sleipner formation
- Test 2&3 - Zone 2A2B - Commingled test - Hugin formation

These tests were conducted in order to yield data about some reservoir properties such as permeability, skin factor, initial pressure and the minimum connected volume value (Ri).

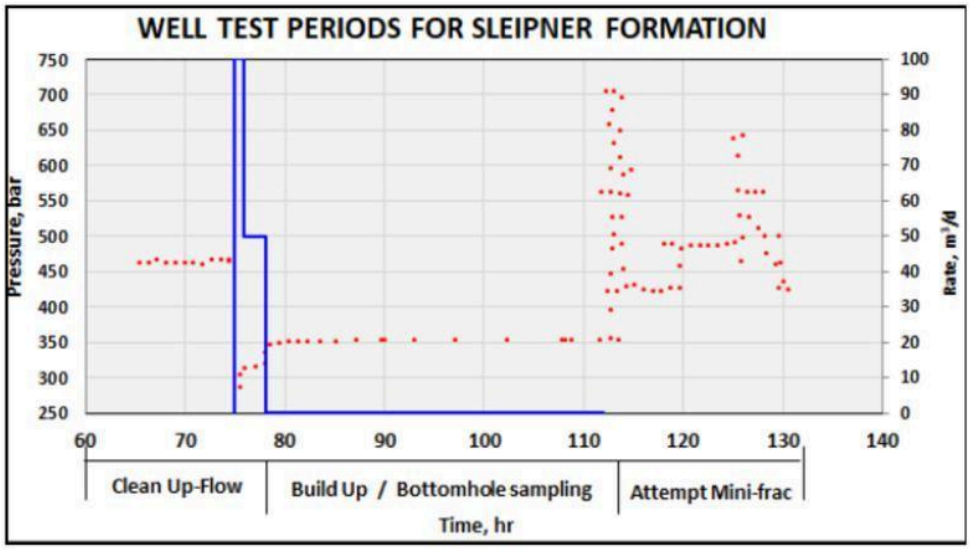

Figure 40. Identified periods for Sleipner formation.

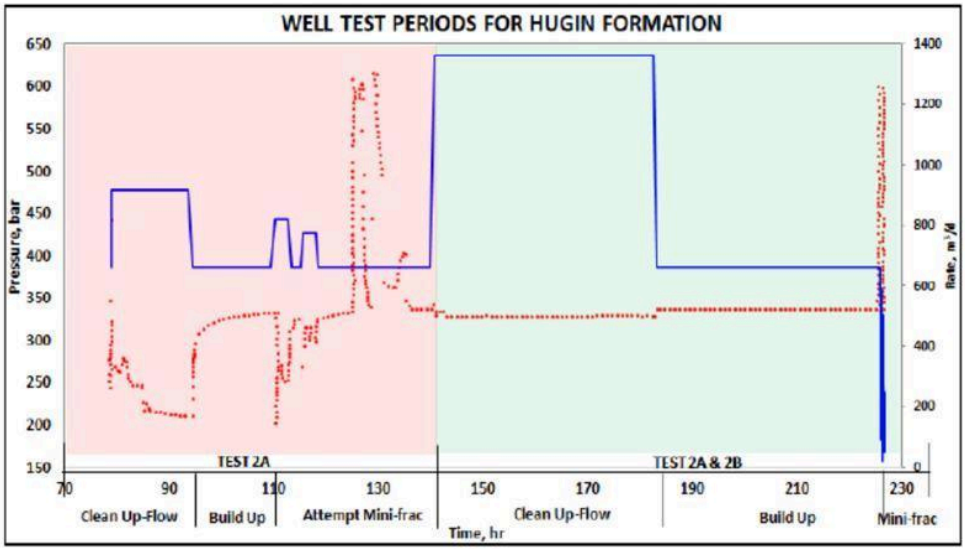

Figure 41. Identified periods for Hugin formation

The figures presented above show the well test periods for each of the formations discovered in this section which is necessary for further analysis. The graph constructed below is a semi-log plot which allows to calculate permeability and skin factor based on the data provided.

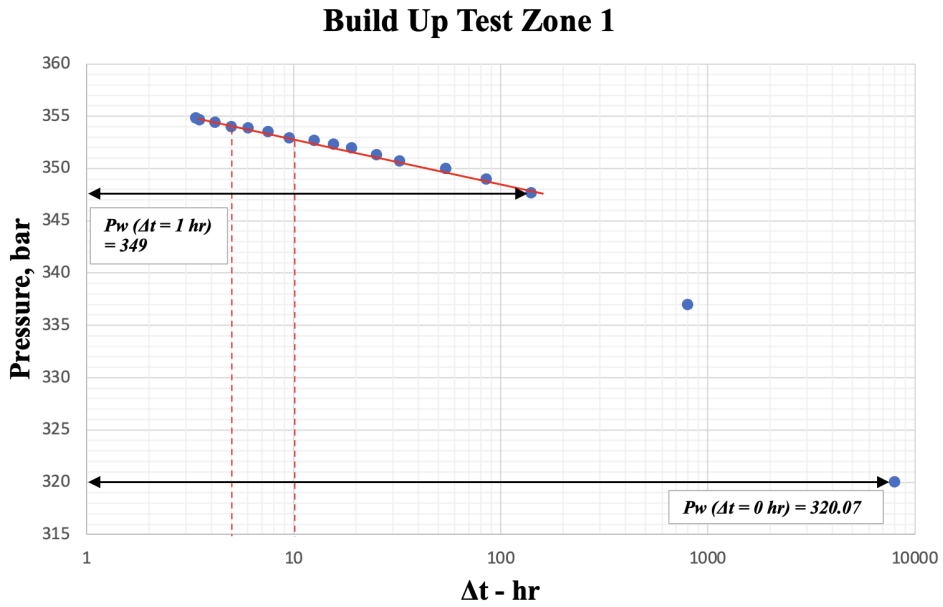

Figure 42. Semi-log Time curve equivalent to the build up Zone 1.

Permeability:

$$m = \frac{353-354}{Log10 - Log5} \tag{4}$$

$$m = -3.3 \frac{psi}{cicle} \tag{5}$$

$$K = \frac{162.6\mu QB}{hm} = \frac{162.6*0.7767*314*1.31}{31.28*3.3} = 503\ mD \tag{6}$$

Skin:

$$t_H(\Delta t = 1hr) = \frac{3+1}{1} = 4 \tag{7}$$

$$P_w(\Delta t = 1hr) = 349\ psi \tag{8}$$

$$S = 1.151 * \left(\frac{(P_w(\Delta t=1hr)) - (P_w(\Delta t=0hr))}{m}\right) - log\left(\frac{k}{\Phi\mu C r_w^2}\right) + 3.23) \tag{9}$$

$$S = 1.151 * \left(\frac{349-320.07}{3.3}\right) - log\left(\frac{503}{0.22*0.7767*(1.3662e^{-5})*4.25^2}\right) + 3.23) = 5.66 \tag{10}$$

The calculated value of Connected Volume Ri is 169 mt.

Secondly, two curves were also constructed for the build up test in the form of log-log plot.

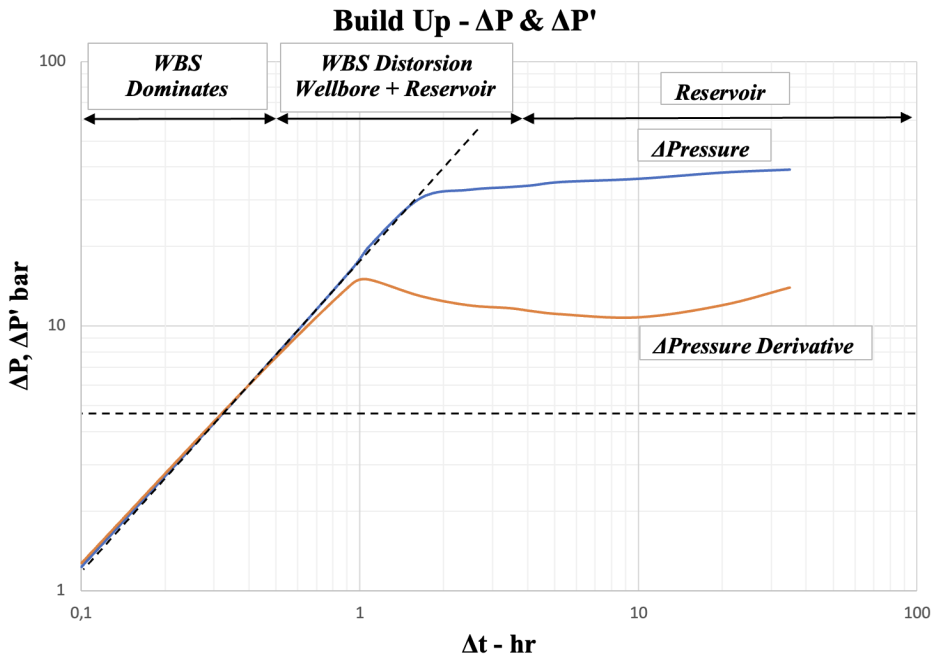

Figure 43. Log-log ΔP & ΔP' equivalent to the buildup Sleipner formation.

The above-provided figure demonstrates that the part with WBS, skin effects and its delta P derivative behavior does not match with a well-defined type of flow called radial flow. In addition, there is an ETR period where constant storage was observed between time intervals of 0.6 to 4 hours which was a result of well geometry, in particular, the damage effect as well as the well effect. As for the MTR period, it shows the presence of semi-IARF close to the well itself. It implies that there is a sealing fault due to the transient that continues to travel till the boundary.

As a result it can be concluded that the model has constant WBS and the skin effects in a semi-infinite acting homogeneous reservoir, sealing fault and low mobility.

Based on the following figure, permeability and skin factor were calculated.

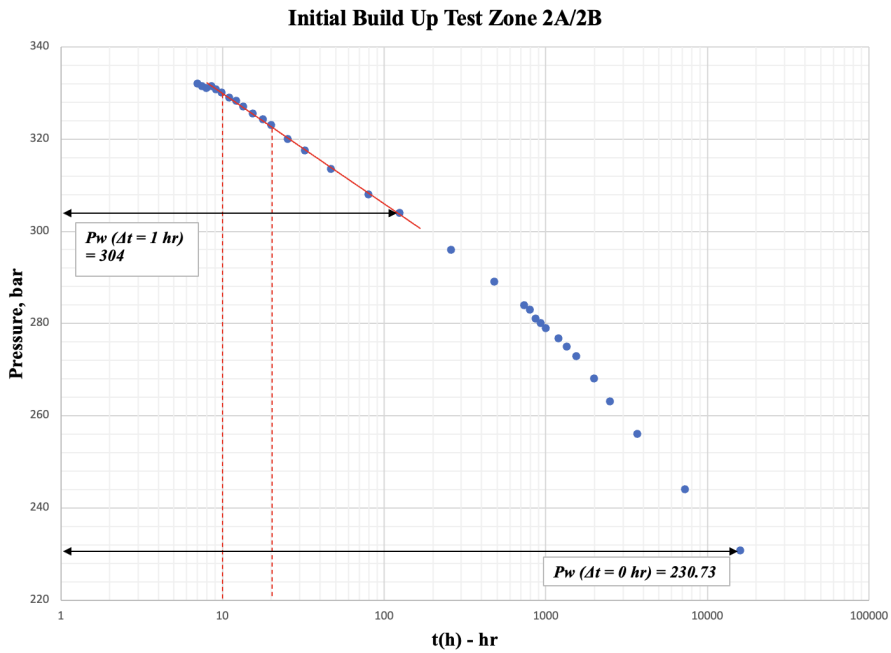

Figure 44. Semi-log Time curve equivalent to the first build up test for Zone 2A/2B.

Permeability

$$m = \frac{322-328}{Log20-Log10} = -19.9\ psi/cycle \tag{11}$$

$$K = \frac{162.6\mu QB}{hm} = \frac{162.6*0.7767*4151*1.31}{31.28*19.9} = 1103\ mD \tag{12}$$

Skin factor

$$t_H(\Delta t = 1hr) = \frac{3+1}{1} = 4 \tag{13}$$

$$P_w(\Delta t = 1hr) = 304\ psi \tag{14}$$

$$S = 1.151 * \left(\frac{(P_w(\Delta t=1hr))-(P_w(\Delta t=0hr))}{m}\right) - log\left(\frac{k}{\Phi\mu C r_w^2}\right) + 3.23) \tag{15}$$

$$S = 1.151 * \left(\frac{304-230.73}{19.9}\right) - log\left(\frac{1103}{0.22*0.7767*(1.3662e^{-5})*4.25^2}\right) + 3.23) = -0.58 \tag{16}$$

In addition, the calculated value of Connected Volume Ri was 480 mt.

The following graph was constructed similarly to the previous figures, but with the focus on the Hugin formation.

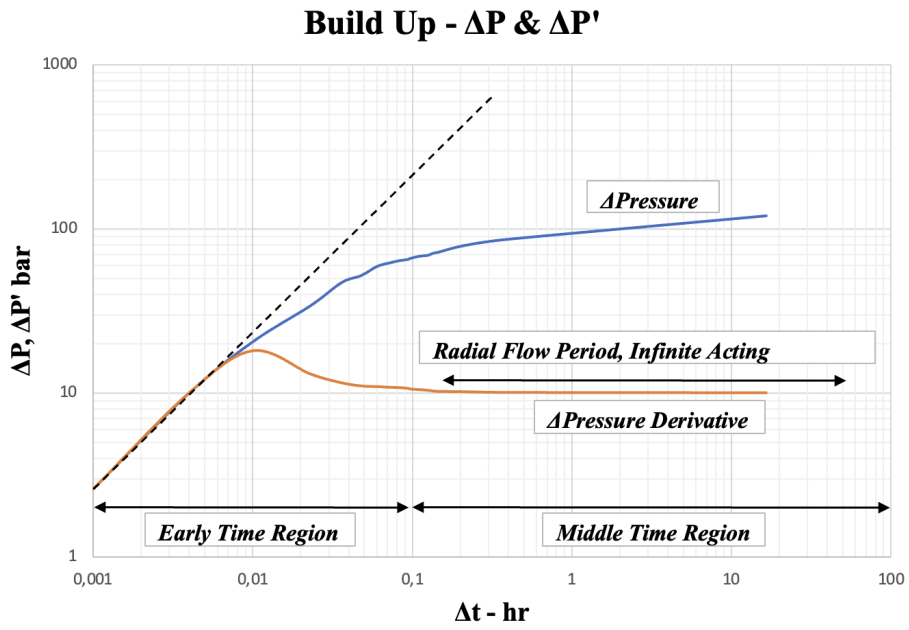

Figure 45. Log-log ΔP & ΔP' curve equivalent to the first build up test of Hugin formation.

The figure above shows that there is a well-defined period of radial flow according to the delta P derivative data points during the period of 0.2 to 0.16 hours. The value was constant at approximately 10 psi.

There is no damage effect due to the small scale of constant storage that was observed during the ETR period within the 0.005 and 0.02 hours. The MTR period reveals that there was also Infinite Acting Radial Flow. In addition, there were no faults observed since the transient does not reach the boundary while travelling. Eventually, the model has minimal constant WBS with IARF, homogeneous behavior and infinite reservoir.

The results show that the permeability in the zone of interest is about 1100 mD which almost matches with the values obtained from the well log interpretations. Moreover, the skin factor being negative means that there was a stimulation procedure to increase the efficiency of oil production.

Chapter IV

4.1. Comparison of Oil Initially In Place (OIIP) Estimation Methods.

In order to validate the reservoir model, three different methods were employed to estimate the initial oil in place (OIIP) for the Volve field including the classical volumetric method, dynamic simulation using ResInsight (simulation models are described below), and official values reported by the Norwegian Offshore Directorate (NPD).

The volumetric method provided an estimate of $122 * 10^6\ bbl$, based on average petrophysical data such as porosity (21%), thickness (300 m), water saturation (30%), and an effective reservoir area of $6000000\ m^2$. This calculation was based on the following formula:

$$N = \frac{\phi * A_o * H_o * (1 - S_w)}{B_{oi}} \tag{17}$$

This method was useful since it assumes homogeneity and static conditions of the reservoir. It was used as an early approximation.

The ResInsight dynamic simulation model yielded an estimate of $138 * 10^6\ bbl$ based on time-step simulation. This method incorporates production history, reservoir pressure behavior, and fluid movement inside the reservoir. So it reflects a dynamic and realistic evaluation of reservoir conditions.

Another method used for the estimation of oil in place was based on the Norwegian Petroleum Directorate (NPD) official report. It showed a value of $118 * 10^6\ bbl$. This method was based on comprehensive geological, seismic, and well data acquired during the field's licensing and operational processes.

The values across all three methods are relatively similar and consistent, with a variation range of approximately 7-8%. This data consistency shows that the results are quite credible and support the use of the ResInsight model as basis for further field development plans. However,

the dynamic model estimate is slightly higher, which could be due to more optimistic sweep efficiency assumptions.

Table 12. Petrophysical parameters.

Petrophysical data	Value	Unit
Thickness	25	m
Oil FVF	1.37	scf/STB
Water saturation	20	%
Porosity	22.13	%
Area	6	km2

Using the values of different parameters such as area, porosity, thickness, water saturation and oil formation volume factor that are tabulated above, it is possible to provide Monte Carlo simulation through the Python coding to demonstrate mean OIIP, P10, P50 and P90 cases.

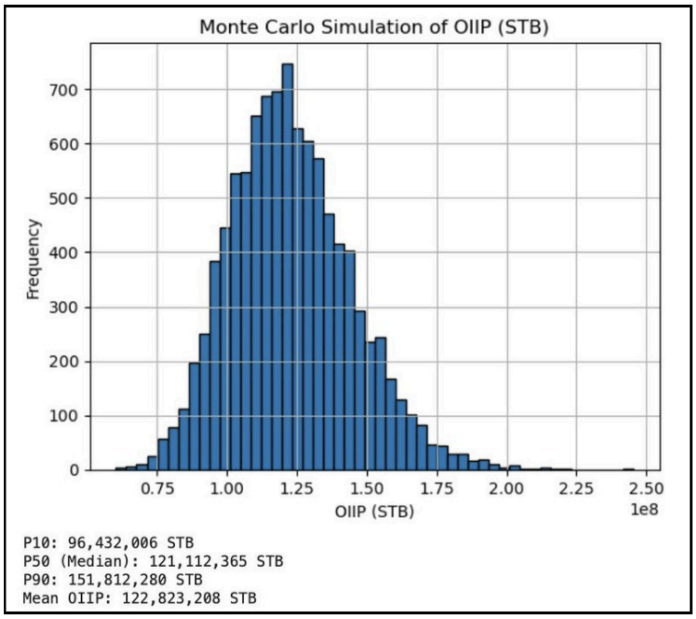

Figure 46. Monte Carlo simulation results.

The figure above shows that the mean OIIP by considering all the parameters on average is about 122 MMSTB which is the result gained through the volumetric method. The P50 case

demonstrates the most likely case which uses the median values and the results is about 121 MMSTB. The P10 case represents the least optimistic situation with 96 MMSTB, while P90 shows the most optimistic case with 152 MMSTB of oil. These numbers help to understand the probability of finding oil in place in such volumes and to avoid underestimating or overestimating the reserves of the field.

4.2. Reservoir Simulation

Accurately simulating and analyzing the dynamic behaviors within a reservoir is a crucial step for optimizing extraction strategies and understanding long-term field development potentials. The purpose of this section is to describe and analyze the reservoir engineering approach used in this field development plan, focusing on the dynamic models and their generated results. In this study, the entire reservoir model for the Volve field was initially constructed in ResInsight.

ResInsight is an open source, 3D visualization and post processing tool for reservoir models and simulations. The system includes various mathematical solvers, seismic data interpretation algorithms, detailed reservoir developer sections, and much more. The user interface is quite easy for utilization due to efficient interpretation of reservoir simulation data with specialized visualizations of properties, faults and wells [6]. Moreover, it enables easy handling of a large amount of data and statistics which is a significant point in FDP. Another benefit is that derived results and computed properties can be directly exported to other softwares such as Eclipse for further simulation analysis and parameter studies. In our case, the major results were exported to Computer Modelling Group (CMG) software. Here is the summary of some other essential features of ResInsight:

- It supports Eclipse, OPM Flow, and other simulation models;
- Advanced 3D visualization capabilities for reservoir data (NNC,MSW, cell edge coloring);
- It uses GNU Octave for additional mathematical modeling and data analysis;
- ResInsight supports geomechanical ABAQUS simulations including the assessment of rock mechanics and deformation properties.

After constructing the complete reservoir model in ResInsight, the most productive area of the Volve field was identified and exported to CMG (Computer Modelling Group) software for more detailed reservoir simulation analysis. This decision was made to leverage CMG's advanced dynamic simulation capabilities for predicting reservoir behavior and hydrocarbon production. In CMG, reservoir simulation was conducted using a combination of historical production data, pressure performance data, and fluid property models to forecast well and field performance. This included the use of PVT data for accurate fluid phase behavior and relative permeability curves for modeling multiphase flow.

Reservoir characterization. Setting geological grid and framework for the ResInsight model.

In order to create a dynamic model, to simulate fluid flow, and predict future production, the following settings were performed in the ResInsight software. The framework for the model consists of the interpreted and depth-converted top and bottom reservoir grid. 14 reservoir zones have been established with the specific outlines generated in ArcGIS. In this model, the outer limiting faults and internal faults were modeled and imported into ResInsight as well. In total, there are 11 active faults in the reservoir model.

The model has dimensions of 108*100*63, with a total cell count of 680 400 and 183 545 active cells. The grid size is 50*50 m with 3 m of thickness. This model can be seen in the following figure:

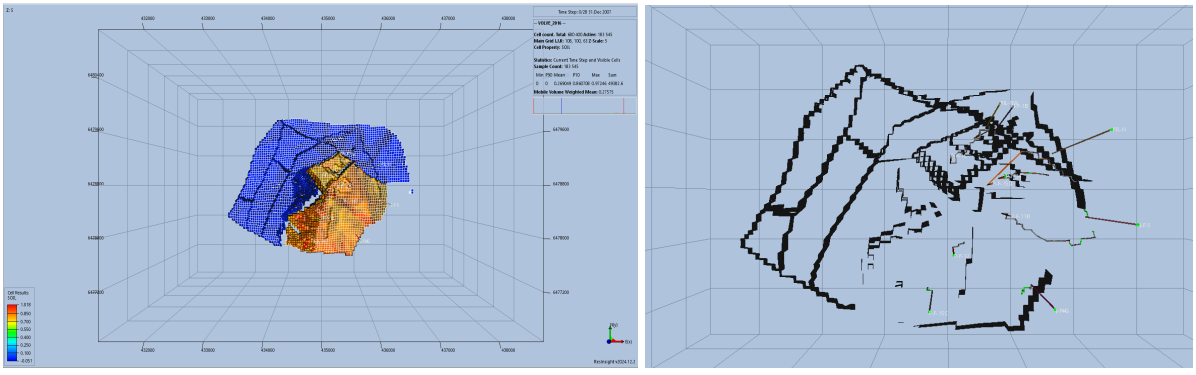

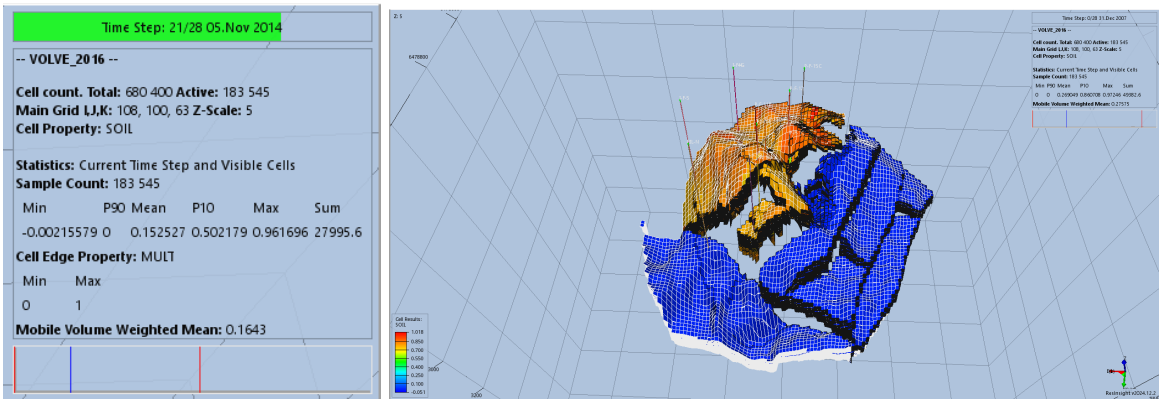

Figure 47. The dynamic reservoir model from the ResInsight.

The initial conditions for the reservoir were set according to the reservoir parameters mentioned in the previous section (1.2.1).

In total 6 production (P-F-15D, P-F-5, P-F-14, P-F-11B, P-F-12, P-F-15C) and 4 injection (I-1, I-2, I-3, I-4) wells were placed across the whole framework based on the well top trajectories given in the official Equinor's report [3]. Table 1 shows the main information on the wells, including the water injection and the oil production wells, entered into the Volve reservoir simulation model. All the wells are inclined, and the maximum inclination value for each of the wells can be seen as well. Moreover, 3 of the 6 production wells, particularly P-F-11B, P-F-14, and P-F-15D are considered as horizontal wells. In total, the Volve reservoir model consists of 10 active objects - 4 water injection and 6 oil production wells.

Table 13. Summary of well data.

Well name	**Well Type (Fluid Type)**	**Operation**		**Total Vertical Depth (TVD), m**	**Measured depth (MD), m**	**Maximum degree of well inclination**
		Starting day	**Ending day**			
I-1	Injector	2028-01-01	2033-05-16	3210.0	3185.2	30.0
I-2	Injector	2028-0101	2033-01-01	3036.0	3230.1	31.0

I-3	Injector	2028-0101	2033-09-15	3144.1	3307.5	20.0
I-4	Injector	2028-0101	2033-08-04	3027.7	4437.9	151.0
P-F-5	Producer	2025-01-01	2033-04-28	3012.8	3013.5	16.5
P-F-11B	Producer	2029-01-01	2033-09-20	3038.2	4285.2	172.7
P-F-12	Producer	2025-01-01	2033-09-24	2890.1	2971.8	11.6
P-F-14	Producer	2025-01-01	2033-06-27	3044.7	3612.4	168.2
P-F-15C	Producer	2025-01-01	2033-10-21	2925.3	2968.0	7.4
P-F-15D	Producer	2028-01-01	2033-07-27	3043.6	4238.2	166.8

Analysis of simulation results of the Volve reservoir model in ResInsight.

The analysis focuses on oil production trends, bottom-hole pressure (BHP), water production, and gas-oil ratio (GOR) over time. These parameters were mainly studied and analyzed to cover the following points:

- Evaluating oil recovery performance over 8-10 production periods.
- Assessing reservoir pressure behavior and the impact of constraints on BHP.
- Identifying water breakthroughs and its impact on oil production.

The following graphs compare the simulation results of yearly oil recovery, water cut, and additionally bottom-hole pressure maintenance for the Volve field.

The BHP trends for each well showed quite significant variations in pressure management over the production period. For instance, for P-F-12 and P-F-14, there was a continuous decrease. BHP fluctuated between 250 - 350 bars over time. These periodic drops might possibly be due to reservoir pressure depletion or some operational constraints. In contrast, P-F-11B and P-F-15D revealed sudden pressure drop and recovery. Particularly, BHP showed an

initial flatline of around 0 bar before sudden production start in 2028-2029. This might indicate well shut-in or some issues related to drilling delay. Once production started, pressure stabilized around 300 bar. Moreover, pressure after 3-5 years steadily increased, indicating pressure maintenance works, particularly water injection support.

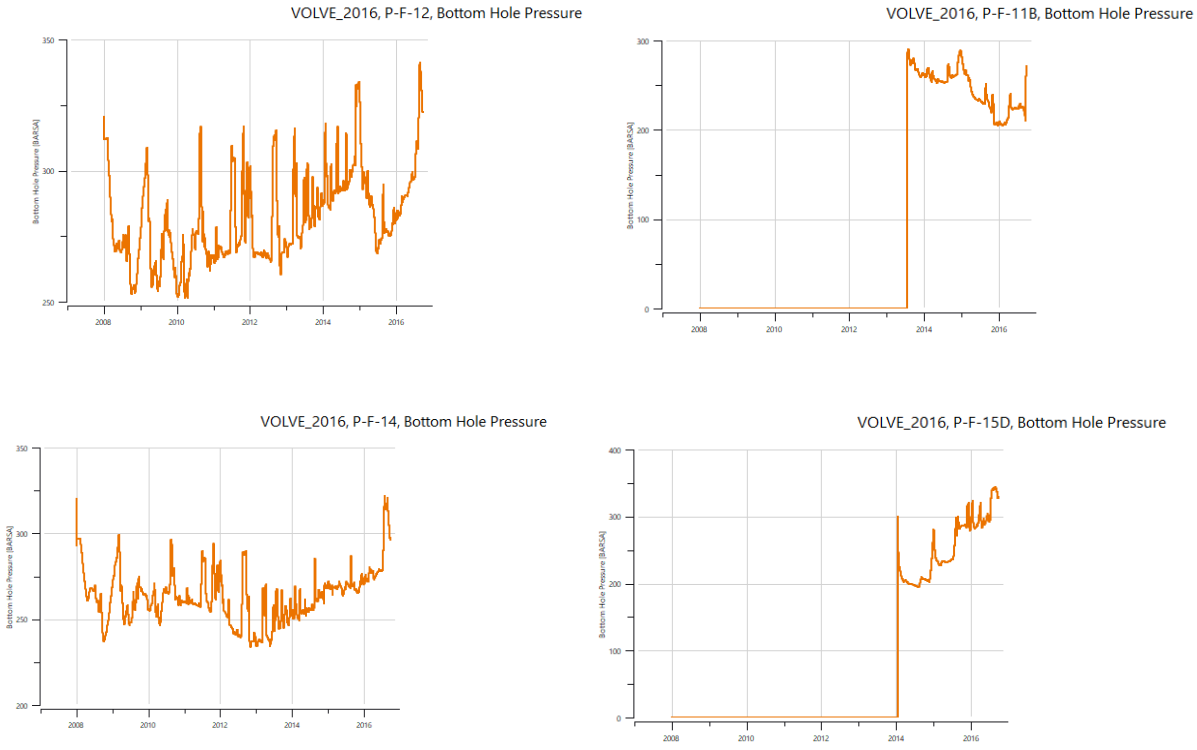

Figure 48. BHP total for producer wells.

Another important point is water production which increased significantly after 2029 across all wells. Based on the given trend, majorly P-F-12, P-F-14, and P-F-15D production wells exhibited a steady increase in water cut. While for the P-F-11B production well, the value for water production rose sharply after 2031 which resulted in the corresponding decline of oil production. This trend suggests early water breakthroughs.

Moreover, another interesting observation is the behavior in P-F-15D being consistent with delayed water breakthrough. Possible reasons might be well positioning, completion strategy, as well as proceeding injection processes. In contrast, wells like P-F-12 and P-F-14

likely experienced early contact with the aquifer or water injection, leading to smoother, earlier water production trends.

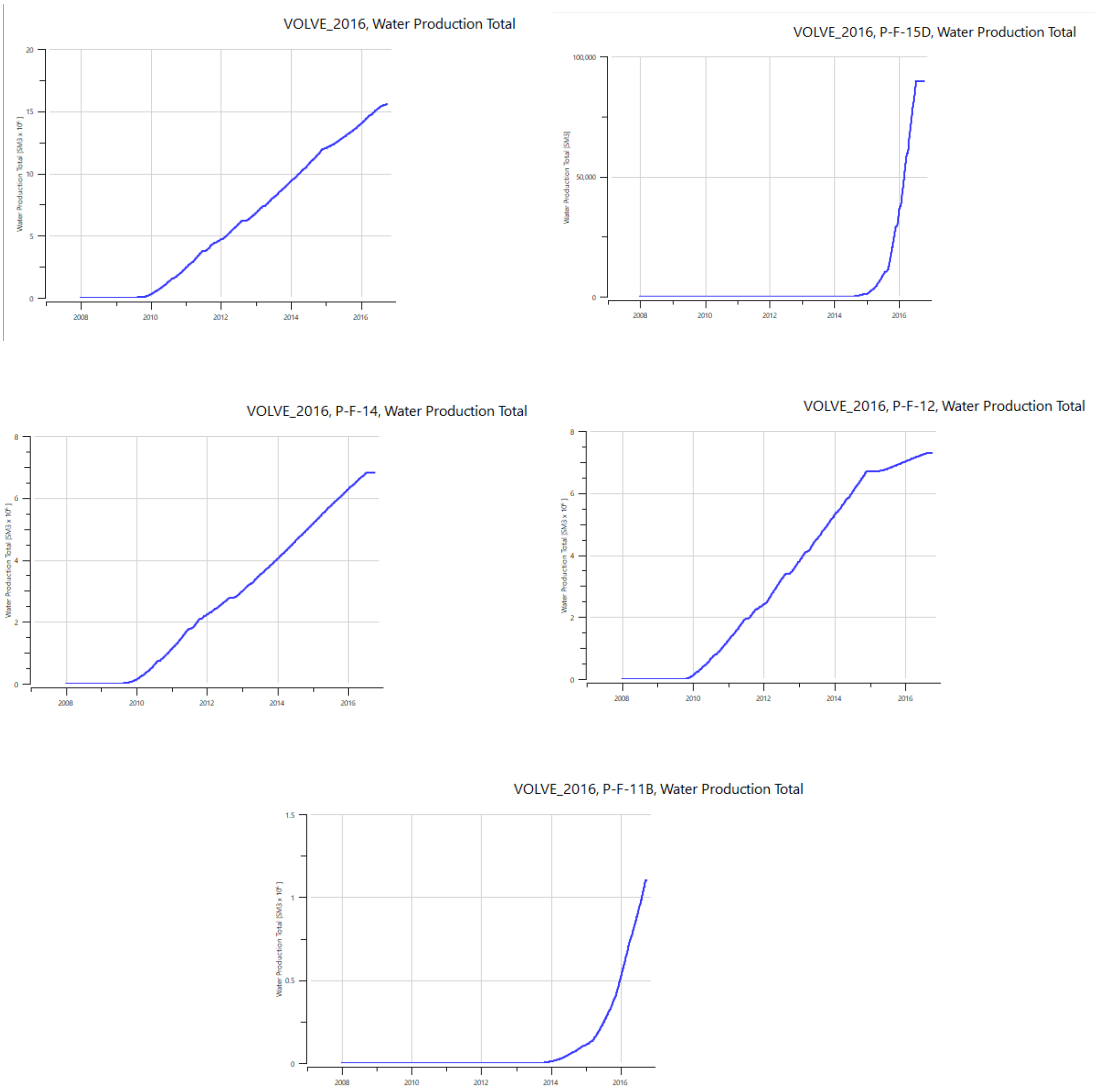

Figure 49. Water production total for producer wells.

The last but not least is the cumulative oil production graphs, as well as oil recovery. At the beginning of production history, there was quite rapid and extensive initial production. Comparing all the production wells, P-F-12 and P-F-14 reached faster and higher ultimate recovery compared to P-F-11B and P-F-15D. Particularly, P-F-15D exhibited a delayed production response, meaning it had a bit different reservoir drainage pattern. Rapid increase in production was followed by stabilization from 2014 till 2016.

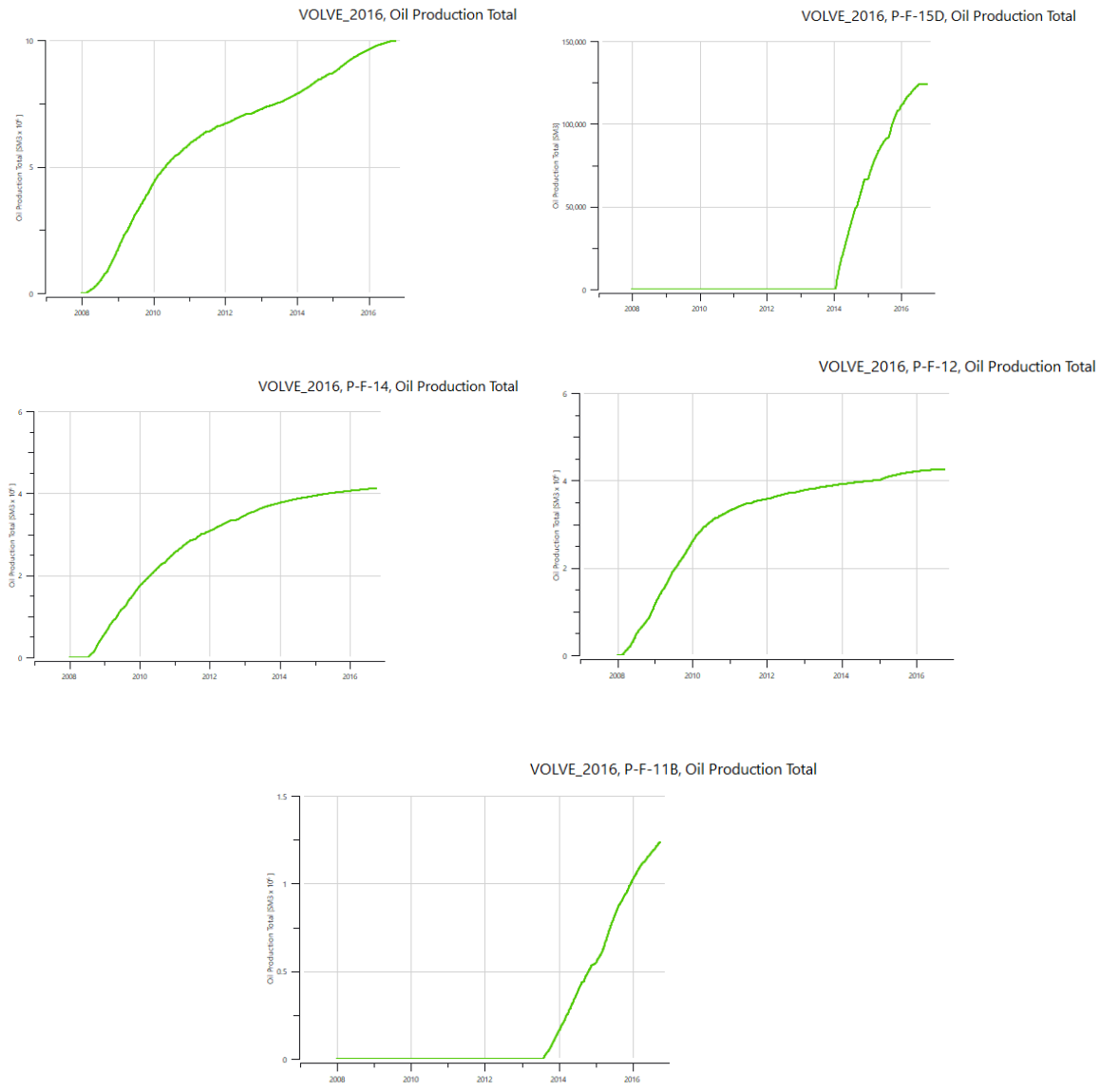

Figure 50. Oil production total for producer wells.

Additionally, across the whole period of production, the GOR profile was monitored which remained relatively stable. It showed values in between 100-150 m^3/m^3, followed by some sudden drops (indicating well shut-ins or operational disruptions). Generally, there was no significant gas breakthrough observed.

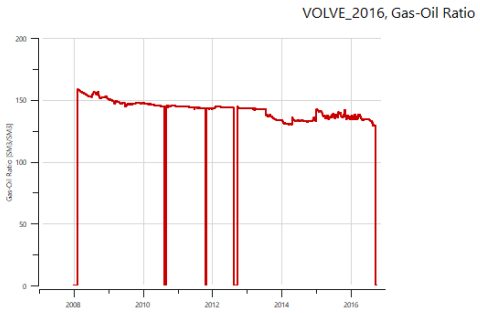

Figure 51. GOR total for producer wells.

The ResInsight simulation results indicate that initial production was strong, however, it declined sharply after 2029 due to reservoir depletion and water breakthrough. Water breakthrough in the Volve field is primarily attributed to the reservoir characteristics of the Hugin Formation. It tends to consist of interbedded sandstone and shale layers leading to quite high heterogeneity and corresponding varied permeability distribution. This geological complexity creates preferential flow paths that can cause injected water to bypass significant volumes of oil. Moreover, the moderate reservoir thickness might also contribute to gravity override, where the denser injected water migrates along the lower layers, reaching the base of producers ahead of the intended sweep front. However, with proper intervention, the field can achieve higher ultimate recovery and increase economic production.

Reservoir simulation analysis performed in the CMG software. Setting initial conditions for the reservoir model.

For the detailed reservoir simulation analysis, the most productive area from the whole field was chosen for the detailed production studies. To create a model in CMG, a specific grid with 6 layers representing 6 main formations of the reservoir with their related properties (given in detail in the next section) were constructed.

Table 14. Grid settings for CMG model.

Grid type	Cartesian	
Number of grid blocks		

I	45	* 50
J	35	* 50
K	6	

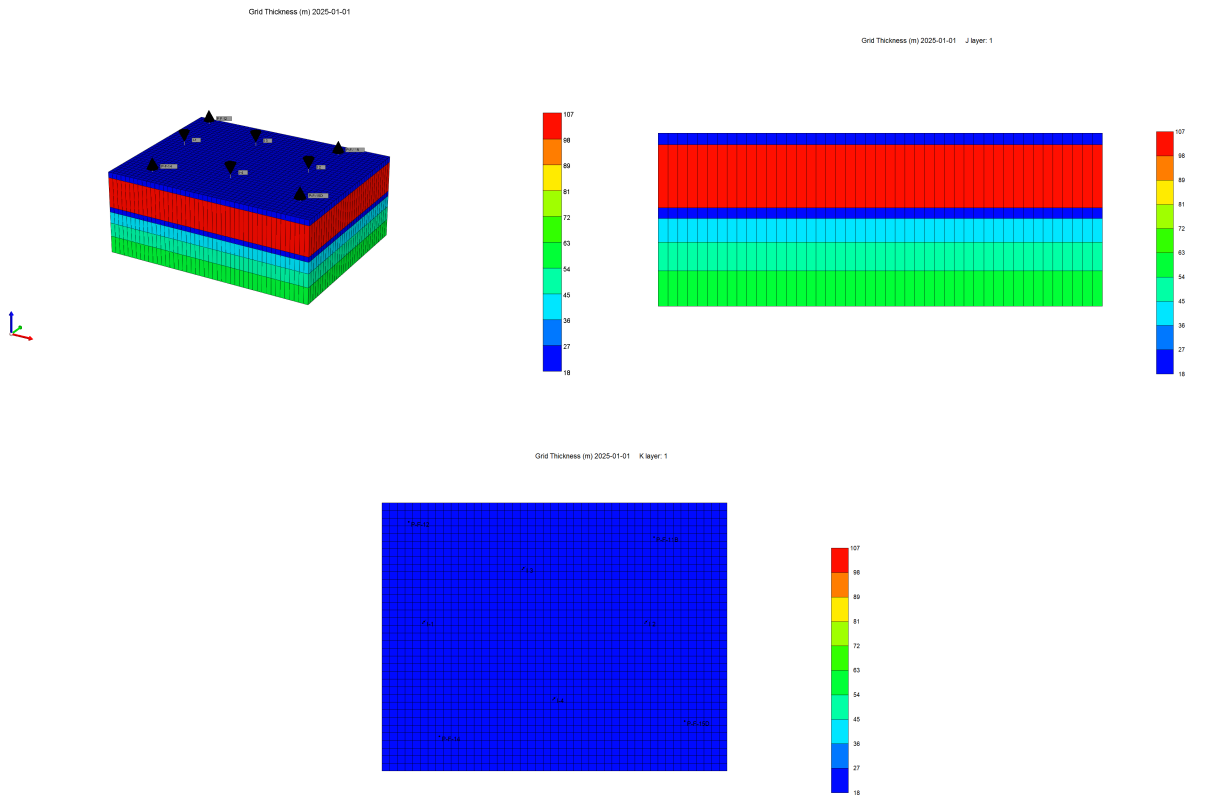

Figure 52. The dynamic reservoir model from the CMG.

The Volve field reservoir is primarily composed of Jurassic-age sandstones with varying degrees of heterogeneity. Taking into consideration this inconsistency in formations, the following key petrophysical parameters for 6 main formations were used in the models:

Table 15. Key petrophysical parameters used for the reservoir characterization in the simulation models.

Formation	**Thickness (m)**	**Porosity (%)**	**Permeability (mD)**	**Water saturation**

Heather	19.7	20.9	1000	0.374
Hugin	107.4	19.8	1200	0.363
Upper Hugin	17.9	20.8	1126	0.414
Middle Hugin	40.5	19.3	1152	0.333
Lower Hugin	49	17.2	1147	0.369
Sleipner	60	19.6	1111	0.936

The PVT model was developed using WinProp software to characterize the phase behavior of reservoir fluids. Additionally, initial conditions such as reservoir temperature, pressure, rock compressibility, and rock-fluid interaction parameters, including relative permeability and capillary pressure curves, were defined. These parameters were carefully calibrated using different correlations to match field conditions and ensure that the simulation output is realistic as possible.

All the assumptions were made to simplify the model while maintaining a realistic representation of reservoir behavior taking into consideration numbers from company reports.

After setting all the assumptions and necessary model conditions, the particular well configurations and constraints were specified. To set the well placement configuration, a dedicated well placement study was conducted to assess the effect of various injection-production strategies on oil recovery efficiency and pressure maintenance. Since the simulation domain was limited to the most productive sector of the reservoir, multiple scenarios were tested, varying injector and producer locations, and operational constraints. Out of all the configurations, two primary scenarios were analyzed in detail due to their superior performance in early simulations:

- **Scenario 1 - Centralized Injection Strategy:** Single injector placed at the geometric center of the reservoir grid surrounded by 4 producers at the chosen production area (P-F-11B, P-F-12, P-F-14, P-F-15D). The central injection strategy was designed to create and analyze a radial pressure sweep, ensuring efficient displacement of oil toward the

peripheral producers. Another point is that this scenario benefits from minimal injection complexity and lower drilling costs.

- **Scenario 2 - Distributed Injection Strategy:** 4 injectors placed in a distributed pattern to ensure the most profitable, uniform, and controlled sweep efficiency + 4 producers at the chosen production area (P-F-11B, P-F-12, P-F-14, P-F-15D). This design significantly improves sweep efficiency and breakthrough control, and minimizes areas of bypassed oil. Like
- **Production Constraints:** Fixed bottom-hole pressure limit at producing wells.
- **Injection Constraints:** Fixed injection rate or pressure limit for injectors.

This sensitivity analysis was performed to evaluate additional configurations, including water injection, vertical-to-horizontal injector combinations, and pattern flooding designs.

Another important factor is well perforation of injection wells. All injectors were tested under two different perforation scenarios to determine the optimal configuration. In the first case, perforations were made across all six layers, while in the second case, only the Hugin, Middle Hugin, and Lower Hugin formations (most productive) were perforated. The recommendations and final decision can be seen in the table below:

Table 16. Perforation recommendations.

Perforating only the most productive zones		**Perforating all 6 layers**		**Final recommendation**
Advantages	**Disadvantages**	**Advantages**	**Disadvantages**	Hugin, Middle Hugin, and Lower Hugin formations have significantly higher
Maximizes injection efficiency by targeting the most permeable	Limits injectivity if 3 layers have lower overall permeability than the full 6	Maximizes injectivity by utilizing all available flow paths.	Less control over injection distribution, meaning water might flow	

and productive layers.	layers combined together.		preferentially into the most permeable zones and bypass less permeable formations.	permeability and contribute most of the production. That is why perforating only these 3 zones is more efficient.
Reduces early water breakthrough.	Might result in uneven vertical sweep efficiency.	Reduces the risk of interlayer crossflow in case permeability variations are not large.	Risk of early breakthrough.	
Minimizes unwanted water injection into non-effective layers.		More uniform pressure support across the whole Volve reservoir.	Inefficient sweep if some layers contribute more to injection but not to production.	
Improves sweep efficiency since these layers have good lateral continuity and high permeability.				

The analysis indicated that perforating 3 major productive layers such as Hugin, Middle Hugin, and Lower Hugin formations would yield better sweep efficiency.

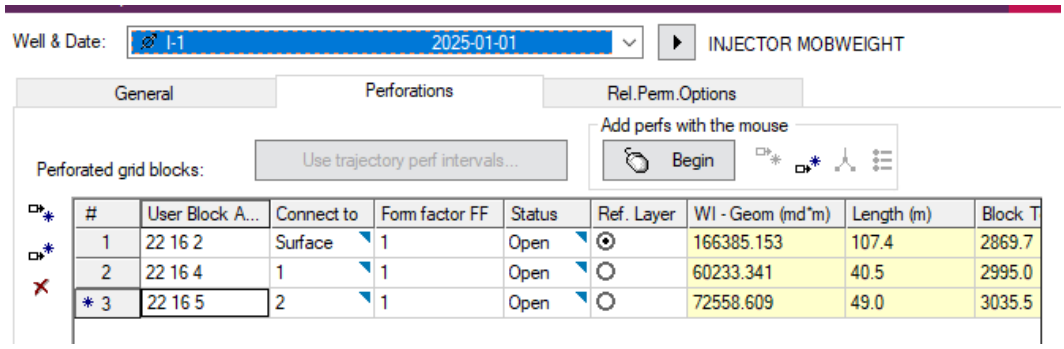

Figure 53. The injectors' perforation settings.

#	Parameter	Limit/Mode	Value	Action	F
* 1	BHP bottom hole pressure	MAX	32760 kPa	CONT REPEAT	

Figure 54. Constraints for the injection wells.

#	Parameter	Limit/Mode	Value	Action	F
* 1	BHP bottom hole pressure	MIN	27300 kPa	CONT REPEAT	
2	STO surface oil rate	MAX	10000 m3/day	CONT REPEAT	

#	Constraint	Parameter	Limit/Mode	Value	Action	Frequency
1	OPERATE	BHP bottom hole pressure	MIN	21000 kPa	CONT	
* 2	OPERATE	STO surface oil rate	MAX	40000 m3/day	CONT	
	select new					

Figure 55. Constraints for the production wells.

Analysis of simulation results of the Volve reservoir model in CMG (injection scenarios).

The analysis focuses on oil recovery, bottom-hole pressure (BHP) trends, water cut percentages, sweep efficiency, and breakthrough time. The following figures compare the simulation results of yearly oil recovery, water cut, and additionally pressure maintenance trends for the Volve field.

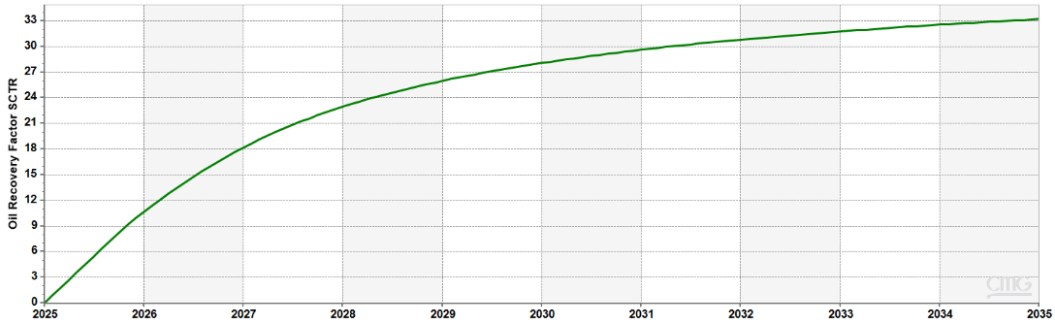

Figure 56. Oil recovery for the entire field (1 injector at the center).

The oil recovery factor for the single-injector scenario revealed a steady increase from 2025, reaching approximately 33% after 10 years of production. The curve increased rapidly in the early years, indicating efficient hydrocarbon displacement, but the slope gradually flattened starting from 2029, suggesting diminishing returns. This plateau effect may result from pressure depletion, reduced injectivity, or approaching residual oil saturation as well.

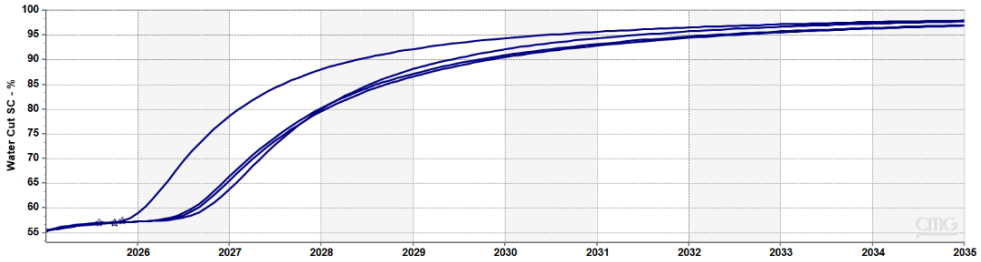

Figure 57. Water cut for 4 production wells (1 injector at the center).

The water cut trend showed a sharp increase starting around 2026, indicating early water breakthrough. By 2028, water cut reaches approximately 80–90%, and after 2030, it stabilizes near 98–100%, suggesting high water and declining oil production. The rapid increase highlighted potential water coning or channeling effects. Further analysis indicated the need in modifying the number of injection wells and strategies that delay water breakthrough.

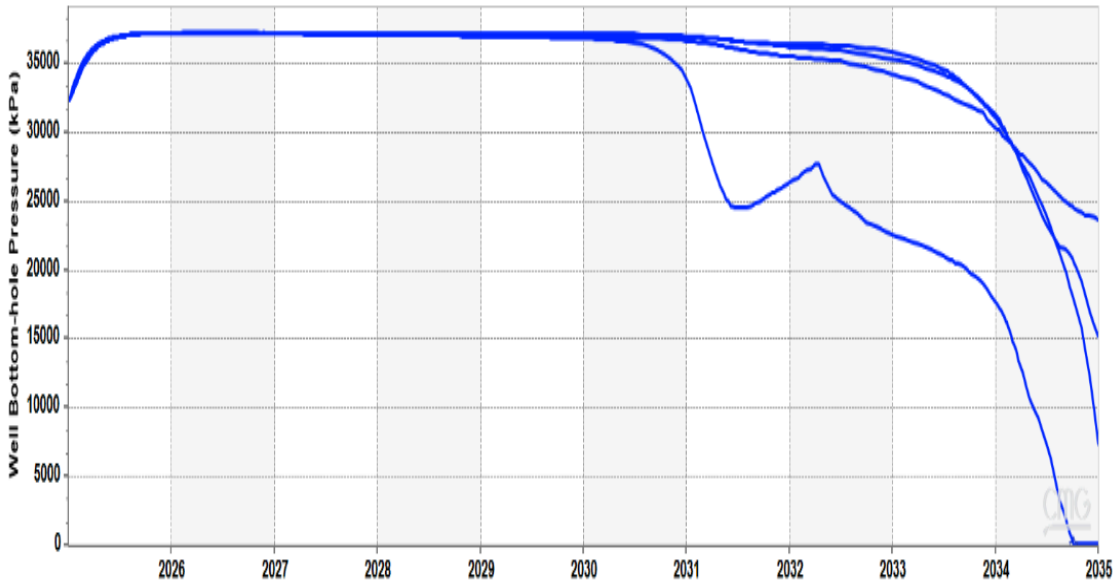

Figure 58. BHP for 4 production wells (1 injector at the center).

The values for BHP remained quite stable around 35 000 kPa until 2031, indicating normal pressure maintenance. After 2030, a sharp decline was observed, suggesting reservoir depletion. Some wells exhibited fluctuations, likely due to water breakthrough affecting pressure support.

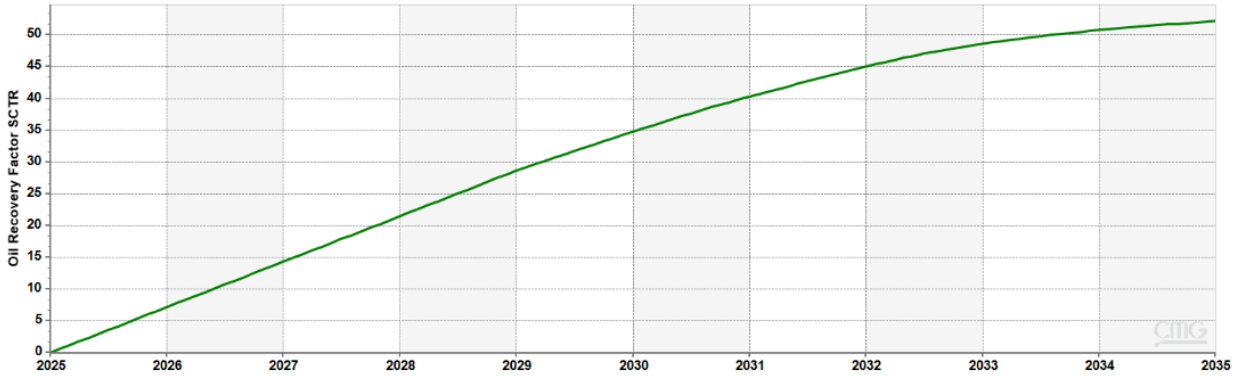

Figure 59. Oil recovery for the entire field (multiple injectors).

The above-mentioned figure (four-injector case) illustrates the distribution of the oil recovery factor values for the period of 10 years. Compared to the one-injector case, the recovery

factor was significantly higher, reaching over 50% by the end of 2035. It seems that the four-injector setup ensured a more stable and linear recovery trend, indicating better pressure support and more efficient displacement. This confirms the whole concept of increasing the number of injectors that enhance overall oil production.

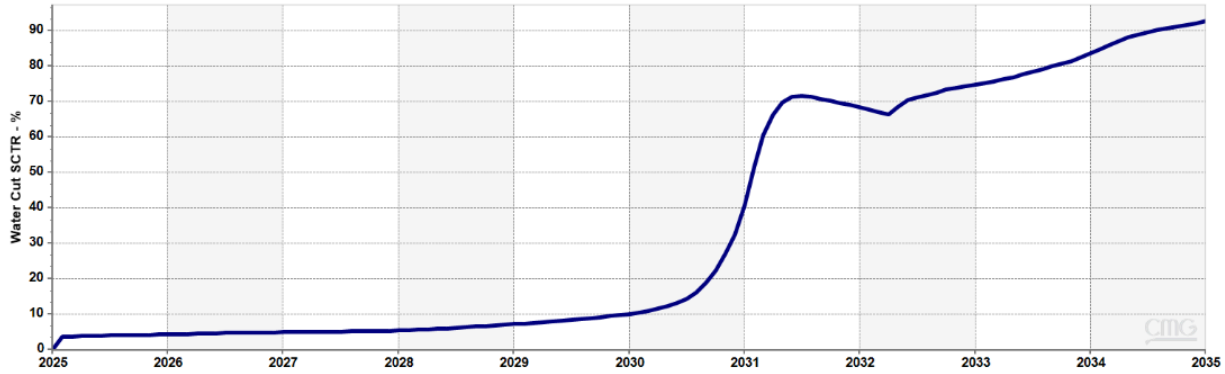

Figure 60. Water cut for the entire field (multiple injectors).

While in the single-injector case the water cut increased sharply, for the second scenario, it was steeper and happened later in 2030. This suggests more rapid displacement of oil but also higher water production challenges after breakthrough in 2030-2031.

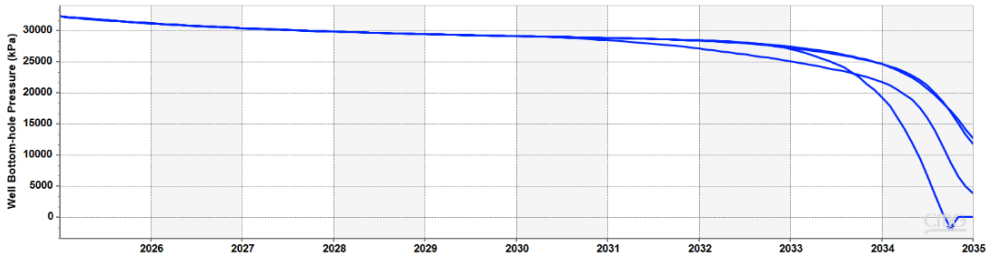

Figure 61. BHP for 4 production wells (multiple injectors).

Comparing pressure maintenance trends, with a single injector, the BHP showed a gradual decline over time, indicating a slower depletion rate due to limited pressure support. In contrast, with four injectors, the BHP remained stable until around 2030, after which a slight drop started to be seen. This suggested that the additional injectors initially helped maintain

reservoir pressure but were unable to prevent eventual depletion. The four-injector case provided better pressure support and maximized oil recovery for a longer period.

The cumulative oil production was significantly higher in the scenario with four injectors compared to the single-injector case. The additional injectors improved sweep efficiency, displacing oil more effectively toward production wells.

Analysis of simulation results of the Volve reservoir model in CMG (EOR implementation).

Another case study was conducted on the implementation of WAG as an EOR method to further increase oil production and improve overall sweep efficiency. As mentioned in the previous section, the Volve field has a heterogeneous sandstone reservoir with a gas cap and an active aquifer, making WAG injection a suitable approach. This method helps mitigate early gas breakthrough while maintaining reservoir pressure, as a result leading to higher oil recovery compared to gas or water injection alone.

To perform this simulation analysis, 2 perforations were created in specific reservoir layers to allow alternating water and gas injection over several periods of time, enhancing sweep efficiency and reducing gas channeling between injectors and producers. Specifically, perforations were made at levels 2 and 5, where gas was injected into the upper layers and water into the lower ones. Gas injection in the upper layers was chosen due to its lower density, buoyancy, and upward migration, ensuring effective contact with oil in higher-permeability zones. Meanwhile, water was injected into the lower layers to sweep oil more efficiently from the bottom while preventing excessive gas override. The following results were obtained based on these scenarios.

The graph shows the oil recovery factor over time for WAG injection, reaching approximately 60% by 2035. A rapid increase was observed between 2025 and 2026, where recovery rose to nearly 55%, indicating efficient early oil displacement due to improved sweep efficiency and mobility control. By 2028, the recovery factor stabilized around 58-60%, showing that most recoverable oil has been produced. This result confirmed that WAG significantly enhances recovery compared to conventional water or gas injection alone.

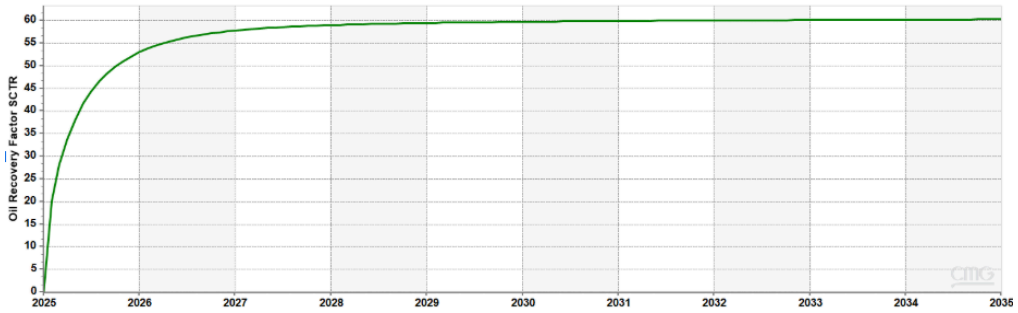

Figure 62. Oil recovery for the entire field (WAG).

The graph elucidates that initially, water cut was near 0% in 2025, but then it increased sharply after injection started, reaching 50% by 2028. This steady increase indicates progressive water breakthrough as more injected water reached the production wells. By 2030, water cut increased to 80%, and from 2032 onward, it reached almost 95-98%. This means that most of the produced fluid is water. The plateau at high water cut suggests that oil recovery has peaked, and further production consists mainly of water, which is typical in mature waterflooded reservoirs.

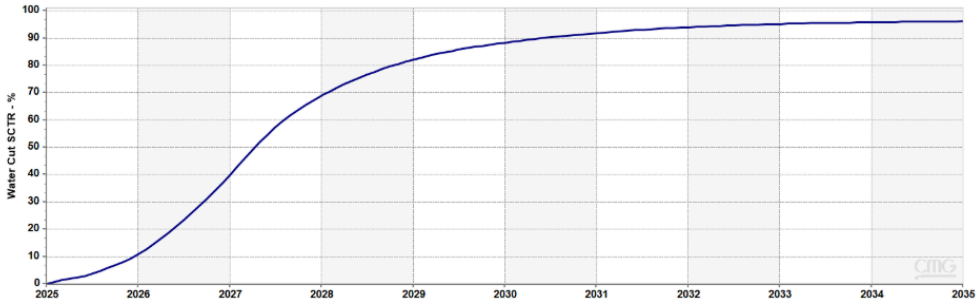

Figure 63. Water cut for the entire field (WAG).

As a result, based on the sensitivity analysis, the following conclusions can be drawn. The four-injector case demonstrated improved sweep efficiency with more uniform displacement of hydrocarbons. However, water breakthrough occurred sooner as expected due to larger injection. Additionally, the pressure profiles indicated that the second scenario achieved better pressure maintenance across the reservoir, reducing bypassed oil. For future work, additional sensitivity analyses on fluid properties could further optimize the reservoir development strategy.

4.3. Carbon Capture and Storage. Saline Aquifer Concept

After the abandonment of the field and cessation of hydrocarbon production, the Volve field presents a promising opportunity for developing carbon capture and storage sites. There are several parameters that make the Volve field viable candidate for long-term carbon sequestration including the presence of a deep saline aquifer, favorable reservoir conditions, and established infrastructure.

The major reservoir formation in the given field is the Hugin Sandstone which is located at a depth of approximately 3040 meters. This formation exhibits highly favorable properties for carbon storage. In particular, it has high porosity of 20%, the average permeability of 1000 mD, as well as reservoir pressure and temperature of 340 bar and 110°C ensuring that gas remains in supercritical state. This is one of the most important factors since gas is denser in this phase and it occupies less volume, enhancing storage efficiency. The calculated density of gas at the given reservoir conditions is $672.6\ kg/m^3$, allowing substantial mass to be stored in a given volume of pores.

Analogous Project at the Sleipner Field

The Sleipner offshore oil field tends to be located in the proximity of our target, which is considered as a current well-known carbon storage site in the North Sea. Supercritical carbon dioxide has been successfully injected into the Utsira formation since 1996. This project is considered to be a great example of the long-term stability of supercritical carbon gas in saline aquifers under North Sea geological conditions. Taking into account that there are quite great similarities in formation depth, pressure-temperature conditions, as well as general regional setting, the Volve field can potentially duplicate the success of the Sleipner Project.

Storage Mechanism and the Main Concept of Saline Aquifers

Carbon dioxide injected into the target permeable formation (Hugin Sandstone) migrates through the pores and fractures, being trapped via several mechanisms including structural and mineral trappings. The below-provided illustration greatly demonstrates the major concept,

emphasizing the role of caprock and saline aquifer creating a barrier outside of the zone and preventing gas leakage.

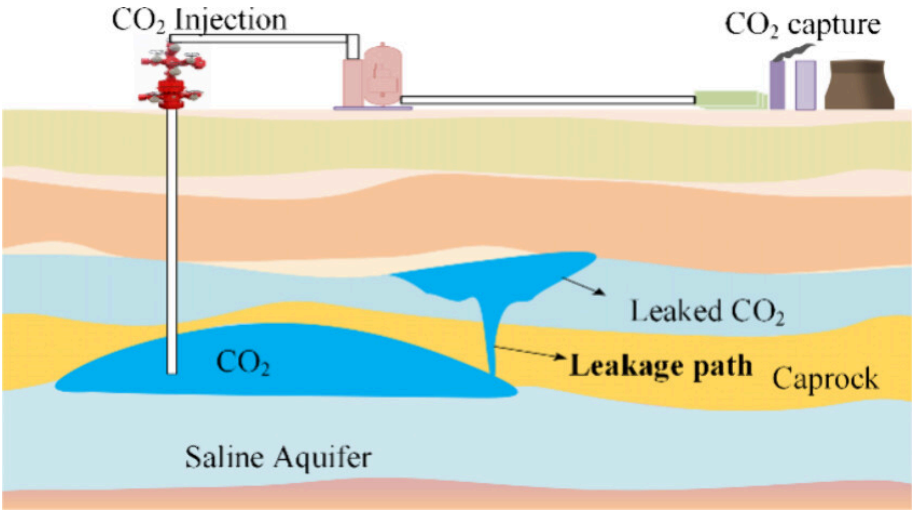

Figure 64. Saline Aquifer Concept [8].

Developing the CCUS project in the Volve field tends to align with Norway's and the EU's main climate goals to achieve net-zero emissions. That is why by integrating this part into the region's CCUS infrastructure, a significant contribution can be made toward carbon mitigation efforts.

Chapter V

5.1. Drilling and Completion Engineering

Drilling and completion engineering - are one of the most important parts of the Field Development Plan (FDP). Drilling engineering stage is aimed at the successful drilling process until the desired depth under the earth both for the fluid production and fluid injection operations. Afterwards, the completion engineering stage has a purpose of installing all the surface and subsurface components in order to provide a functioning and safe environment for the wells.

The Volve field was planned to be developed with three oil production wells and three water injection wells. In addition, two water production wells were planned to be drilled into the Utsira formation to produce water that should have been injected. Drilling on Volve was scheduled to begin at the turn of 2006/07. However, there was a risk of delay due to possible setbacks related to the installation deployment during winter.

Volve field had to have valve trees on the platform and a drilling facility available during the production phase, providing easy access to the wells for interventions, sidetrack drilling, or drilling into nearby prospects. The three production wells were planned to be completed with gas-lift equipment. The drilling location had been chosen to minimize the risk of shallow gas and to allow drilling access to all identified prospects for Volve. The number of wells was determined based on the reserves, drainage efficiency, the planned production plateau, and the need for water injection. The injectors were to be drilled with a maximum deviation of 30 degrees, while the producers were drilled horizontally or with high deviations through the reservoir.

Additionally, the location was within drilling range of all identified prospects in the area. A wellhead module was placed outside the platform under the drilling tower. There were slots and manifolds prepared for drilling up to 13 wells, with the possibility of considering additional 2 wells. Drilling was scheduled to begin at the turn of 2006/2007 and was expected to be

completed by the second quarter of 2008. Table 15 provides a summary of the well trajectories. Optimization of the drilling program, including well paths and casing programs, was to be carried out in close collaboration with reservoir engineers until the completion of each individual drilling and completion program.

Table 17. Summary of the planned well trajectories [9].

Well	Start deviation construction, mTVD/mMD	Stop deviation construction, mTVD/mMD	Deviation build rate degrees, degrees/30m	Sailing angle, degrees	Total depth, mTVD/mMD	Well orientation
I-F10	300/300	634/649	2.5	29	3228/3618	Deviated
I-F15	300/300	479/481	2.5	15	3110/3206	Deviated
I-F5	300/300	570/577	2.5	23	3125/3355	Deviated
P-F2	300/300 2168/2268 2862/3813	486/490 2867/3332 2891/4049	3 3 3	19 91 75	3081/4804	Horizontal
P-F9	300/300 2186/2209	409/409 2804/3010	2.5 3	9 73	2991/3641	Horizontal
P-F5	300/300 2190/2231	483/485 2871/3130	2 3	12 78	2959/3538	Horizontal

The table above shows the depth, deviation, angles and orientation for both injection and production wells that were actually present in the Volve field project. As it can be seen injection wells are mainly deviated, while production wells are mostly horizontal according to the measured depth and the deviation angles. This information further provides an opportunity to construct completion schemes for different wells.

5.1.1. Well completion design

There are three well types that will be discussed further: oil production well, water production well and water injection well. Three types of wells are actively involved in the field development plan since they contribute to efficient oil and gas production from the reservoir.

Based on the type of the well, there are different components and drilling operations considered. Therefore, the figures below provide a schematic overview of three types of wells with their corresponding unique properties.

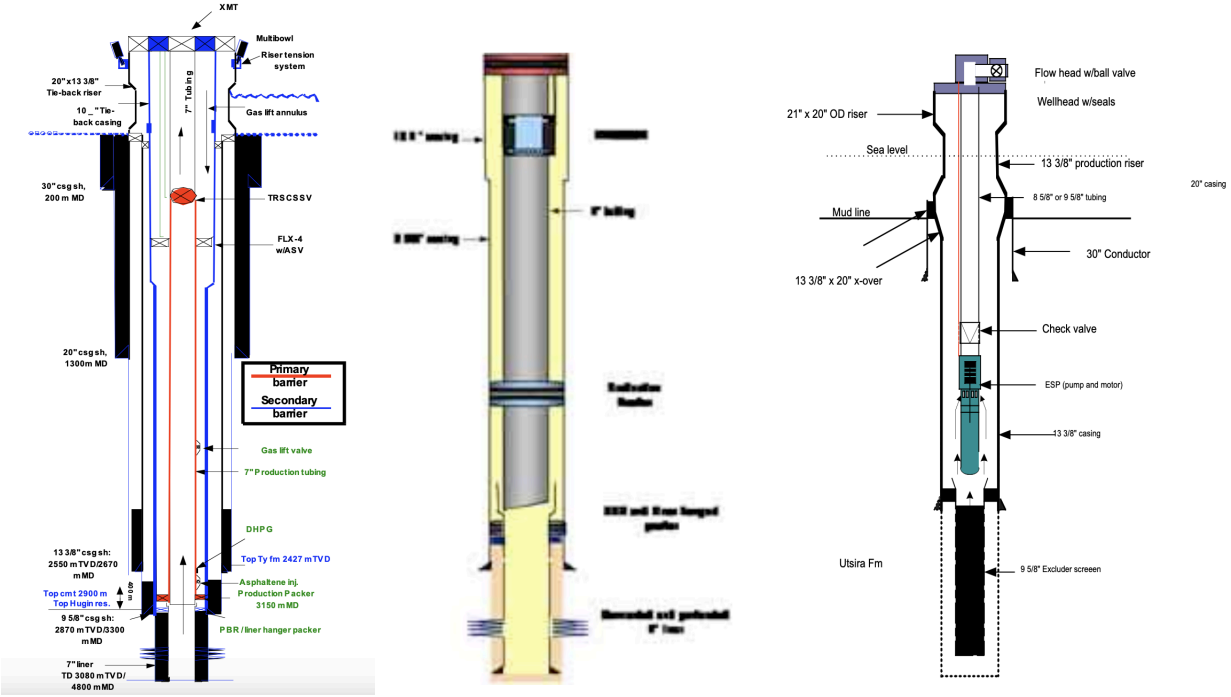

Figures 65-66. Oil producer well with gas lift and water injection well schemes [9].

The oil production wells and water injection wells were completed with production packers and safety valves in the production tubing. The production wells were planned to be completed with gas-lift equipment, including annulus safety valves, downhole pressure and temperature gauges. The two water production wells were planned to be supplemented with downhole electric driven pumps to pump the water to the surface. The water production wells into the Utsira formation were planned to use 30" and 13 3/8" casings. Both production wells and injection wells were planned to be completed with 7" production tubing. Gathering all the necessary information about the completion schemes of three different types of wells, the summary is presented in the following table.

Table 18. Summary of the planned well completion schemes [9].

Well type	Casing / Tubing type	Size, in	Depth, ft

Oil producer	Conductor casing	30	656
	Surface casing	20	4265
	Intermediate casing	13 ⅜	8760
	Production casing	10 ¾ x 9 ⅝	10827
	Production liner	7	15748
	Production tubing	7	10663
Water producer	Surface casing	30	-
	Production casing	13 ⅜	-
Water injector	Surface casing	20	4265
	Intermediate casing	13 ⅜	8760
	Injection liner	9 ⅝	10827
	Injection tubing	7	8800

Based on the provided data from the table presented below and considering other important details of completion engineering there were constructed well schemes using PIPESIM Schlumberger software. This software allows to fully create the schematic model of any well in 2D and 3D view if all the necessary information is provided. Apart from the completion engineering purposes, it is widely used in production engineering, for instance, for nodal analysis. Therefore, the figures below demonstrate the well schemes of oil production and water injection wells.

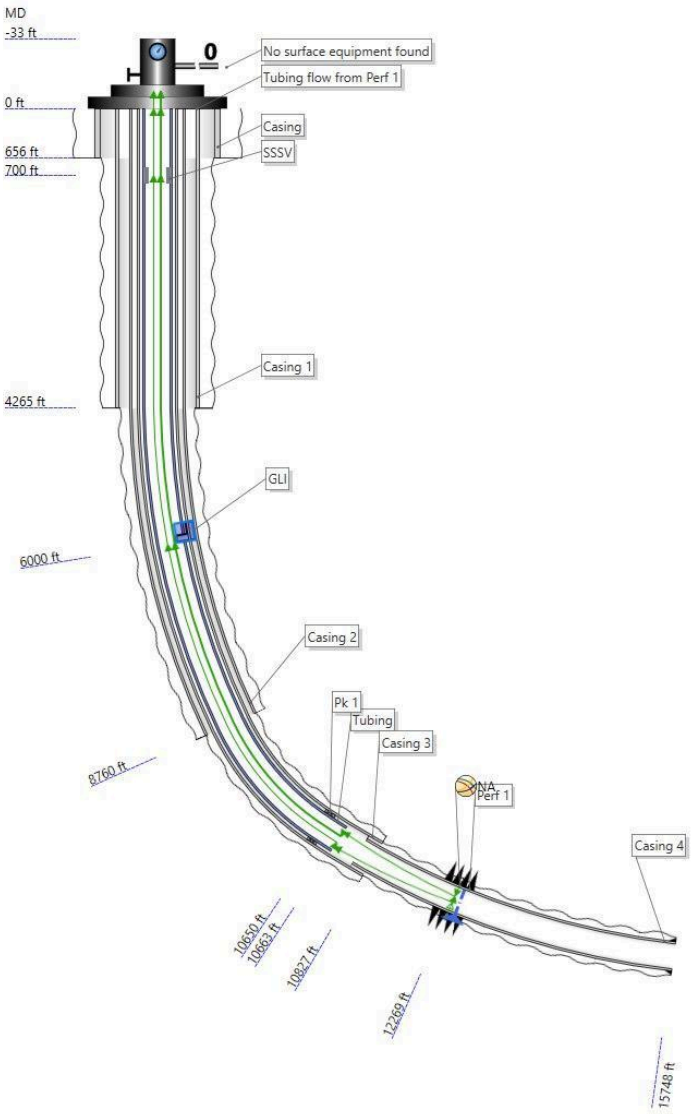

Figure 67. Completion scheme for the oil producer well [PIPESIM].

As it can be seen from the above-provided schematics, the completion scheme was constructed in the PIPESIM Schlumberger software based on the criteria presented in Table 18. The construction consists of several casings and a tubing with a size of 7 inches. In order to allow fluid flow in the wellbore, perforations were made at the depth of 12269 feet. The gas lift section was added in the well completion at the depth of 6000 ft for gas injection that helps oil flow when natural producing pressure is not sufficient. Packers were located at the depth of 10650 feet in order to have control over the fluid flow between casing and tubing. In addition,

one of the main components is SSSV which is accountable for automatic shut off in case of any emergency situation which is located at the depth of 700 ft.

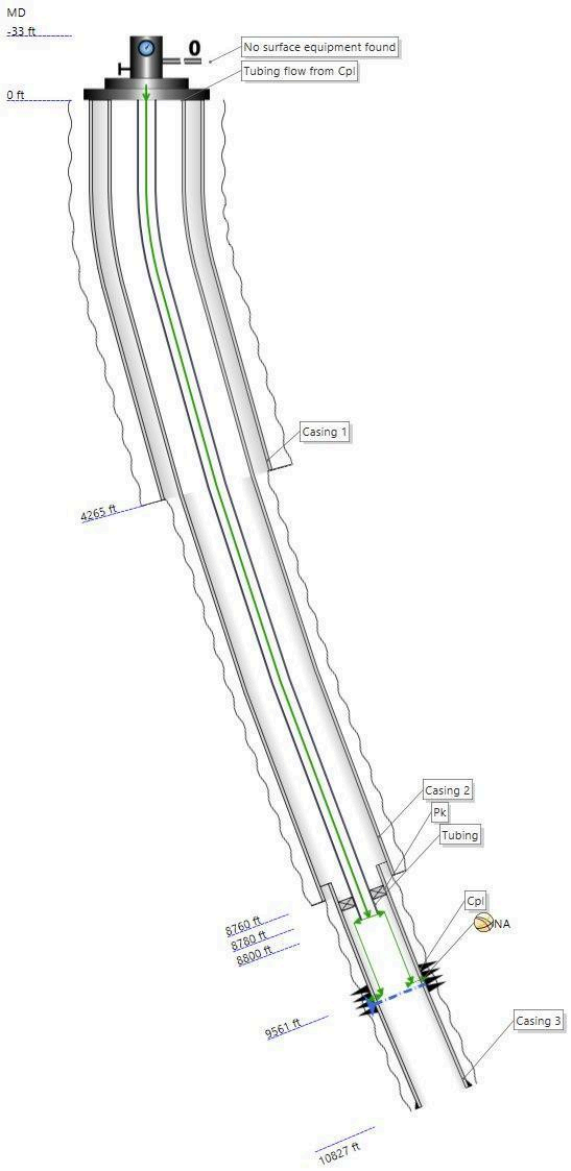

Figure 68. Completion scheme for the water injection well [PIPESIM].

The above-provided schematics demonstrates the completion scheme that was also constructed in the PIPESIM Schlumberger software based on the criteria presented in Figure 7. The three casings are situated up to 4265 feet, 8760 feet and 10827 feet respectively. The construction consists of several casings and a tubing with a size of 7 inches. In order to allow fluid flow in, perforations were made at the depth of 9561 feet. Packers were located at the depth

of 8780 feet in order to have control over the fluid flow between casing and tubing. Due to the fact that this is an injection well, there is no gas lift, ESP or sucker rod pump defined.

It is also crucial to consider the equipment and details that should be located on top of the implemented casings, namely, wellhead components and Xmas tree components. Wellhead and Xmas tree components are essential since they allow the wells to produce the oil and gas, inject fluids in reverse, have control over the pressure in the annulus and keep the wells under a safe environment. The figures shown below are the schemes of wellhead and the Xmas tree components that should be included in the completion engineering stage.

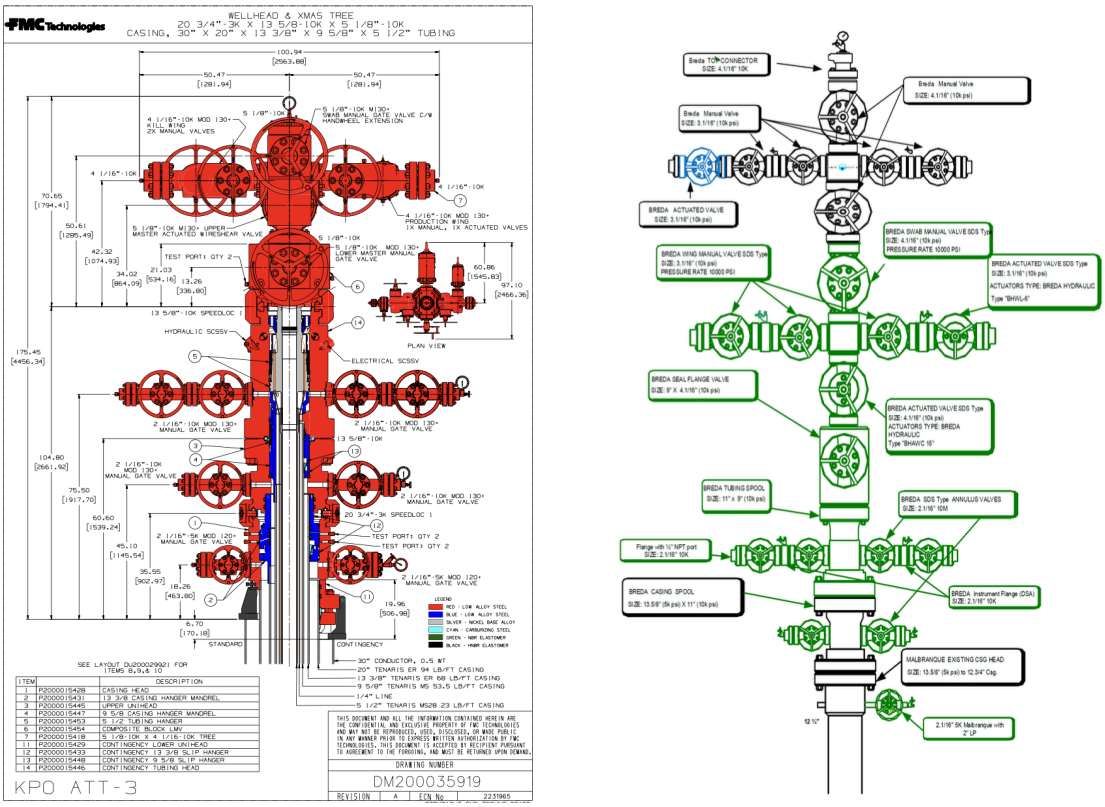

Figures 69-70. Wellhead and Xmas tree schemes [KPO].

The schemes include different valves to control the conditions inside the well and surface safety valves in case of any emergency cases. Moreover, the casing head helps to support surface casing and the tubing head that is attached to the top of the casing head supports the production tubing. In general, a wellhead suspends the casing and provides pressure seals for the casing string. Regarding Xmas tree components, there is kill wing valve, SWAB valve, production wing

valve, upper and lower master valves. While the production wing allows production of oil and gas, the kill wing allows injection of fluids such as mud or brine. The SWAB valve is useful for wireline operations and coiled tubing operations. Lastly, upper and lower master valves are helpful for shut in periods and emergency cases if, for example, blowout occurs.

5.1.2. Drilling system

The mud program for the sections to be drilled will protect the environment, provide a primary pressure barrier against formation fluid pressure as well as provide needed lubrication and cooling for drilling equipment. In addition, the mud will incorporate additives such as lost circulation material, (LCM). The addition of LCM to be mud would prevent losses into the formation as the seismic section showed faults begin crossing and well tests indicate fault boundaries. The summaries of the mud weights and property are shown in the table presented below.

Table 19. Summary of the planned mud types [9].

Hole section	Mud type	Mud weight, SG	Additive
8 ½ - in Mill-out	Water based mud	1.2-1.3	Tandem Pill – to sweep clean mill casing swarf Shale Inhibitor LCM PAC
6-in Production	Oil based mud	1.35-1.45	LCM PAC
Completion	Brine	1.3	KCl

As it can be seen from the table, there should be used both water based mud and oil based mud for drilling operations. Water based mud is usually used in the upper parts of completion, while oil based mud is mostly used in lower parts of well completion. The reason is that water based mud is utilized due to its environmental friendliness, cheaper cost and drilling through non water sensitive formation to maintain the stability of the wellbore. On the other hand, oil based mud should be used because of its superior lubricity, stability in reactive formations, better

thermal stability and minimization of formation damage. Different types of additives are used, for example, lost circulation materials (LCM) are helpful to plug zones with fractures to avoid increase in non productive drilling time and mud losses.

One of the main tasks of drilling engineering is to work with the Mud density vs. True vertical depth chart since it contains all the information concerning fracture gradient, mud weight window and pore pressure. This information is essential for placing the casing at the right position, using appropriate mud weight, avoiding kicks and blowouts as well as formation testing. Figure 71 presented below provides data on these parameters to have certain conclusions for the drilling engineers.

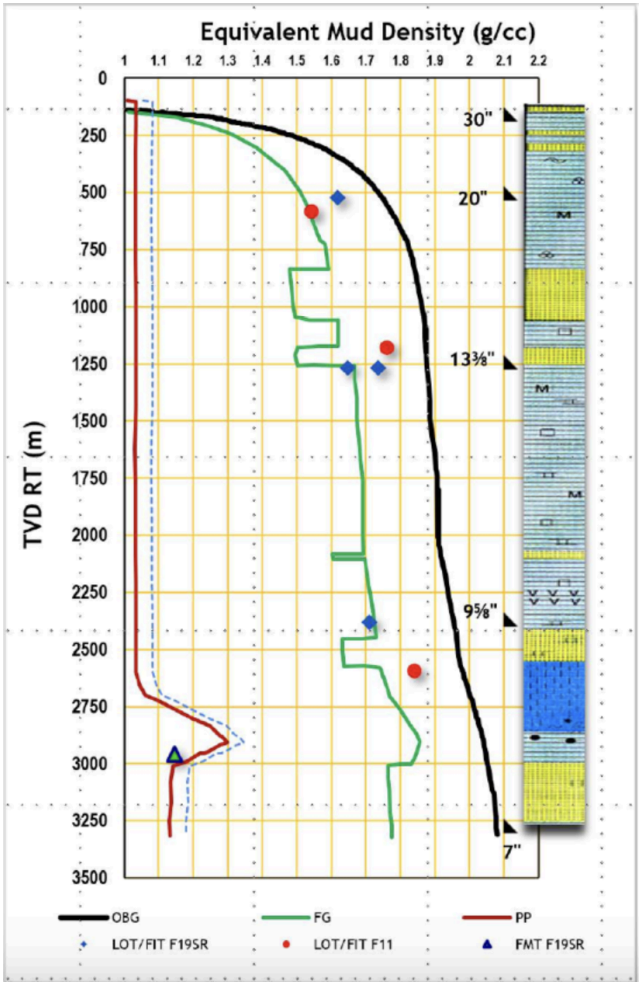

Figure 71. Equivalent mud density vs. True vertical depth graph [9].

The figure shows curves of fracture gradient, pore pressure and overburden gradient with corresponding depth and casings for the oil production well. For each depth appropriate mud weight should be used according to the graph, meaning that safe mud weight should be between pore pressure and fracture pressure. Therefore, drilling fluid should be heavier compared to pore pressure to avoid kicks and must be lighter than fracture gradient to be safe from fracturing the formation that is being drilled. From this figure it can be seen that at the depth of about 2500 meters there is a high risk zone due to the decreasing mud weight window because of an increase in overpressure.

Mud weight can be calculated using the following equations:

$$Mud\ Weight\ (ppg) = \frac{Formation\ pressure\ (psi)}{0.052 \times TVD(ft)} \tag{18}$$

$$Mud\ Weight\ (g/cc) = \frac{Formation\ pressure\ (kPa)}{9.81 \times TVD(m) \times 1000} \tag{19}$$

Considering the fact that the reservoir lies in the true vertical depth of 3060 meters and has a pressure of 340 bar, the suitable mud weight can be calculated for these conditions.

$$Mud\ Weight\ (ppg) = \frac{Formation\ pressure\ (psi)}{0.052 \times TVD(ft)} = \frac{4931.28}{0.052 \times 10039.37} = 9.45\ ppg = 1.13\ g/c \tag{20}$$

This means that at the depth of 3060 meters mud with 9.45 ppg or 1.13 g/cc density can be used for safety conditions. This value also matches with the graph above where 1.13 g/cc lies between pore pressure gradient and fracture gradient values at the depth of 3060 meters.

Bits selection is also an integral part of the drilling operation preparedness. Based on the formations available and rock properties available for drilling engineers, there may be changes of

drill bits. Hence, the figures below present two of the most suitable drill bits for the drilling process in the Volve field.

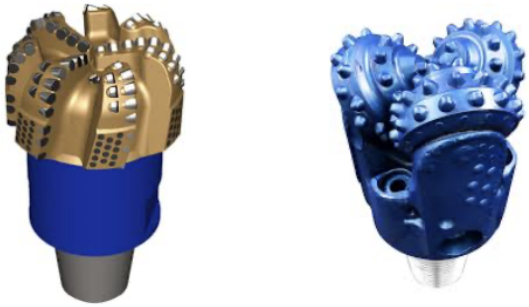

Figure 72. PDC and tricone bits.

PDC drill bits are usually used for rapid drilling in softer formations due to its shape, mechanical properties and the mechanism of rotation. However, tricone drill bits are utilized for harder sections also due to its unique shape and having three rotating cones.

5.1.3. Drilling and completion operations schedule

It is important to consider the time spent on both drilling and completion operations for both operating and service companies. The time span predetermines and affects the production period and the economics of the project. It is efficient to drill and complete the wells in as little time as possible to earlier begin the production operations. Moreover, the best strategy is not to wait once a well is drilled, but to drill and complete a couple of wells at the same time to save time. The table below shows the time spent on such procedures for different categories of wells.

Table 20. Drilling and completion time [9].

Category	I5	I10	I15	P9	P2	UP1	UP2	Tech	Total
Drilling days	38	36	36	40	40	53	12.5	12.5	307
Completion days	19	19	19	22	24	23	10	10	165
Total days	57	55	55	62	64	76	22.5	22.5	475

It can be understood from the table that the drilling procedure takes almost twice the time of the completion operations due to the difficulties and carefulness of actions on this stage. The drilling operation for one well takes on average 35-40 days, whereas the completion process takes up to 24 days at maximum. Overall, for the list of these wells it took approximately a year to drill the wells and around half a year to complete the wells.

5.1.4. Surface Equipment and Rig Selection

After defining the completion schemes and all the constitutes of the drilling process, it is important to construct the network schematic of all the surface equipment. Network schematic provides an opportunity to see how the produced fluid flows through the tubulars until the desired location. Therefore, the Figure below demonstrates the surface equipment scheme necessary to the oil production well.

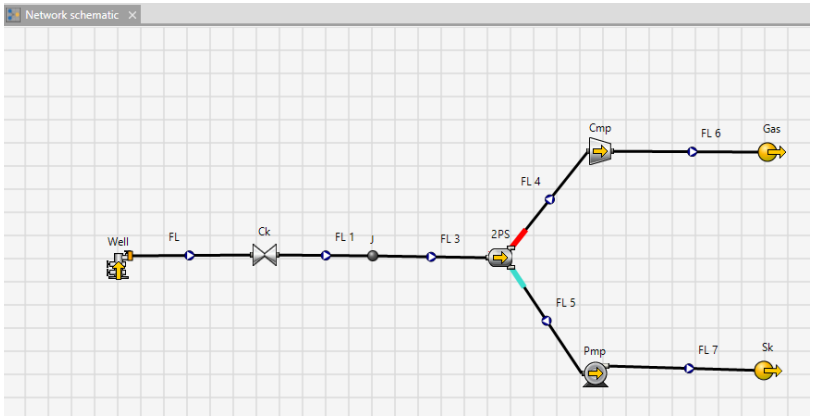

Figure 73. Surface equipment scheme [PIPESIM].

The surface equipment contains the oil production well as a source, choke, joint point, two phase separator, compressor, generic pump and several flowlines. The process commences when the fluid from the well flows through the flowline 1 to the choke valve which is necessary to restrict and control the flow rate and the downstream pressure of oil and gas. Then the transport of the fluids continues via flowlines to the joint point and reaches to the two phase separator. The separator's function is to provide efficient fluid phase separation and deal with the mixture of oil and gas before coming to the storage. Furthermore, the gas line has a compressor needed for reducing the volume of a gas by having higher pressure and to meet the requirements

of the process. At the same time there is a generic pump in the oil flowline because it helps to move fluids by means of mechanical actions with appropriate flow rate and pressure.

For every offshore drilling operation it is necessary to appropriately choose the best and the most suitable type of rig in order to operate efficiently and safely. There are different types of rigs based on different purposes and the depth of the sea. The figure below summarizes the most popular types of rigs with a short explanation.

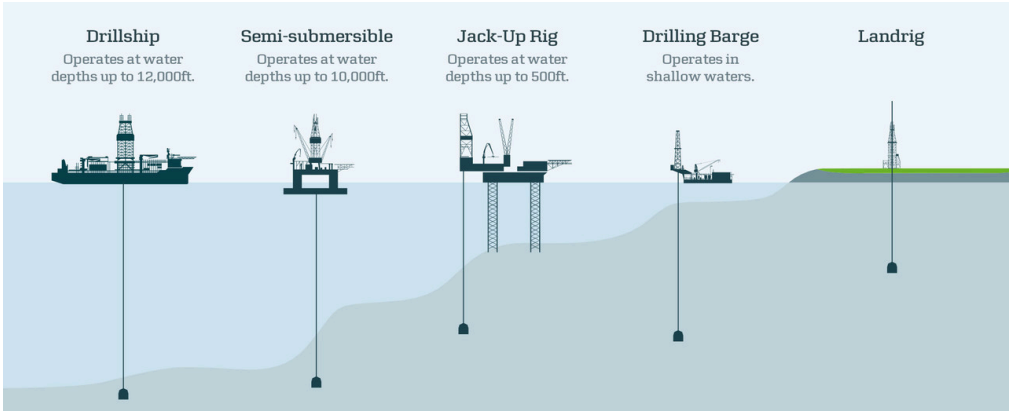

Figure 74. Offshore drilling rig types [25].

Due to the fact that the Volve field's sea depth is about 80 meters, it is considered to be a shallow offshore field. Therefore, the Jack-Up type of rig is suitable since it operates at water depth up to 500 ft and has a strong construction that allows doing operations in the best conditions.

Figure 75. Jack-up offshore drilling rig type [25].

Chapter VI

6.1. Production Engineering with PIPESIM

Production engineering workflows benefit from PIPESIM implementation because it enables engineers to study multiple operational conditions and judge equipment behavior and determine system production constraints. The most valuable application of the software is nodal analysis. Nodal analysis is based on the principle of pressure continuity, the values of which are unique for each individual point of the system (for each node) throughout the entire path of the liquid from the reservoir to the separator (or vice versa for injection wells). As the pressure and temperature change, the properties of the fluids also change. And in order to simulate the flow, it is necessary to "break" the system into a number of discrete nodes that divide the system into separate elements, where calculations of the properties of liquids will be performed. The analysis of the system at these nodes is actually a nodal analysis. The most common example given in the literature is the intersection of inflow curves (IPR) and vertical lift curves (VLP or TPR) to determine the flow rate of a well under these conditions. The separation point (node) in this case is the bottom of the well. PIPESIM helps to perform detailed nodal analysis by integrating well data, fluid properties and surface conditions. The goal of this study is to explore the implementation of this software to construct the well design and perform the nodal analysis based on the literature data.

6.1.1. Nodal analysis

The construction of a wellbore model took place through PIPESIM within a well-centric workspace before its export to the network canvas for additional development. The network canvas obtained the model which required linking to flowlines before integrating it with surface facilities to finalize the system configuration.

For the downhole tubulars, including casings and tubing strings were created using the data from Figure 76.

Mode: ○ Simple ◉ Detailed
Dimension option: ◉ OD ○ Wall thickness

CASINGS/LINERS

	Section type	Name	From MD	To MD	ID	OD	Roughness
			ft	ft	in	in	in
1	Casing	Casing	0	656.168	27.5	30	0.001
2	Casing	Casing 1	0	4265.092	18.73	20	0.001
3	Casing	Casing 2	0	8759.843	12.347	13.375	0.001
4	Casing	Casing 3	0	10826.77	8.435	9.625	0.001
5	Liner	Casing 4	10823.49	15748.03	5.92	7	0.001

TUBINGS

	Name	To MD	ID	OD	Roughness
		ft	in	in	in
1	Tubing	10662.73	6	7	0.001

Figure 76. Downhole tubulars.

Then, the deviation survey for the production well was constructed based on the information in Table 15 that states the well trajectory and deviation angles.

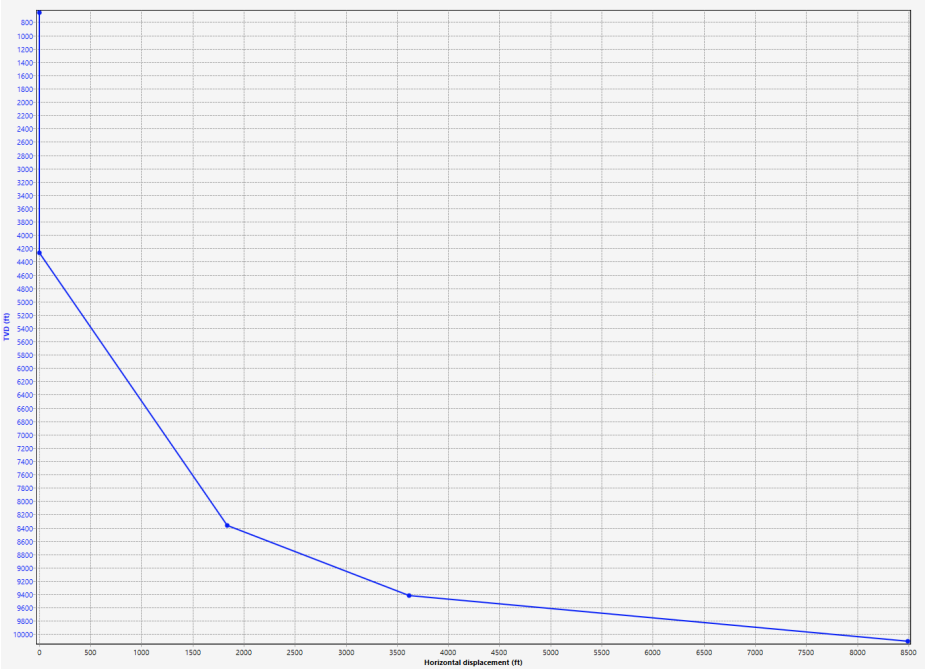

Figure 77. Deviation survey of Production wells.

Downhole equipment, including single packer at 10650 ft MD and subsurface safety valve at 700 ft TVD/MD with 4.25 inches bean diameter. The thermal gradient section requires a single option for overall heat transfer coefficient and ambient temperature. The heat transfer coefficient value of 2 Btu/h/ft²/°F combined with an ambient temperature of 60°F was applied in this section. To run the simulation of horizontal wells in the software, reservoir properties should

be defined. In discussion with reservoir engineers and literature review, the reservoir properties were stated as below (Figure 78).

Reservoir pressure:	4931.283	psia
Reservoir temperature:	230	degF
IPR basis:	◉ Liquid ○ Gas	
Productivity index:	19.42292	STB/(d.p...
Radius of reservoir extent:	50	ft
Reservoir thickness:	262.4672	ft
Permeability X (Perpendicular to well):	1000	mD
Permeability Y (Parallel to Well):	630	mD
Parameter option:	◉ Ratio ○ Absolute	
Permeability anisotropy (kv/k):	0.6	fract.
Horizontal section length :	25	ft
Well radius:	4.25	in
Well eccentricity:	10	ft
Fluid OFVF:	1.31	
Fluid viscosity:	0.7767	cP

Figure 78. Used reservoir properties for model simulation.

The Pipesim offers several types of fluid property modeling, either standard black oil correlation or compositional fluid modeling. The project was constructed based on a compositional fluid model since the Volve field contains undersaturated oil with 52% of C10+ aromatics composition as stated in the PVT Analysis section. From C1 to C36+ (see Fig. 79) components were implemented in the model and phase envelope was obtained (see below).

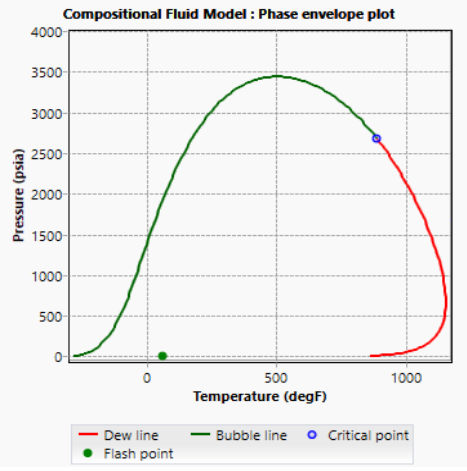

Figure 79. Phase envelope generated in the Pipesim.

As the well definition has finished, the further study will focus on nodal analysis. It is important to understand the core of nodal analysis. Principal of nodal analysis can be expressed by the following formula:

$$q = f_{in}(P_{wf}) = f_{out}(P_{wf}) \tag{21}$$

- q - flow rate, STB/d
- P_{wf} - bottom hole pressure (BHP), psia
- f_{in} - inflow function (IPR)
- f_{out} - outflow function (TPR)

As it is stated above, the reservoir is undersaturated with high content of heavy components. For undersaturated oil, the inflow performance curve is straight-line. Joshi S. D. proposed an equation to evaluate inflow performance for horizontal well in undersaturated conditions:

$$q_o = \frac{2\pi kh(P_{res} - P_{wf})}{\mu_o B_o * [Ln(\frac{4L}{d_e}) + S]} \tag{22}$$

- h - reservoir thickness, ft
- k - reservoir permeability, mD
- d_e - wellbore diameter, ft
- μ_o - oil viscosity, cP
- B_o - FVF
- S - skin factor

Skin factor was defined as -0.58 in the model, based on the calculation in the Well Test section. The next thing that should be discussed is the tubing performance relationship. In Pipesim, it is calculated numerically using multiphase pressure drop correlation:

$$P_{wf} = P_{well\ head} + \Delta P_{friction} + \Delta P_{hydrostatic} + \Delta P_{acceleration} \quad (23)$$

The main input variables for tubing performance are:

- Pressure and temperature profiles
- Fluid properties
- Tubing geometry, it includes tubing diameter, roughness and inclination

After running the simulation, the nodal point that is considered as the operating point was obtained (Table 22). The sensitivity analysis should be performed in order to understand the impact of changes in main parameters such as reservoir pressure, water cut, gas-oil-ratio etc.

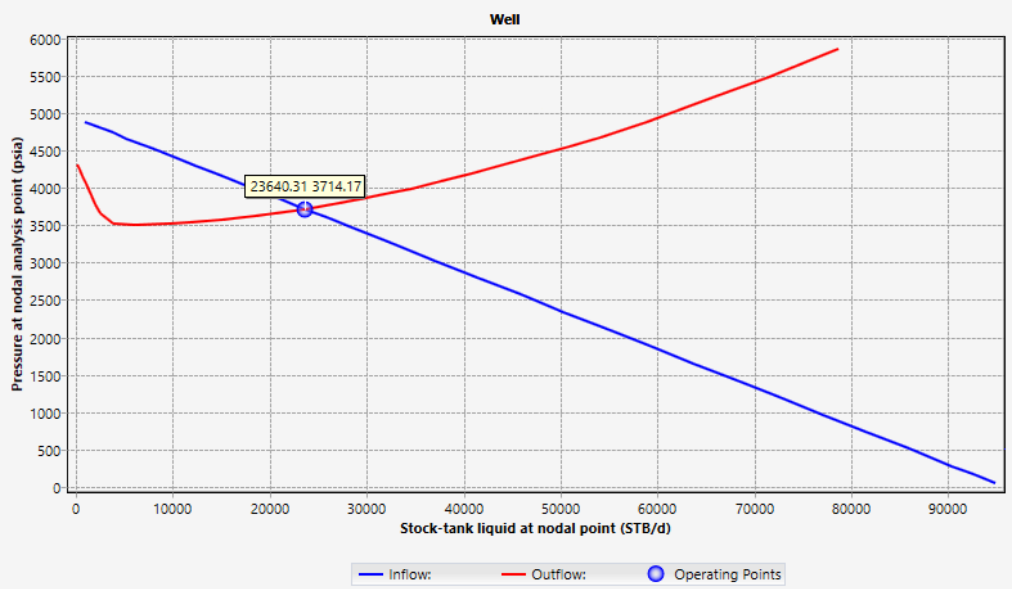

Figure 80. Original operating point based on Nodal Analysis.

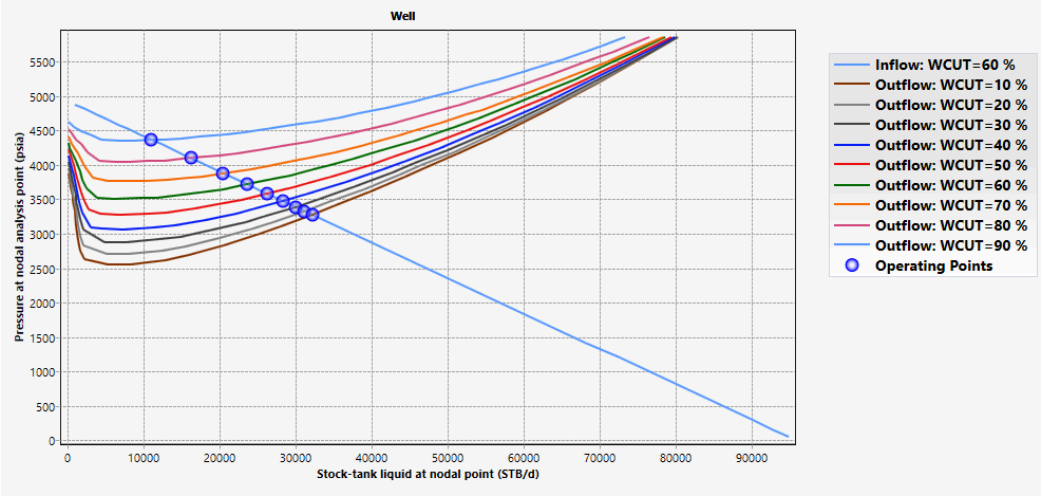

	Operating point	ST Liq. at NA	P at NA
		STB/d	psia
1	WCUT=10 % F...	32136.81	3276.725
2	WCUT=20 % F...	31157.2	3327.161
3	WCUT=30 % F...	29926.52	3390.523
4	WCUT=40 % F...	28331.76	3472.629
5	WCUT=50 % F...	26252.86	3579.662
6	WCUT=60 % F...	23601.35	3716.176
7	WCUT=70 % F...	20403.73	3880.807
8	WCUT=80 % F...	16161.58	4099.215
9	WCUT=90 % F...	10978.28	4366.079

Figure 81. Effect of water cut.

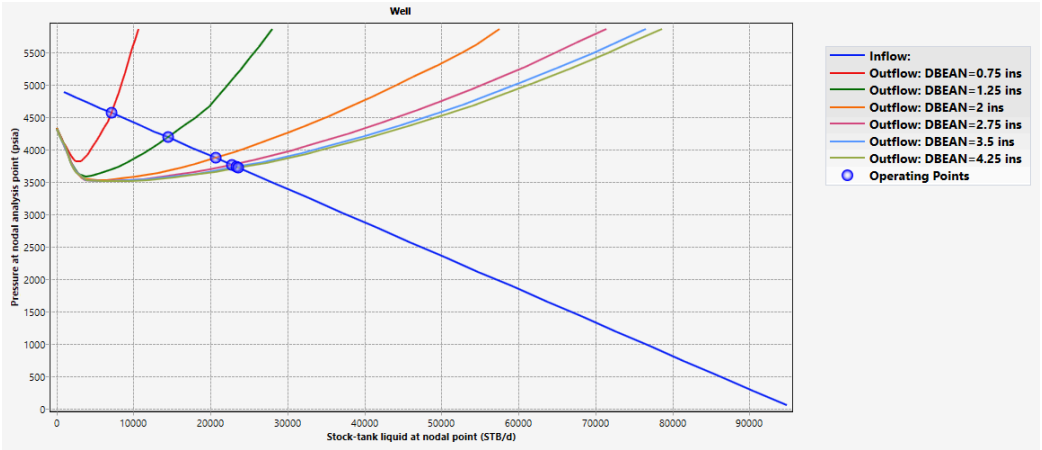

	Operating point	ST Liq. at NA	P at NA
		STB/d	psia
1	DBEAN=0.75 i...	7208.598	4560.163
2	DBEAN=1.25 i...	14488.89	4185.334
3	DBEAN=2 ins...	20682.52	3866.453
4	DBEAN=2.75 i...	22776.99	3758.619
5	DBEAN=3.5 in...	23415.87	3725.726
6	DBEAN=4.25 i...	23648.71	3713.738

Figure 82. Subsurface safety valve sensitivity bean diameter effect.

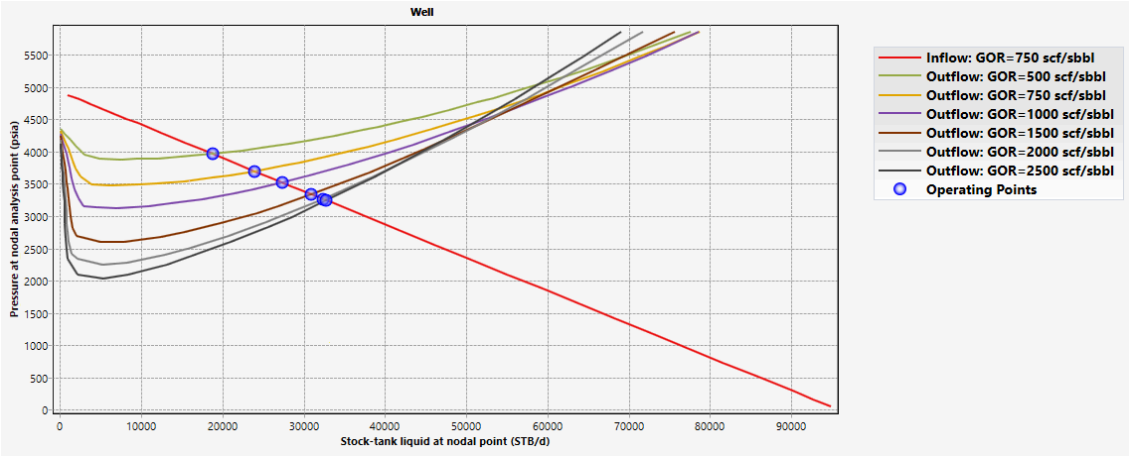

	Operating point	ST Liq. at NA	P at NA
		STB/d	psia
1	GOR=500 scf/s...	18761.59	3965.353
2	GOR=750 scf/s...	23983.54	3696.499
3	GOR=1000 scf...	27371.26	3522.081
4	GOR=1500 scf...	30927.81	3338.971
5	GOR=2000 scf...	32328.77	3266.842
6	GOR=2500 scf...	32771.6	3244.042

Figure 83. Increased Gas-Oil-ratio effect.

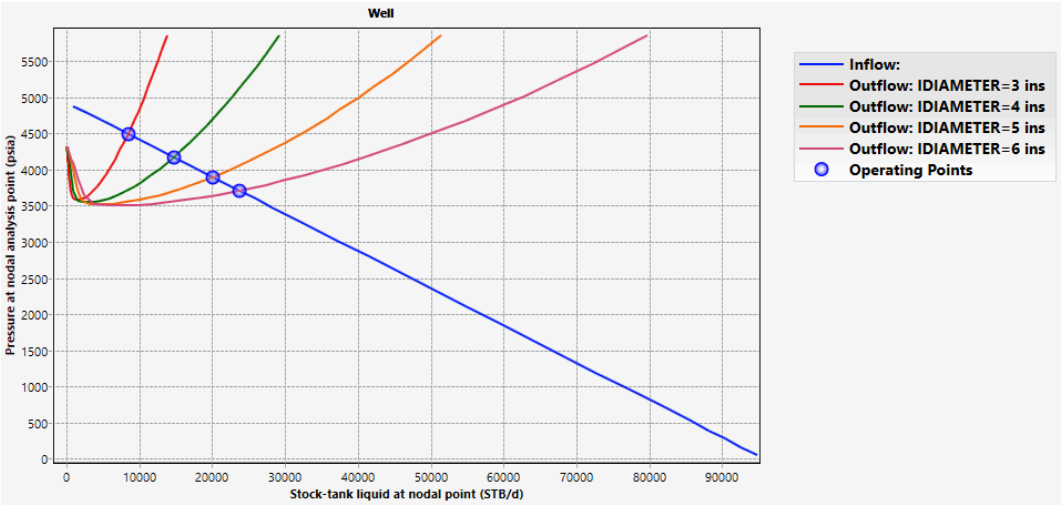

	Operating point	ST Liq. at NA	P at NA
		STB/d	psia
1	IDIAMETER=3...	8470.541	4495.191
2	IDIAMETER=4...	14779.51	4170.372
3	IDIAMETER=5...	20163.42	3893.179
4	IDIAMETER=6...	23767.32	3707.631

Figure 84. Different Tubing Sizes.

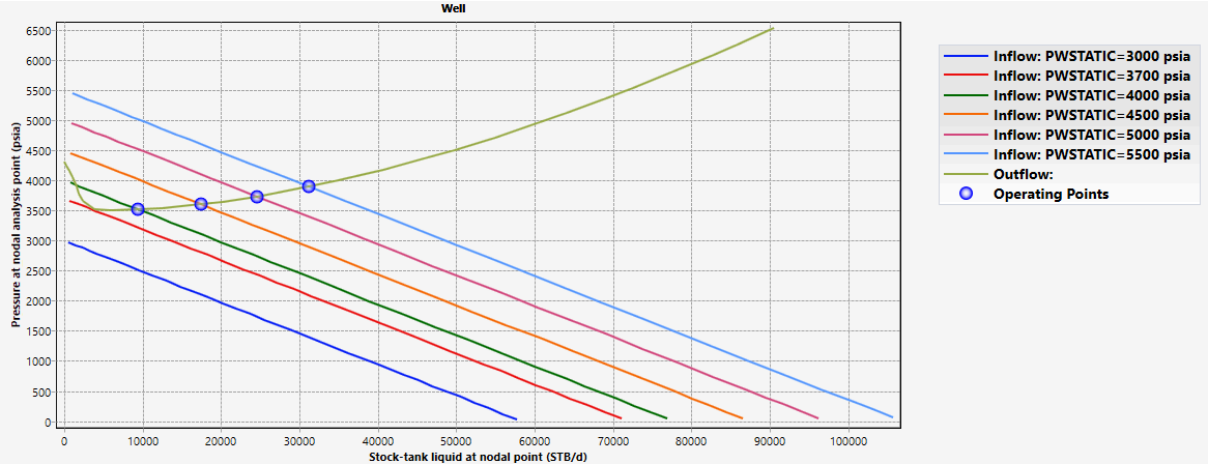

	Operating point	ST Liq. at NA	P at NA
		STB/d	psia
1	UNCONVERGE...		
2	UNCONVERGE...		
3	PWSTATIC=40...	9372.646	3517.446
4	PWSTATIC=45...	17423.41	3602.95
5	PWSTATIC=50...	24599.28	3733.497
6	PWSTATIC=55...	31225.98	3892.319

Figure 85. Different Reservoir Pressure.

The table below shows the result of sensitivity analysis. The notable thing that should be discussed is the unconvergence of IPR and TPR when the reservoir pressure is below 4000 psi. The pressure should be maintained in order to continue production. Different methods were proposed to stimulate the production at lower reservoir pressure. Reservoir engineer proposed to initiate water injection from the beginning of the operation. Moreover, several artificial lift techniques, gas lift and ESP, were suggested to implement when the reservoir pressure falls below 4000 psi.

Table 21. Nodal analysis results with sensitivity.

Parameter	**Value/Effect**
Operating production rate	23 640 STB/d
Operating pressure	3714 psia

Subsurface safety valve sensitivity	Higher bean diameter more production rate
Reservoir Pressure	Production rate increases with high reservoir pressure
Effect of water cut	Operating rate decreases with increasing WC
GOR sensitivity	Flow rate increases with increased GOR, but up to 2000 scf/STB
Tubing size changes on production	Larger tubing less friction more production rate

6.1.2. Gas lift implementation

In the certain period of production, the well is considered to be dead since liquid flow has stopped. To enhance the production, gas lift should be implemented as a type of artificial lift. After the gushing stops due to a lack of reservoir energy, gas lift should be implemented, which is a mechanized method of well operation in which additional energy is introduced in the form of compressed gas. The method is usually used after the gushing stops due to a lack of reservoir pressure. The figure below shows the workflow of simulation with implementing the gas lift method to the Pipesim model.

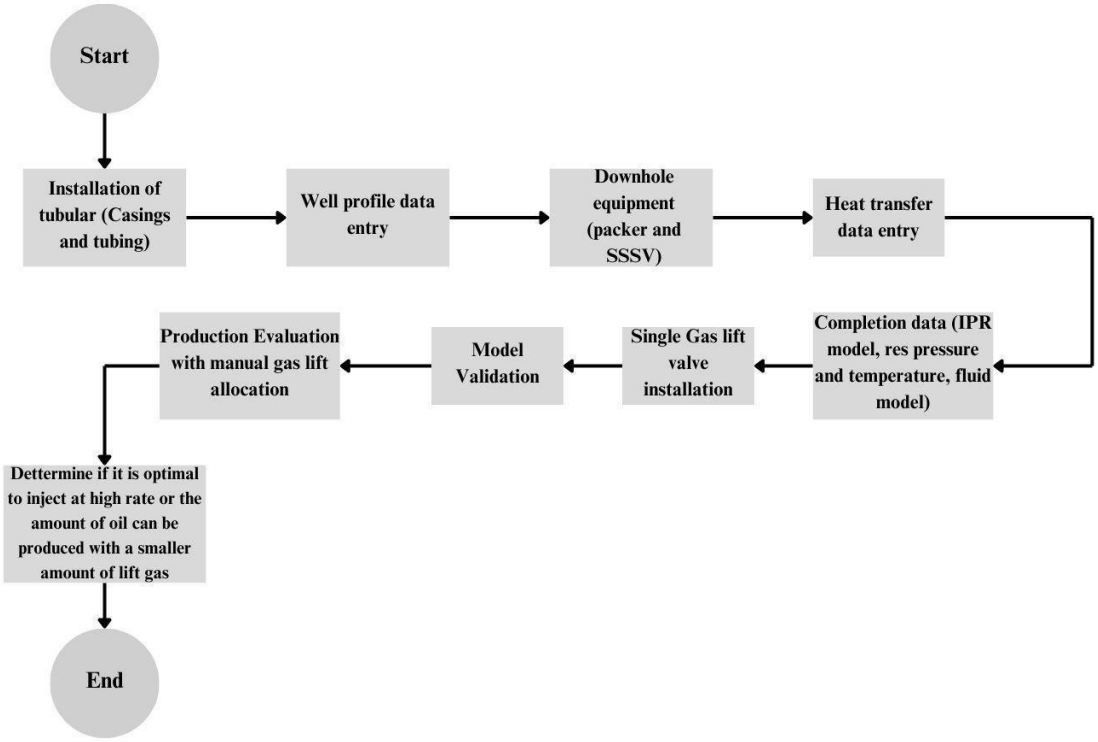

Figure 86. Simulation WorkFlow for Gas Lift Optimization.

Based on the reservoir engineers, the values of reservoir pressure and water cut at no flow point were obtained, 3800 psia and 64% respectively.

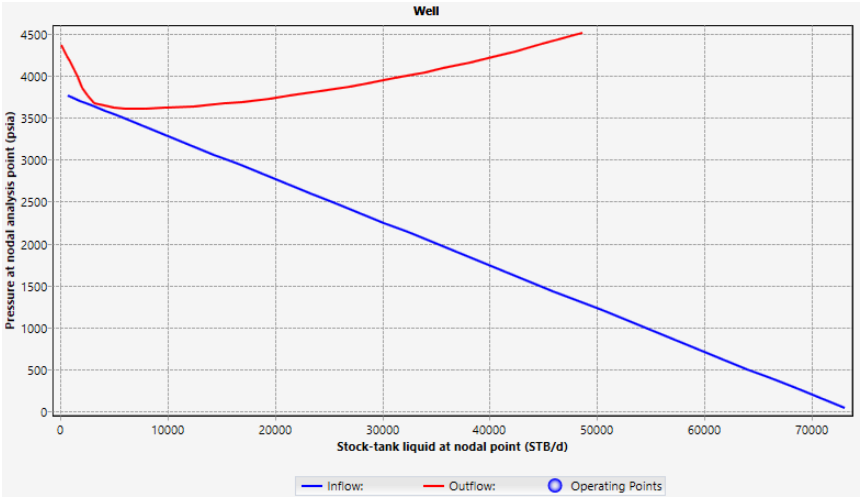

Figure 87. No operating point for lower reservoir pressure and increased WC.

The goal of this study is to create the optimum gas lift model. It is achieved by conducting sensitivity analysis for different cases. Table 23 and Fig. 88-89 show the case of changing production rate and operating pressure by increasing the injection rate of the gas lift.

Table 22. Sensitivity analysis for different gas injection rates.

Gas Lift Injection rate $(10^3\ m^3/d)$	**Production rate** (STB/d)	**Pressure at NA** $(psia)$
0	-	-
5	5509	3516
10	6673	3456
25	8874	3343
50	11 084	3229
75	12 610	3150
100	13 760	3091
150	15 420	3006
200	16 516	2949
250	17 258	2911
300	17 771	2885
350	18 142	2865
400	18 379	2853
450	18 539	2845
500	18 634	2840
550	18 681	2838
600	18 702	2837

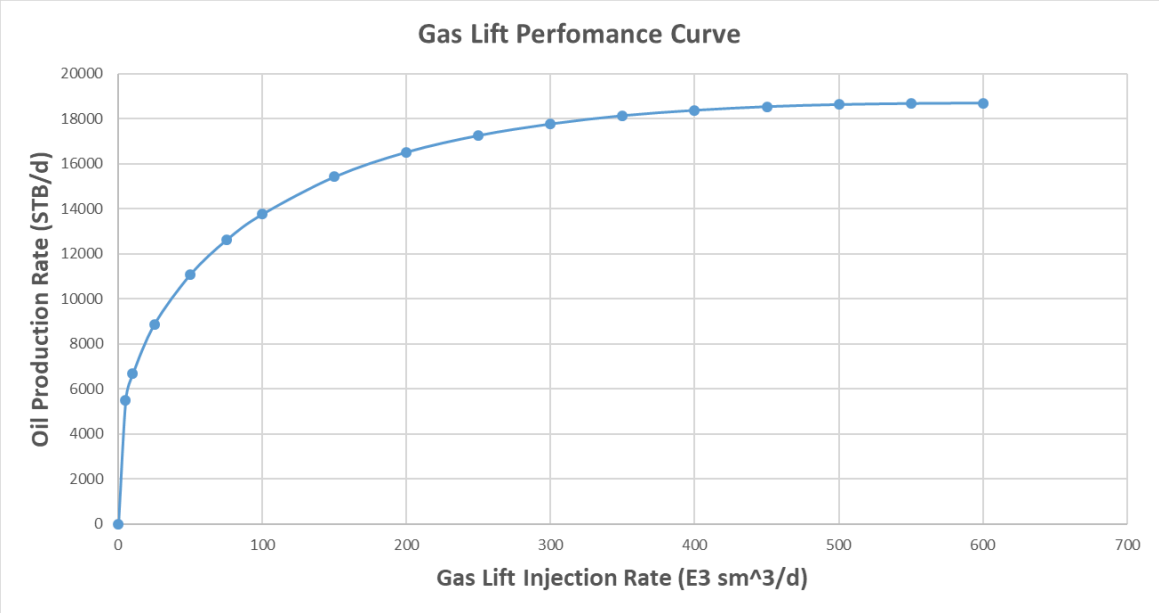

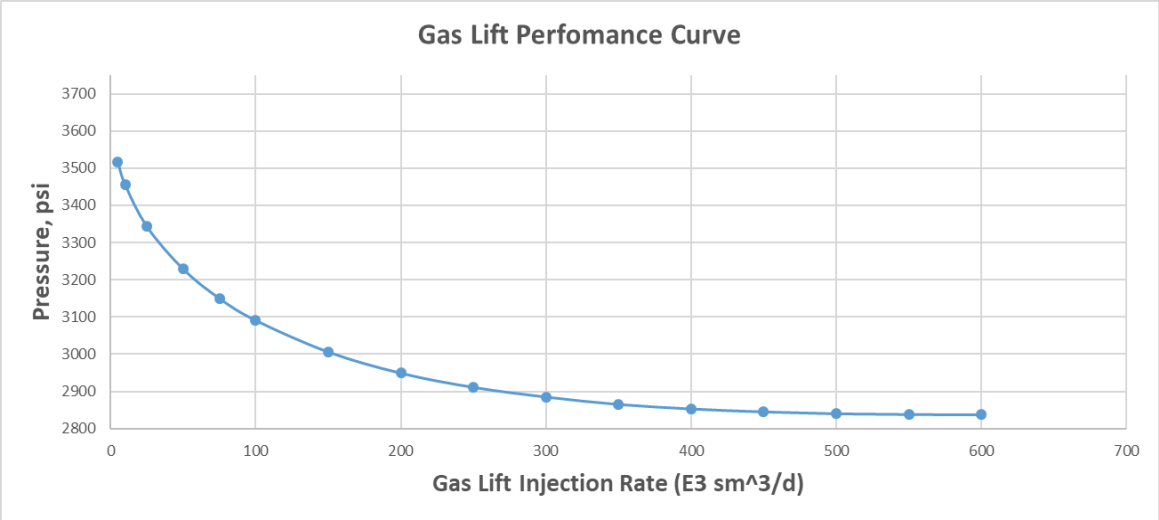

Figure 88-89. Gas lift performance curve.

Gas lift performance curve shows the optimization plot for gas lift made in Pipesim. Comparing the Figure 90, 91 and 92, the optimum injection rate to reach the best efficiency, including economical part, is considered to be 400E3 cubic meters of gas.

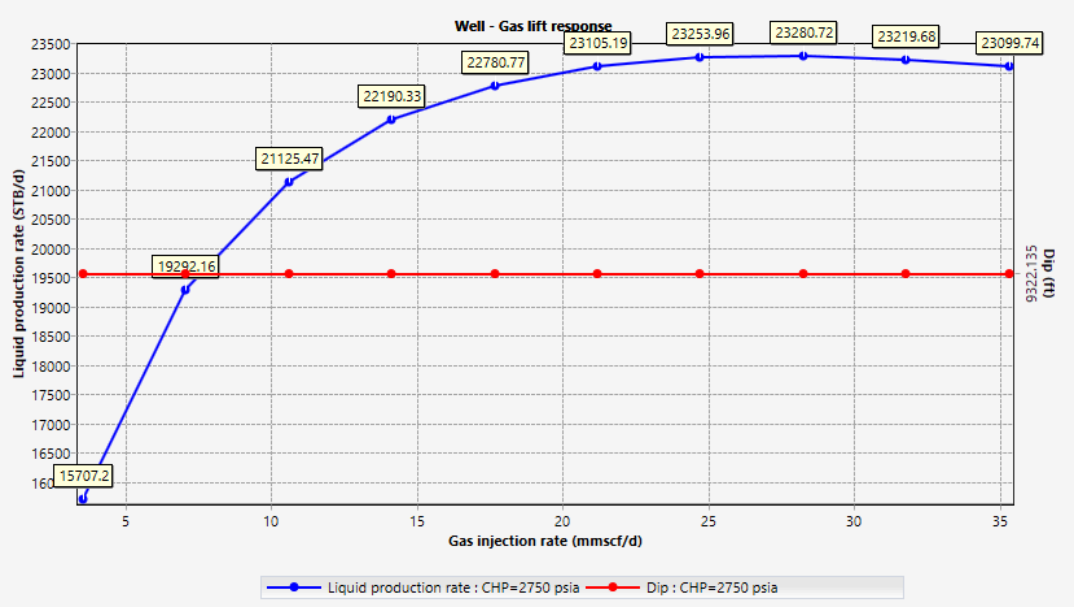

Figure 90. Gas Lift Optimization Plot.

Since the optimal gas lift injection rate was found, the next thing that should be defined is the deepest injection point. The plot below shows that the maximum allowable injection depth is 9151 ft TVD. The gas lift valve should be installed before this point.

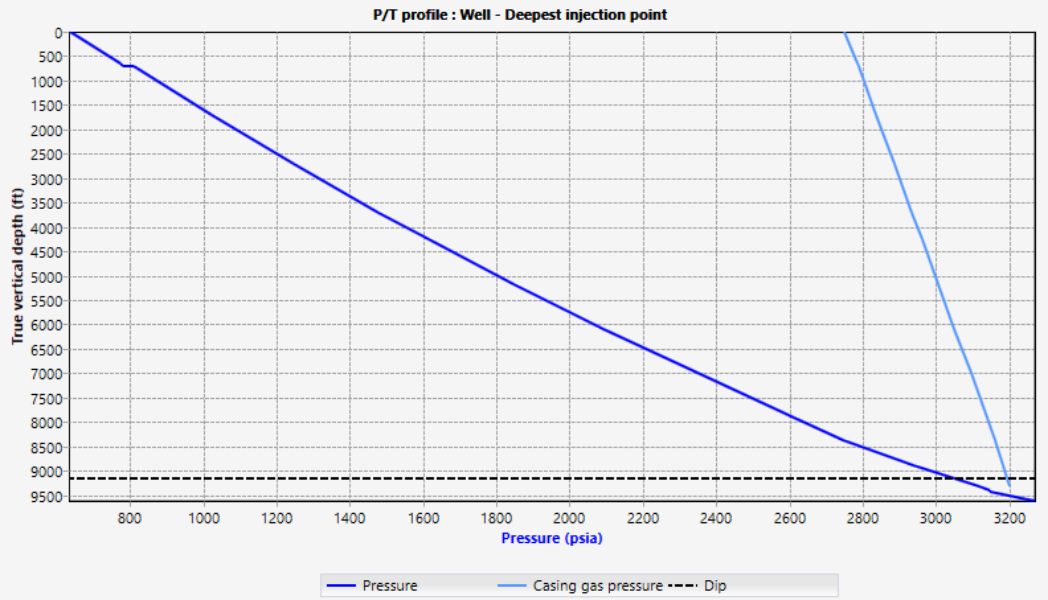

Figure 91. Deepest Injection Point (9151 ft).

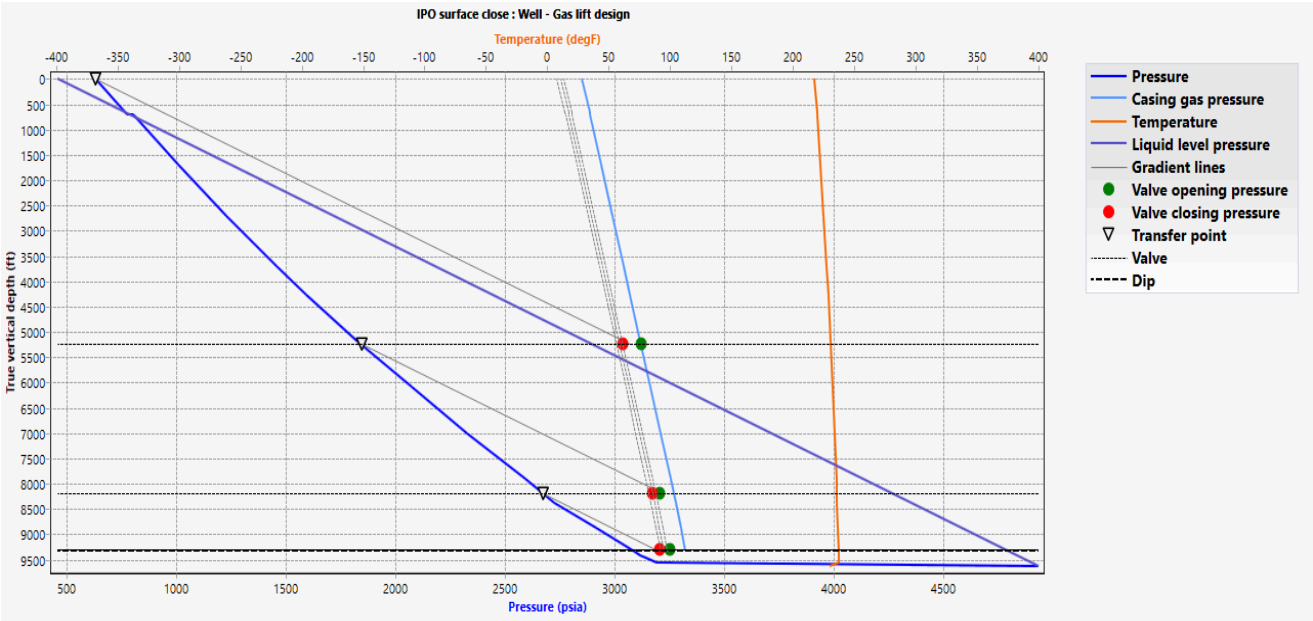

Figure 92. Gas lifts design plot.

The Pipesim offers "Gas Lift Design" analysis to identify the optimum numbers of gas lift valves and their installation depth. The plot above illustrates that three valves should be implemented based on the model properties. The first valve is recommended to be located on the 5250 ft TVD depth, while the second valve is located on 8180 ft TVD. The third valve is near the deepest injection point (DIP). The second and third valve should be discarded. The literature

review states that for producer wells, F-12, F-14 and F-15, a single gas lift valve system was used. The suggestion of Pipesim valve design should be discarded. The deep installed gas lift valve has several limitations, and one of them is difficulty to keep gas injection pressure at high values to reach deeper valves.

6.1.3. Implementation of Electrical Submersible Pump

ESP is the most suitable for use during the development of high-flow oil wells. With high values of the production rate (from 100 to 500 cubic meters per day and above), use of centrifugal pumps ensures maximum efficiency of the process, which at the same time requires the least effort for equipment maintenance. For ESP, there are a number of criteria that determine the possibility of their use. Among the mandatory conditions, work must be carried out with WC ratio no more than 99% and no more than 0.01% solid particles (sand) (Bagci, 2010). The Volve field has no issues with sand production, that means ESP could be implemented. Pipesim offers many types of ESPs based on manufacturers and min/max flow rate. Optimal pump type (REDA H22500N) was selected for flow rate between 20,000 and 30,000 STB/D. The plot below shows the performance of this type of ESP. At the same conditions as simulated for gas lift, 3800 psi reservoir pressure and 64% water cut, the project runned with implemented ESP. The nodal analysis gives the operation rate as 24,000 STB/D and operating pressure as 3572 psia above bubble point.

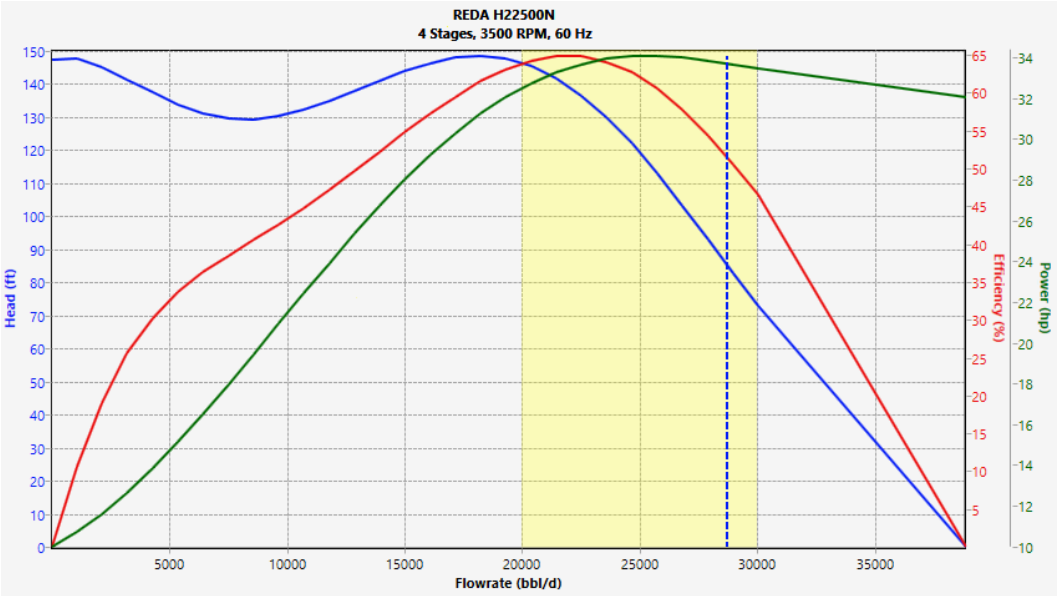

Figure 93. ESP Performance Curve (REDA H22500N).

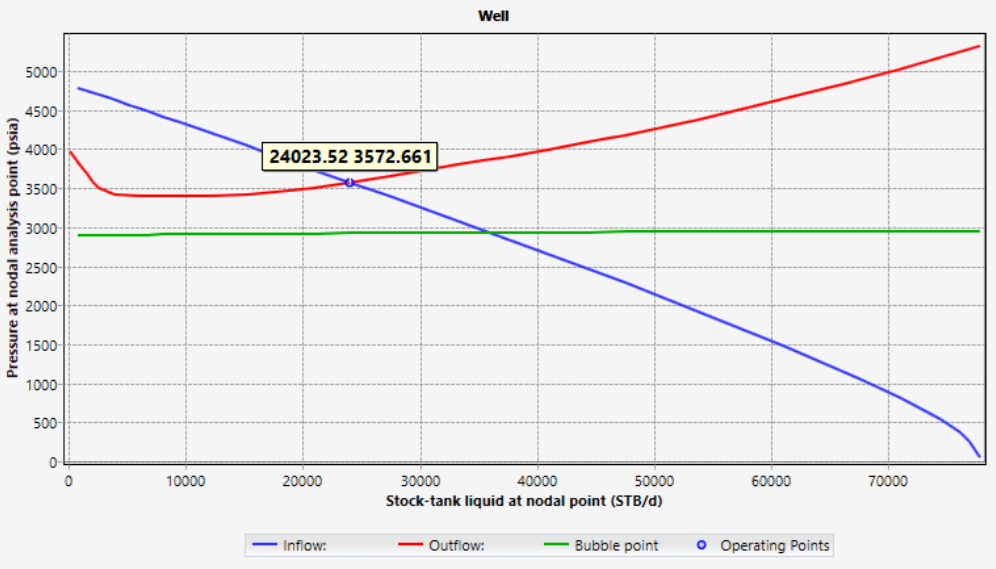

Figure 94. Nodal Analysis for ESP.

The main variables that affect to the performance of the ESP are:

- Power
- Number of Stages
- Frequency of electric current

The sensitivity analysis was conducted for each input variable of ESP. The outputs were shown in the figures below.

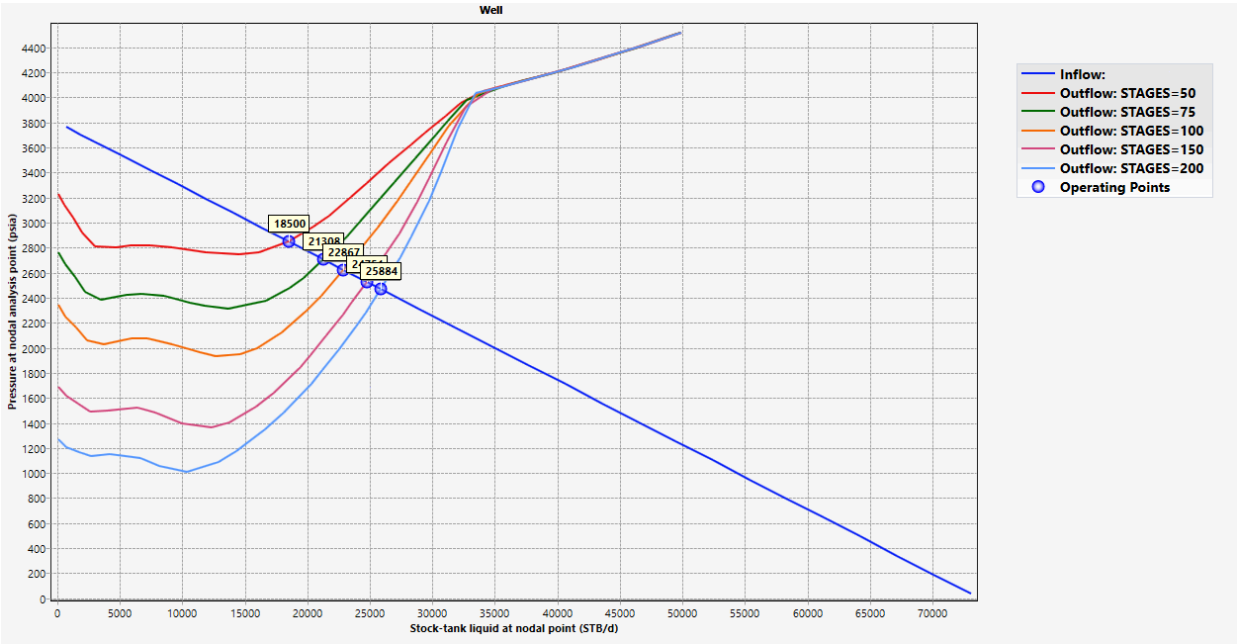

Figure 95. Different Stage number.

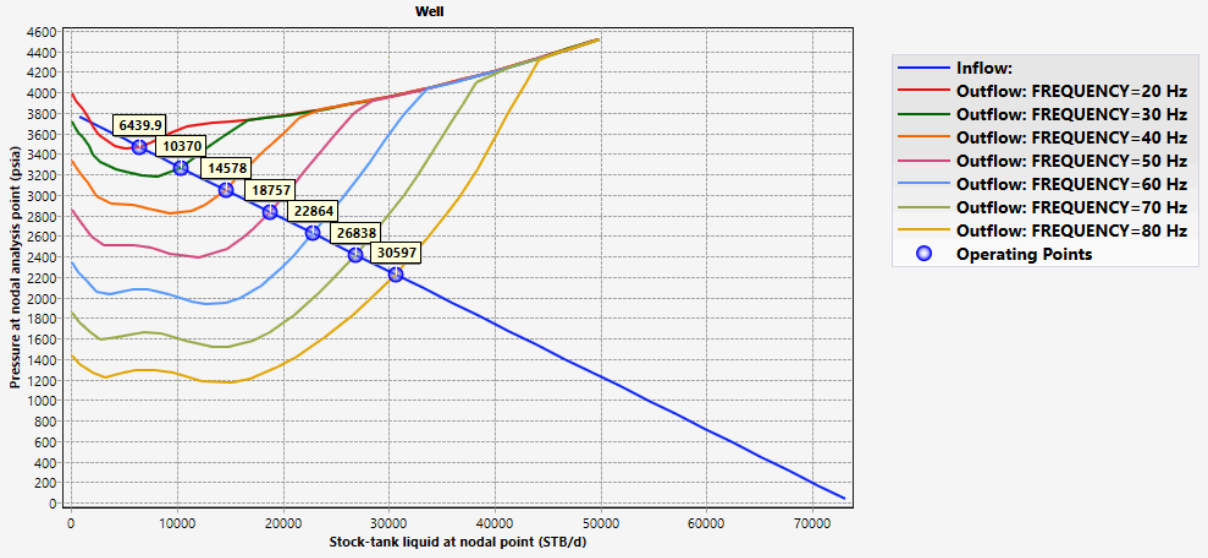

Figure 96. Different Frequency.

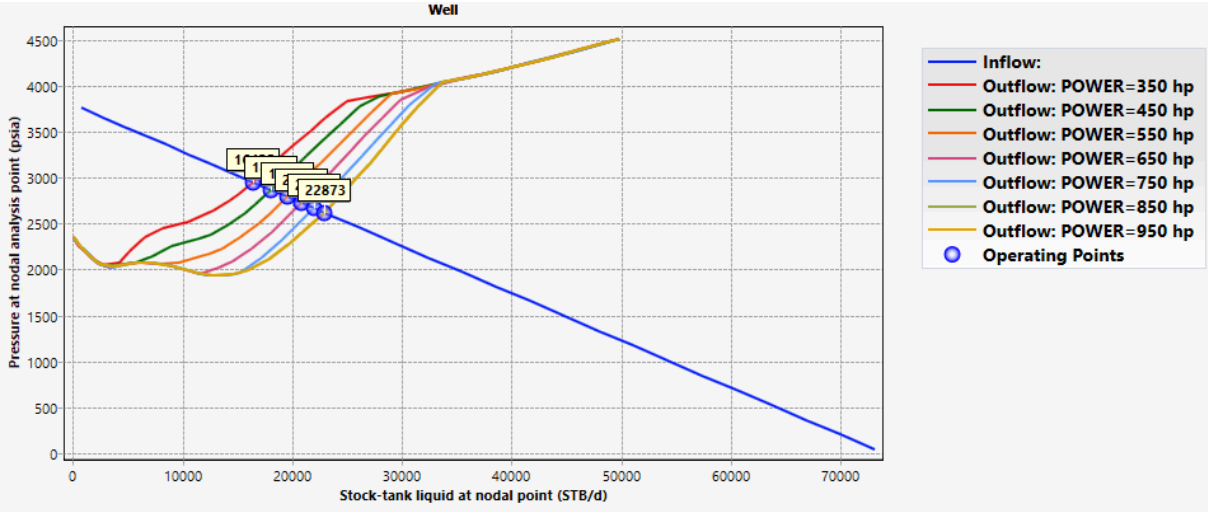

	Operating point	ST Liq. at NA	P at NA
		STB/d	psia
1	POWER=350 h...	16425.42	2954.332
2	POWER=450 h...	18088.33	2868.716
3	POWER=550 h...	19526.17	2794.688
4	POWER=650 h...	20798.55	2729.179
5	POWER=750 h...	21944.76	2670.166
6	POWER=850 h...	22872.67	2622.393
7	POWER=950 h...	22872.67	2622.393

Figure 97. Different Power.

Table 23. Sensitivity analysis for ESP artificial lift.

Parameter	**Effect**
Number of Stages	With an increasing number of stages, the production rate generally increases.
Power increase	With increasing motor power, the production rate can increase, but up to 850 HP
Frequency	Flow rate increases proportionally within design limits.

Comparative analysis should be done for both artificial lift methods. ESP results outperform the outputs of the gas lift method. The higher production was obtained by implementing an electric submersible pump. The optimum design for ESP is 850 horsepower, 60 hz frequency and 100 stage number while the optimum design for gas lift is 400E3 cubic meters

per day injection rate and 5250-6000 ft installation depth. Table 44 also states that ESP implementation is economically efficient. However, the repair works and run life of ESP should be taken into consideration. ESP fails more often, especially in wells with 650-750 scf/STB gas-oil-ratio.

6.1.4. Nodal Analysis for Water Injection Well

After the definition of the water injection well, the well completion model was constructed in the PIPESIM software to provide nodal analysis and sensitivity analysis for some of the properties that influence the water injection flow rate into the layer.

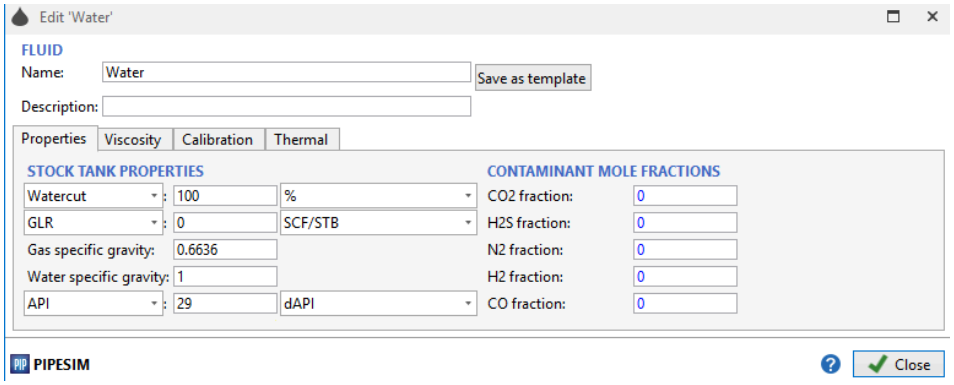

Figure 98. Fluid model for water injector well.

The figure above demonstrates the fluid model of the fluid used to inject into the layer, where 100% water was defined with no other components. The water specific gravity is 1.

Subsequently, after the stages of creating completion scheme and fluid model definition, the nodal analysis can be done in order to identify optimum injection rate and the pressure value. The inlet pressure was set at 635 psia.

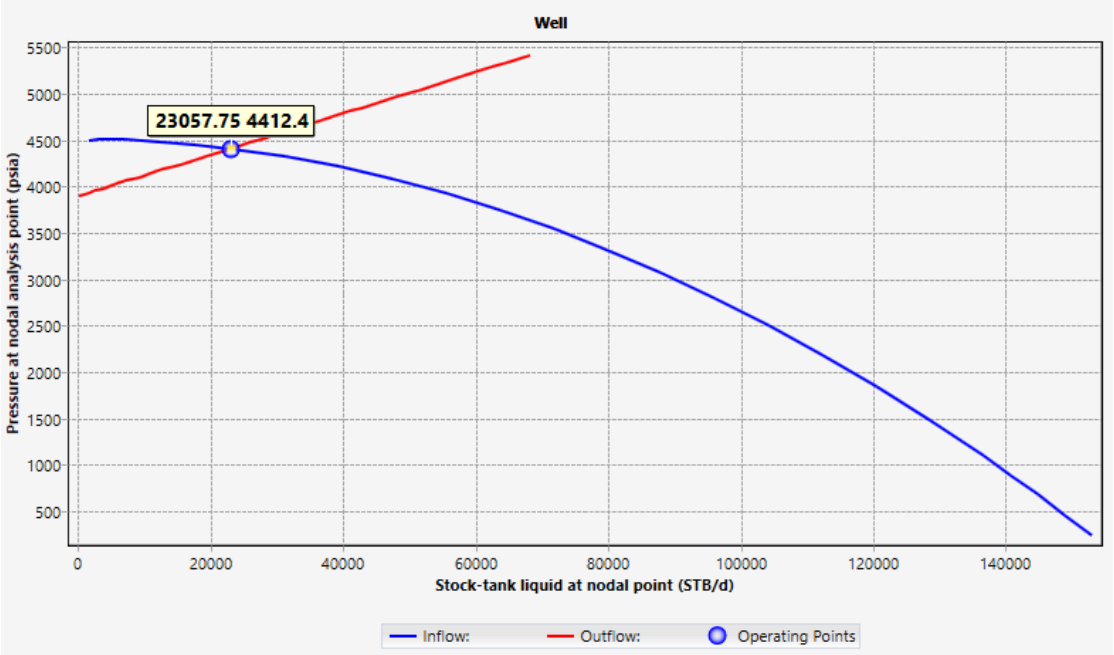

Figure 99. Operating point for water injection well.

The results of the nodal analysis are presented in the Figure above. The intersection of IPR and TPR curves gives that the optimum injection rate is 23058 STB/day, while the pressure is 4412 psia. This means that in the reservoir modelling it should be set that the water injection well should have a value of around 23000 STB/day to give the appropriate results at the end.

The sensitivity analysis for the water injection well includes analyzing the effect of tubing inner diameter and liquid injectivity index. The results of changing the tubing size are presented in Figure 100 and Table 22. They state that as the inner diameter of the tubing increases, the injection liquid rate that passes through it also rises. Similarly, the increase in tubing size causes operating pressure to increase as well. As a result, it is better for engineers to have a larger inner diameter of the tubing to inject water as effectively as possible.

Table 24. Tubing diameter sensitivity analysis values.

Tubing inner diameter, in	**Liquid rate, STB/day**	**Pressure, psia**
3	7786.916	4073.221

3.5	10757.7	4139.509
4	13815.46	4207.119
4.5	16713.89	4271.442
5	19286.61	4327.939
5.5	21395	4375.244
6	23059.9	4412.381

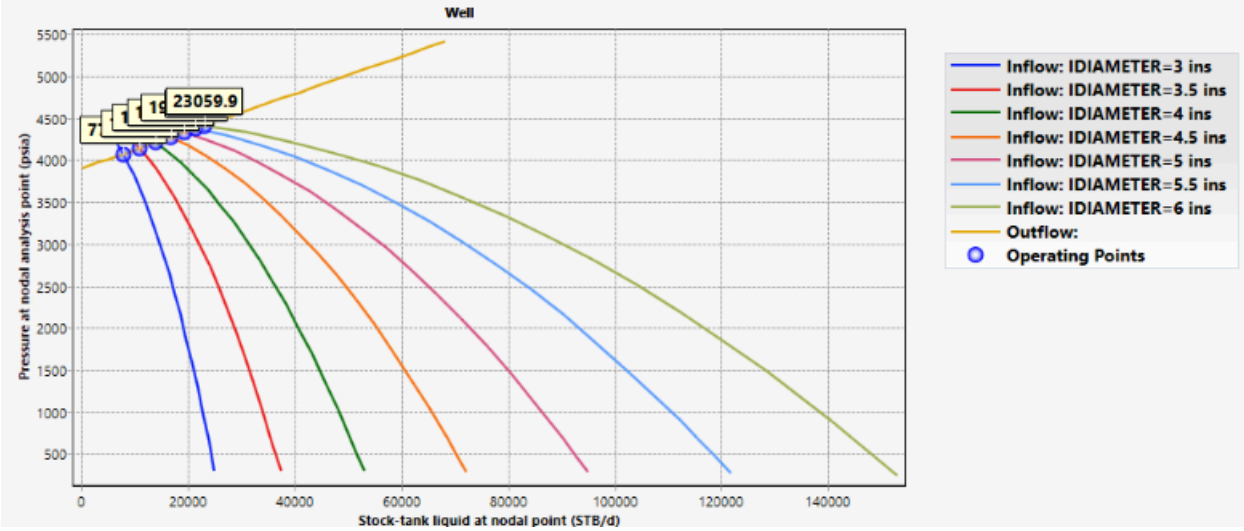

Figure 100. Tubing inner diameter sensitivity test.

The results of the liquid injectivity index sensitivity test are presented in Figure 101. The figure demonstrates that as the injectivity index increases from 1 stb/day/psi to 100 stb/day/psi, the operating injection flow rate increases in value. Conversely, the operating injection pressure declines when the injectivity index increases from 1 stb/day/psi to 100 stb/day/psi. This implies that in order to have better injectivity results, it is better for engineers to have a higher liquid injectivity index.

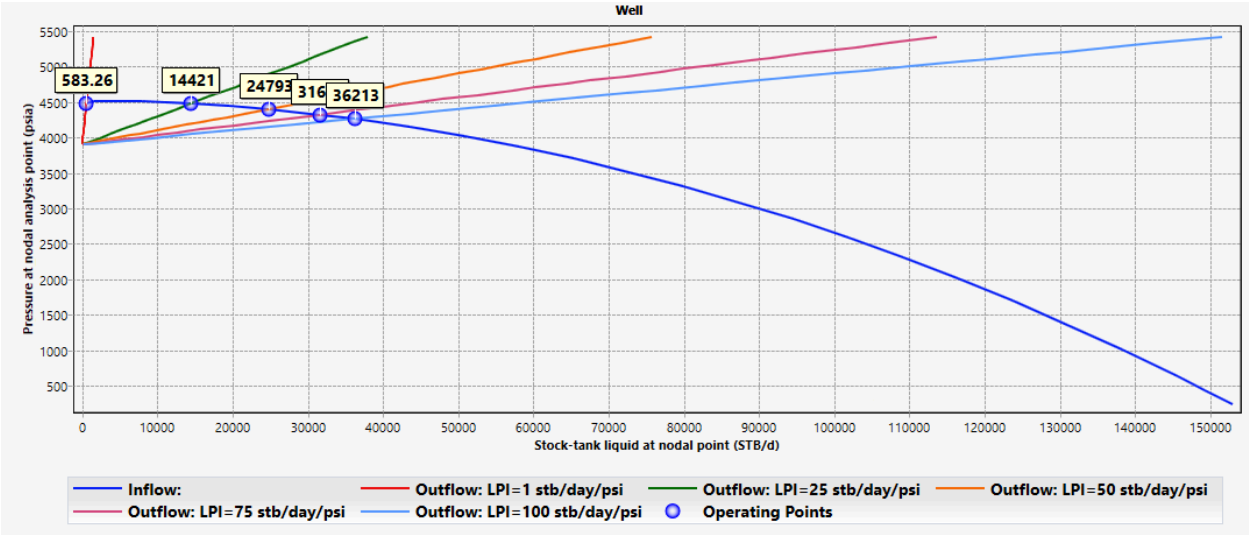

Figure 101. Liquid injectivity index sensitivity analysis.

6.2. Production Engineering. Implementation of Machine Learning

The Equinor database comprises daily and monthly oil and gas production data, featuring 15,634 samples across 24 variables from 7 wells over an 8-year period (2008-2016). Initially, the data were reviewed to assess the types of information available and to ensure consistency. Out of the 5 wells in the database, 3 were excluded due to having less than 3 years of data, leaving only wells F-12 and F-14 for the study. Additionally, daily production records showing zero (indicating a shut-in period) or values below 100 STBD were discarded to eliminate noisy data. The data file was loaded to the pandas data frame and analyzed. Some variables were dropped based on those correlations and the usability of the measure to predict oil and gas production. The resulting cleaned data had the choke size, well head pressure, downhole pressure, pressure at choke, tubing pressure difference, temperature, oil volume, gas volume, and water volume measures for two wells. Null values and shutdown period rows were dropped. Categorical columns were also not taken into consideration. The train and test data were split randomly across data points from all wells in a 5:1 ratio. The models used as below:

6.2.1. Random Forest Regression (RFR)

Random Forest Regressor (RFR) is an ensemble learning method that constructs multiple decision trees and aggregates their outputs to improve predictive performance and reduce

overfitting (Breiman, 2001). The model follows a bagging (Bootstrap Aggregating) approach, where each tree is trained on a different bootstrap sample of the original dataset. Given a set of training data points $\{(x_i, y_i)\}_{i=1}^{n}$, the algorithm randomly selects subsets of data with replacement and builds decision trees independently. The final prediction is obtained by averaging the outputs of all trees:

$$\hat{y} = 1/T \sum_{t=1}^{T} h_t(x) \tag{24}$$

where T represents the total number of trees, and $h_t(x)$ is the prediction made by the t-th tree.

6.2.2. Extreme Gradient Boosting (XGBoost)

XGBoost (Extreme Gradient Boosting) is an optimized gradient boosting algorithm designed for high performance and efficiency. It extends traditional Gradient Boosting Machines (GBM) by incorporating second-order Taylor expansion to approximate the loss function, making training more accurate and stable (Chen & Guestrin, 2016). The objective function in XGBoost consists of a loss term and a regularization term:

$$L(\theta) = \sum_{i=1}^{n} l(y_i, \hat{y}_i) + \sum_{i=1}^{n} \Omega(f_t) \tag{25}$$

where, $l(y_i, \hat{y}_i)$ is the loss function (e.g., squared error for regression, log loss for classification), and $\Omega(f_t)$ represents the regularization term that penalizes model complexity. To improve computational efficiency, XGBoost introduces an advanced split-finding method based on histograms and uses column subsampling to reduce overfitting (Ke et al., 2017). The algorithm optimizes decision tree structure by maximizing the gain function:

$$Gain = 0.5[\frac{G_L^{\,2}}{H_L+\lambda} + \frac{G_R^{\,2}}{H_R+\lambda} - \frac{(G_L+G_R)^2}{H_L+H_R+\lambda}] - \gamma \tag{26}$$

where, G and H denote the first and second-order gradients of the loss function, and L and R refer to the left and right child nodes. These improvements make XGBoost faster and more scalable compared to traditional gradient boosting models, making it highly effective for structured data problems. These features will be implemented in the modeling.

6.2.3. Gradient Boosting Regressor (GBR)

GBR is an ensemble learning technique that sequentially builds decision trees, where each new tree corrects the errors of the previous ones by minimizing a differentiable loss function (Friedman, 2001). The model is mathematically expressed as:

$$F_m(x) = F_{m-1}(x) + \gamma h_m(x) \tag{27}$$

Where, $F_m(x)$ represents the boosted model at step m, $h_m(x)$ is the weak learner (typically a decision tree), and γ is the learning rate that regulates the contribution of each tree. At each iteration, the algorithm computes the negative gradient of the loss function with respect to the model's predictions from the previous step:

$$r_i^{(m)} = -\frac{dL(y_i, F_{m-1}(x_i))}{dF_{m-1}(x_i)} \tag{28}$$

These residuals serve as the target values for the next tree, which is trained to approximate them. The optimal weight for this new tree is found by minimizing:

$$\gamma_m = argmin \sum_{i=1}^{n} L(y_i, F_{m-1}(x_i) + \gamma h_m(x_i)) \tag{29}$$

GBR incorporates techniques like shrinkage (learning rate reduction), subsampling (stochastic gradient boosting), and tree complexity constraints to prevent overfitting (Hastie, Tibshirani, & Friedman, 2009). Unlike XGBoost, which employs second-order derivatives and advanced regularization, GBR relies solely on first-order gradient information, making it computationally simpler but less optimized for large-scale problems (Chen & Guestrin, 2016).

6.2.4. Artificial Neural Network (ANN)

Artificial Neural Network represents a machine learning model that draws its concept from the brain functions of a human. The structure contains synthetic neurons that are also known as units. A system of ANN consists of units which form integrated layers through arrangement. The number of units that make up such a layer can vary from one up to multiple millions based on how deep and sophisticated the neural network needs to be in generating hidden models from the dataset. ANN includes various layers with output layer, input layer and hidden layers as its main categories. Similar to human neural networks the outside world information streams through input layers so these information components are needed for analysis and learning. The input layer transports data through multiple hidden layers during information processing until reaching output results. ANN features an architecture that appears in Figure 102 below.

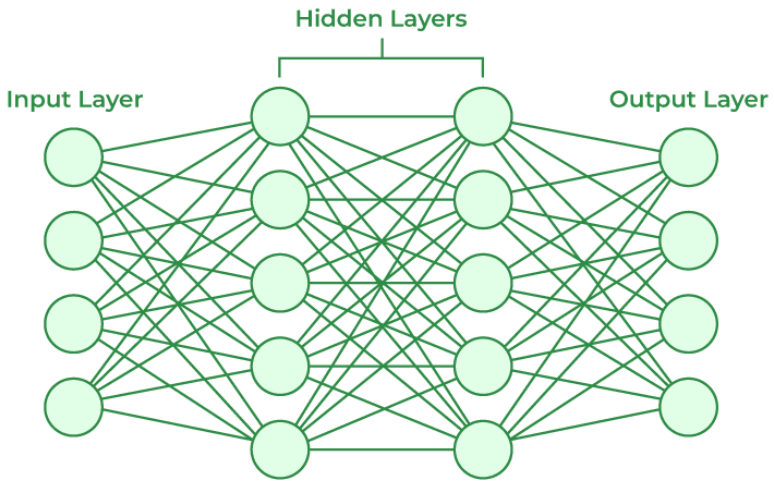

Figure 102. Connection between input, hidden and output layers [25].

6.2.5. Multilayer perceptron (MLP)

Multilayer perceptron (MLP) is a subset of ANN. It is widely used for classification and regression tasks. There are several working models of MLP:

Forward propagation

In forward propagation information from the dataset flows from the input layer to the output layer, passing through hidden layers. Every neuron in the hidden layer processes in input follows:

1. Weighted sum: the neuron computers the weighted sum of all input data.

$$z = \Sigma_i w_i x_i + b \ [25] ,$$

(30)

Where, x_i is an input feature, w_i is a corresponding weight, b is a bias term.

2. Activation function: main goal is to introduce linearity by activation function of weighted sum z. Common activation function include:

- Sigmoid:

$$\sigma(z) = \frac{1}{1+e^{-z}}$$

(31)

- ReLu (Rectified Linear Unit):

$$f(z) = max\,(0, z)$$

(32)

- Tanh (Hyperbolic Tangent):

$$tanh(z) = \frac{2}{1+e^{-2z}} - 1$$

(33)

Optimization

The training procedure of MLPs performs an iterative process where optimization algorithms adjust the biases and sum z weights. This project employs Adam optimizer as a methodology during this implementation.

The Adam optimizer extends the SGD to include adaptive learning features combined with momentum for achieving better training results.

$$m_t = \beta_1 m_{t-1} + (1 + \beta_1) * g_t$$

(34)

$$v_t = \beta_2 v_{t-1} + (1 + \beta_2) * g^2_t \quad (35)$$

Here, g^2_t indicates gradient at time t, β_1/β_2 are decay rates.

6.3.6. Batch size

Batch size is another hyperparameter in the neural network training that determines the number of samples processed before the model's parameters are updated. A larger batch size results in faster processing and better utilization of hardware resources, but a smaller batch size provides a more fine-grained update to the model's parameters. A common batch size is 32, 64, or 128, although the optimal batch size depends on the size of the dataset, the complexity of the model, and the amount of available memory. A batch size that is too small can lead to slow convergence, as the model's parameters are updated infrequently, while a batch size that is too large can cause memory issues or stability problems during training. The batch size can have a significant impact on the model's performance and its ability to generalize to new data, so it's important to experiment with different batch sizes to find the best value for a specific use case.

6.2.6. Objective Functions

Machine learning algorithms try to minimize (or maximize) the objective function. A widely used and simple objective function in supervised learning is the summation of all the differences between predicted values and the actual values of the output. Since the summation of positive and negative errors may cancel out each other, a square or absolute value function can be used. Objective function is sometimes called cost function, error function or loss function and is quantifying how the entire model performs for a given set of weights. Table 2-3 shows the most popular objective functions in a supervised regression problem.

Table 25. Objective function equations.

Objective Function Name	Equation
Mean Absolute Error (MAE)	$J = \frac{1}{m}\sum^{m} \lvert y_{actual} - y_{predicted} \rvert$

	(36)
Mean Squared Error (MSE)	$J = \frac{1}{m}\sum^{m}(y_{actual} - y_{predicted})^2$ (37)
Mean Squared Log Error (MSLE)	$J = \frac{1}{m}\sum^{m}(log(1 + y_{actual}) - log(1 + y_{predicted}))^2$ (38)

Other metrics are utilized for classification problems, such as accuracy, precision, recall, and f1-score. Coefficient of determination (R^2) and the square root of mean squared error (RMSE) are metrics to judge the quality of the training and cannot be used as a cost function, but MAE, MSE, and MSLE could be used as metrics as well. Table shows the mathematical equations to calculate R^2 and RMSE

Table 26. Metrics Equation.

Metric Name	**Equation**
RMSE	$\sqrt{\frac{1}{m}\sum_{i=1}^{m}(y_i - \hat{y}_i)^2}$ (39)
R^2	$1 - \frac{\sum_{i=1}^{m}(y_i - \hat{y}_i)^2}{\sum_{i=1}^{m}(y_i - \bar{y}_i)^2}$ (40)

6.2.7. Machine Learning Results

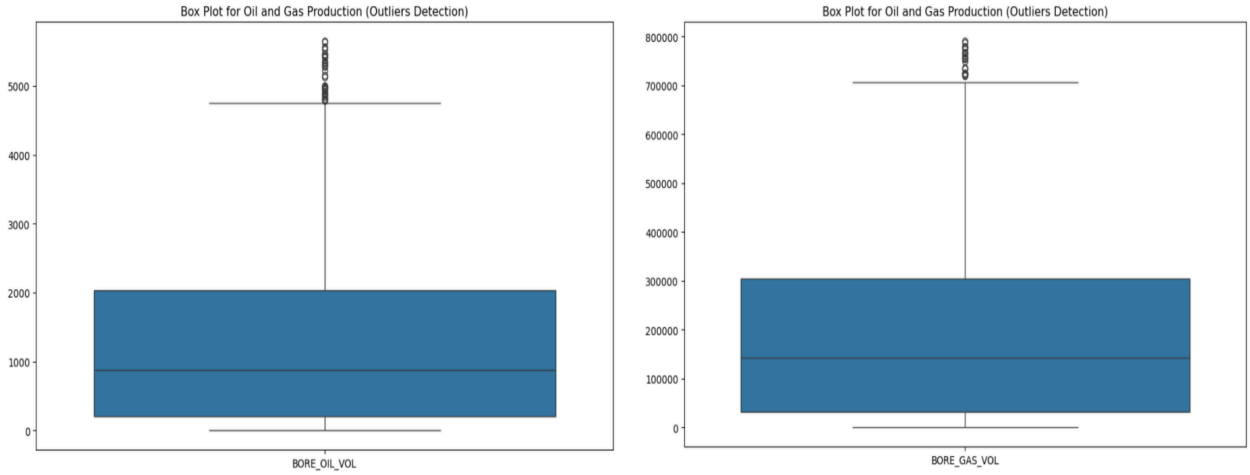

Figure 103. Outlier Detection.

The outliers were identified and it was decided to remain them since these outliers were considered as natural data.

All three regression models (RFR, GBR, and XGBoost) were optimized using RandomizedSearchCV with 20 iterations and 3-fold cross-validation, scoring based on the R^2 metric.

In this study, ANN (MLP type) uses eight feature input nodes followed by three consecutively nested hidden layers with 128, 64 and 32 ReLU activation neurons and single-neuron output layer for regression. The model is compiled using Adam optimizer with 0.001 learning rate. The model is trained for 100 epochs with 32 batch size and 5:1 data split. Some problems occurred with large numbers of gas production, and it was overcomed by applying MinMaxScaler function.

Tables 18-21 and Figure 55 summarize the outcomes for both Well F-12 and Well F-14, covering the oil and gas phases. Additionally, the three metrics outlined in the "Validating the model" section are presented. Furthermore, Figures 56-83 display the predicted vs actual production values for both wells.

Table 27. Models of F-12 Oil Prediction

ML Models	Training	Test

	R^2	MAE	RMSE	R^2	MAE	RMSE
ANN	0.9641	183.01	304.57	0.9458	215.04	378.1
XGBoost	0.9938	80.565	128.0	0.9824	111.94	214.8
RFR	0.996	0.5117	0.7545	0.9632	1.2974	2.023
GBR	0.9966	65.39	93.79	0.9859	103.3	191.8

Table 28. Models of F-12 Gas Production

ML Models	Training			Test		
	R^2	MAE	RMSE	R^2	MAE	RMSE
ANN	0.9477	0.1800	0.2603	0.9323	0.1870	0.2979
XGBoost	0.9764	0.1132	0.1762	0.9538	0.1421	0.2393
RFR	0.9885	0.076	0.1228	0.9603	0.1188	0.2217
GBR	0.9881	0.0841	0.1253	0.9629	0.1274	0.2144

Table 29. Models of F-14 Oil Production

ML Models	Training			Test		
	R^2	MAE	RMSE	R^2	MAE	RMSE
ANN	0.9738	120.99	207.49	0.9718	127.68	220.43
XGBoost	0.9955	46.647	86.252	0.9873	72.684	147.61
RFR	0.9969	29.884	70.633	0.9851	66.094	160.12
GBR	0.9989	27.651	42.101	0.9909	61.69	124.88

Table 30. Models of F-14 Gas Production

ML Models	Training	Test

	R^2	MAE	RMSE	R^2	MAE	RMSE
ANN	0.9756	0.1205	0.1748	0.9677	0.1331	0.2078
XGBoost	0.9941	0.0554	0.0857	0.9840	0.0734	0.1462
RFR	0.9963	0.0242	0.0684	0.9697	0.0676	0.2011
GBR	0.9964	0.0447	0.0663	0.9843	0.0683	0.1446

This study faced the problem of overfitting for XGBoost and GBR classifiers when the first results showed a high difference in metrics between Training and Testing data. It happens because the model learns too much from the training data and the size of training data is too high. Several steps were taken to overcome this issue. For the GBR model, decreasing learning rate, reducing the sample size for each tree, more samples to split nodes and limiting tree depth helped to handle the overfitting. Since the XGBoost was more overfitted compared to the GBR, that's why more techniques were applied. It includes L1 (Lasso) and L2 (Ridge) regularizations. In the result, it was managed to reduce overfitting.

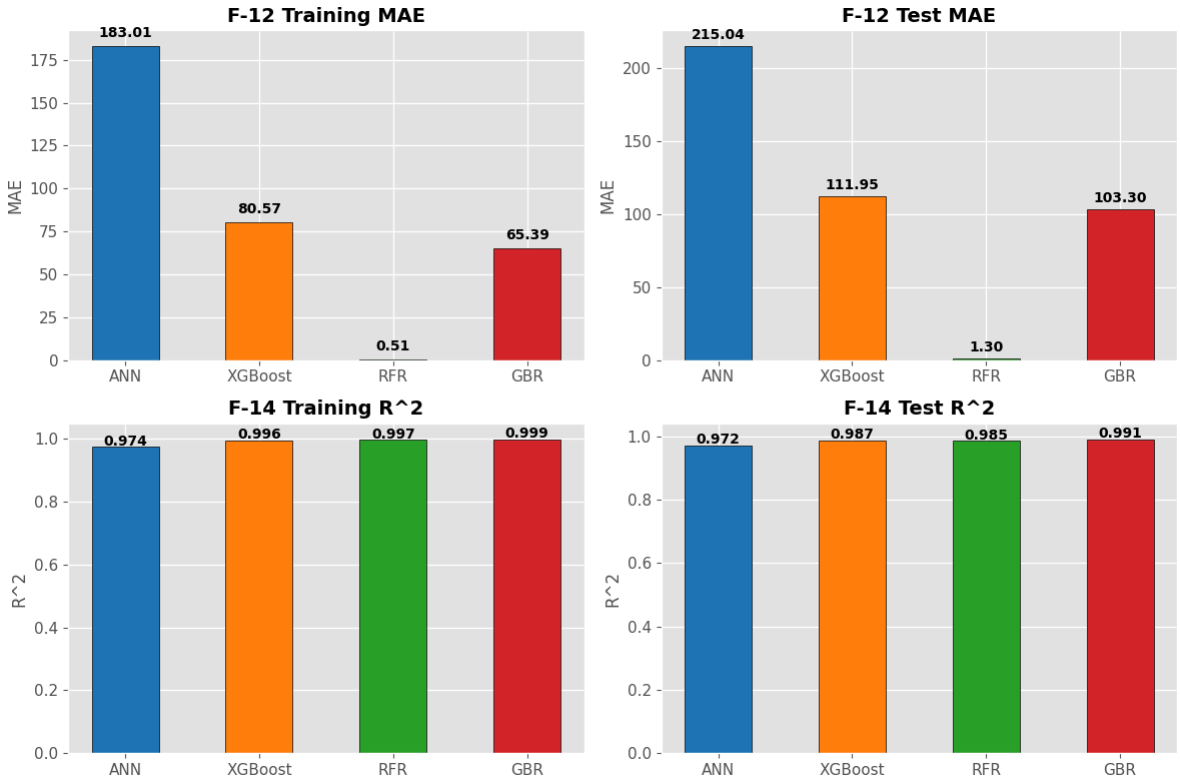

Figure 104. R2 _Score and MAE comparison for machine learning models used for the Volve field dataset.

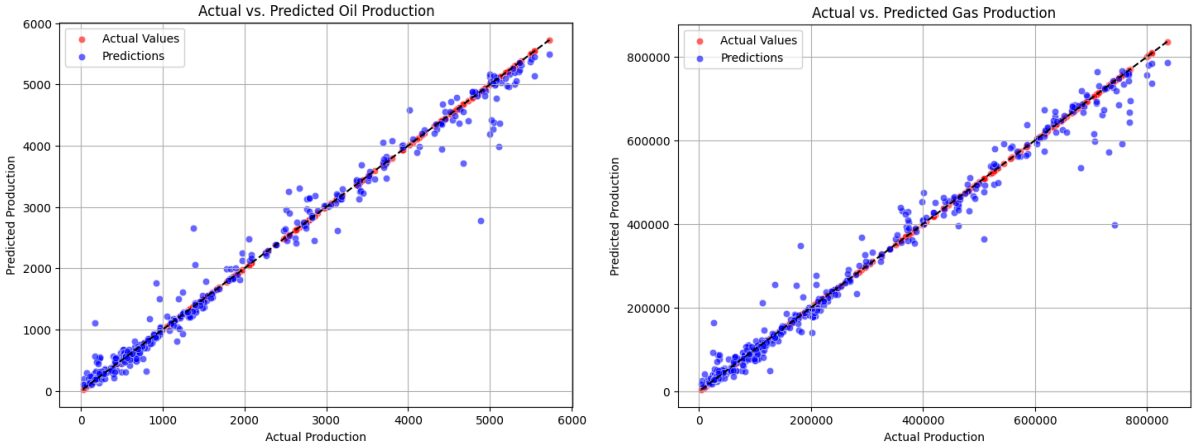

Figure 105-106. Test data (Real vs. Predicted) oil & gas production volume for Well-F-12 (RFR).

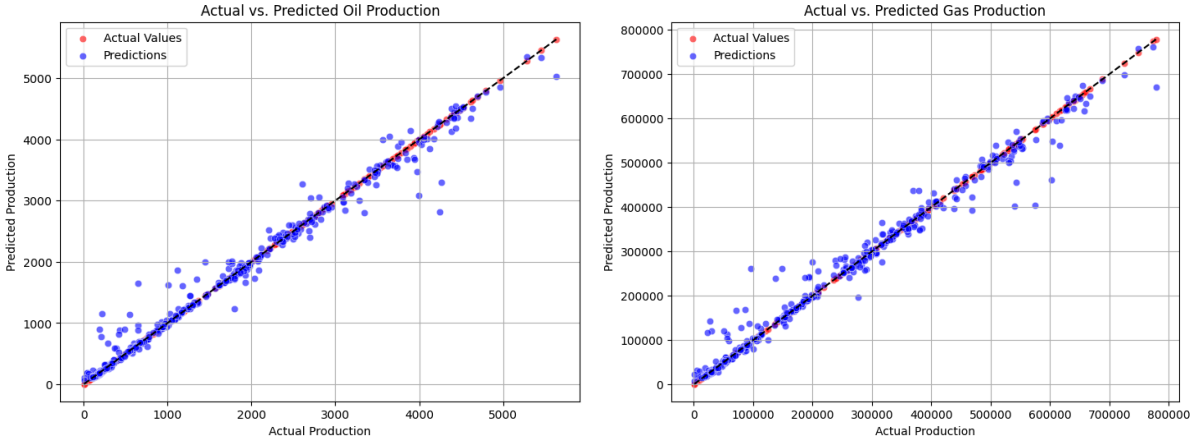

Figure 107-108. Test data (Real vs. Predicted) oil & gas production volume for Well-F-14 (RFR).

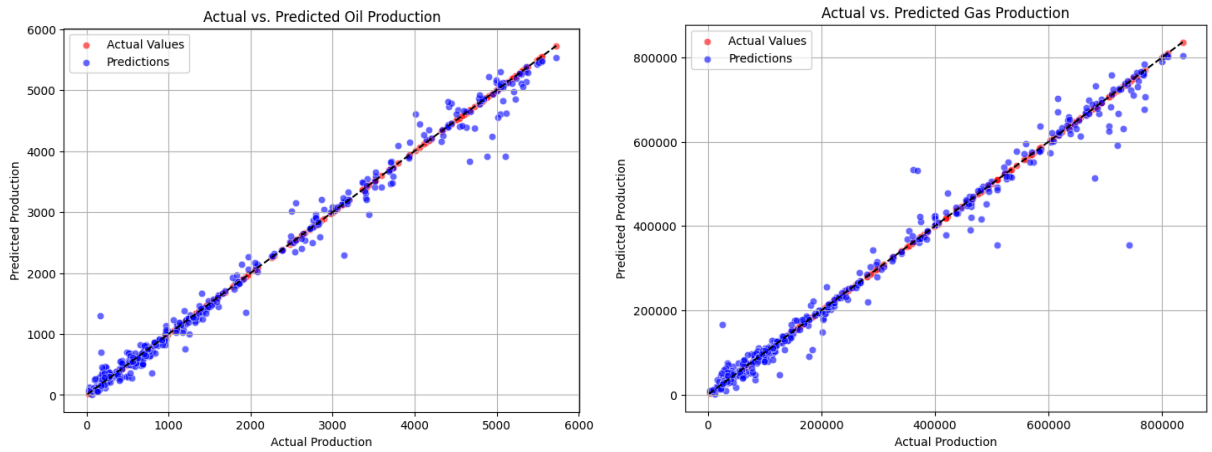

Figure 109-110. Test data (Real vs. Predicted) oil & gas production volume for Well-F-12 (GBR).

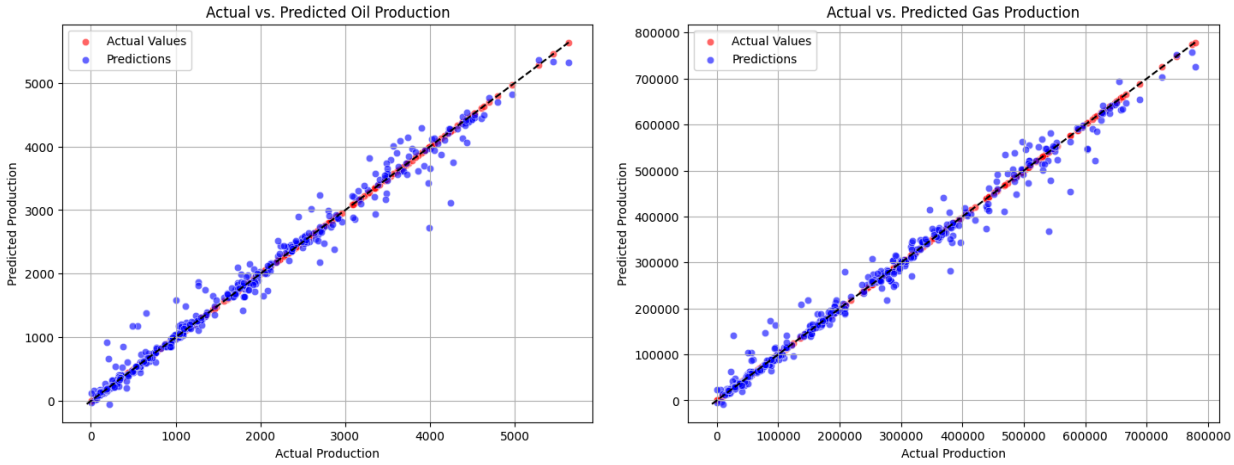

Figure 111-112. Test data (Real vs. Predicted) oil & gas production volume for Well-F-14 (GBR).

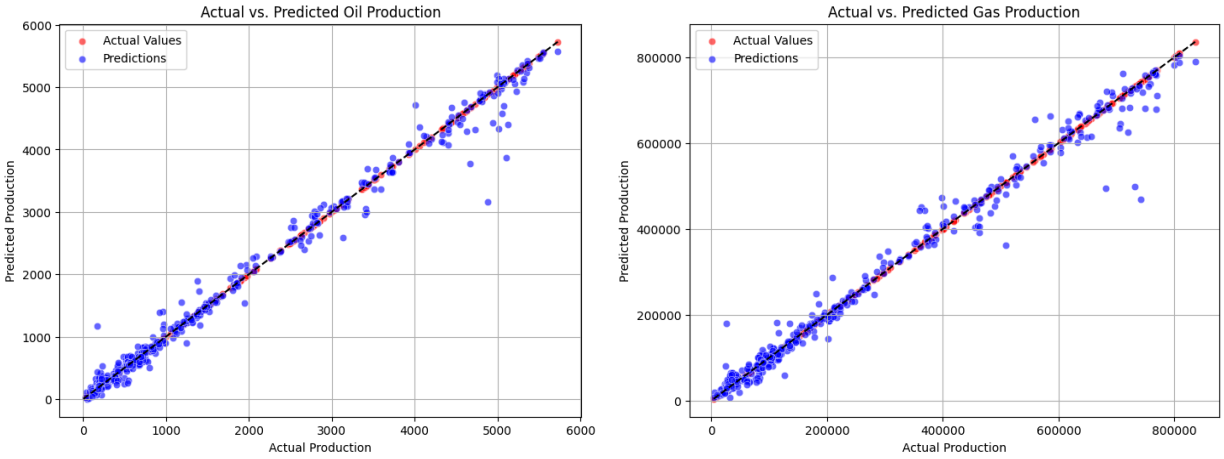

Figure 113-114. Test data (Real vs. Predicted) oil & gas production volume for Well-F-12 (XGB).

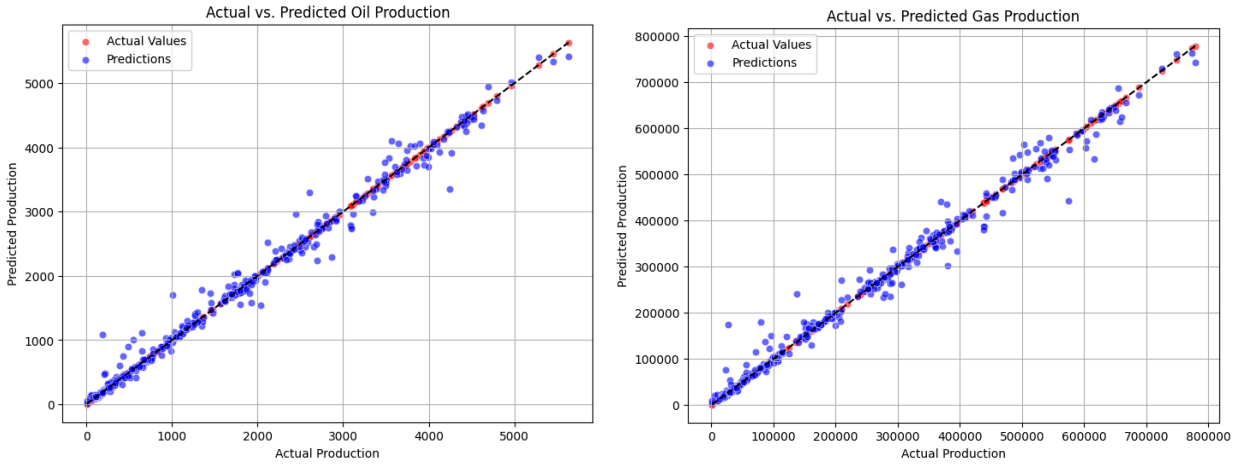

Figure 115-116. Test data (Real vs. Predicted) oil & gas production volume for Well-F-14 (XGB).

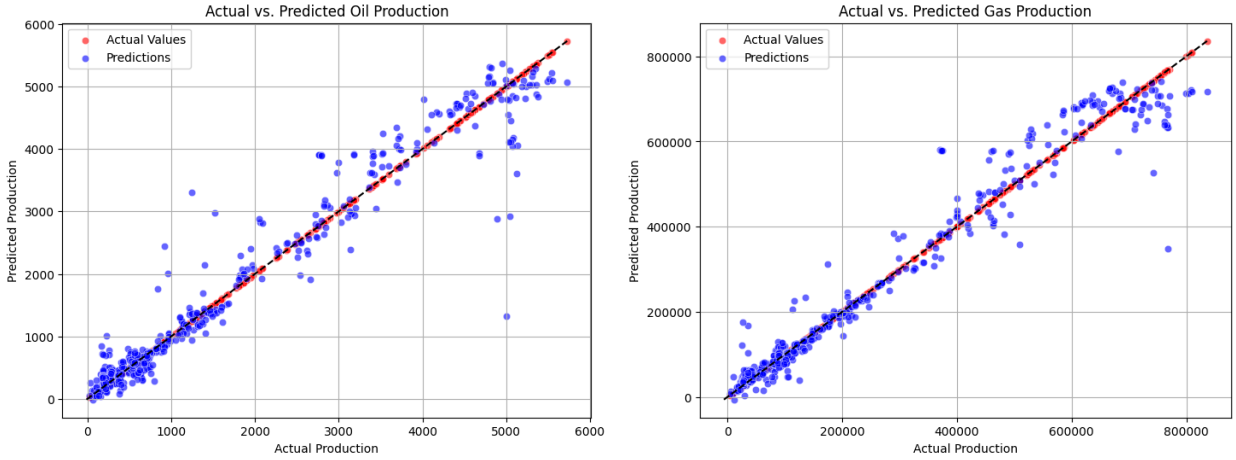

Figure 117-118. Test data (Real vs. Predicted) oil & gas production volume for Well-F-12 (ANN).

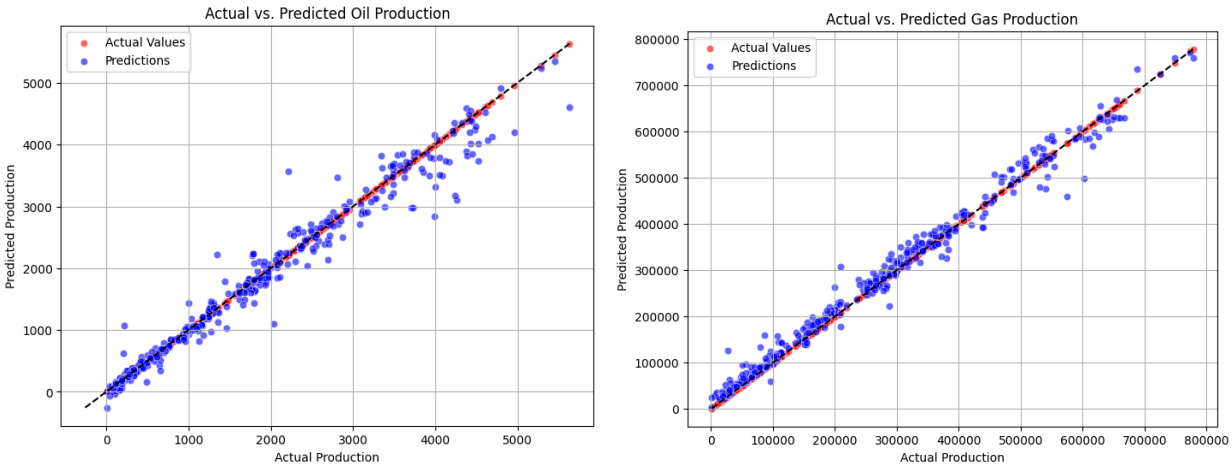

Figure 119-120. Test data (Real vs. Predicted) oil & gas production volume for Well-F-14 (ANN).

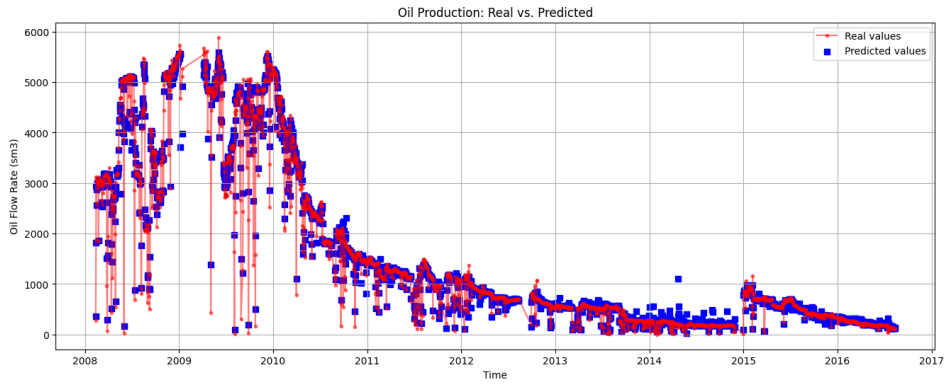

Figure 121. Test data (Real vs. Predicted) oil flow rate for Well-F-12 (RFR).

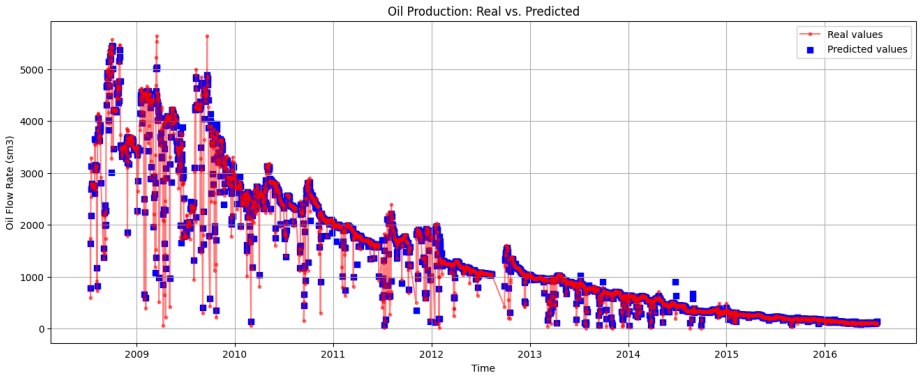

Figure 122. Test data (Real vs. Predicted) oil flow rate for Well-F-14 (RFR).

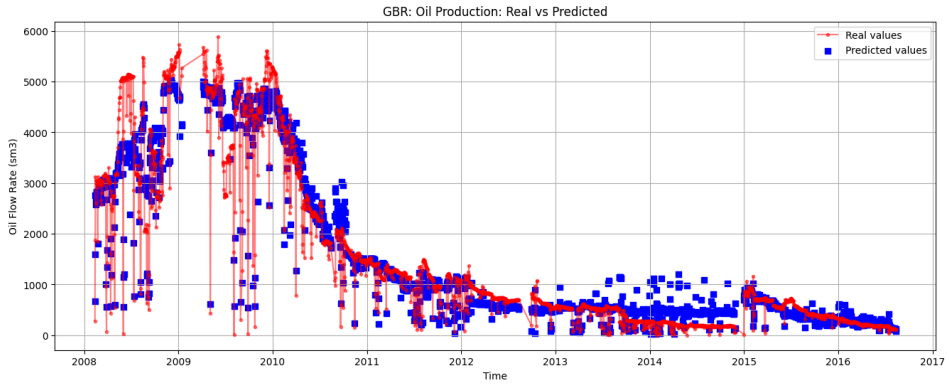

Figure 123. Test data (Real vs. Predicted) oil flow rate for Well-F-12 (GBR).

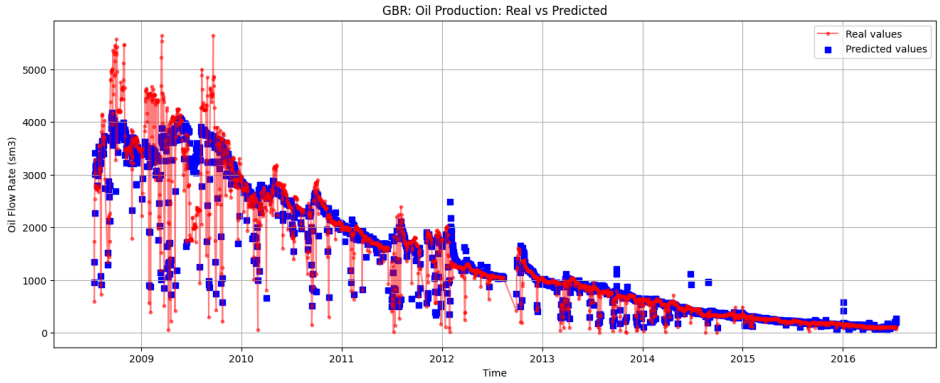

Figure 124. Test data (Real vs. Predicted) oil flow rate for Well-F-14 (GBR).

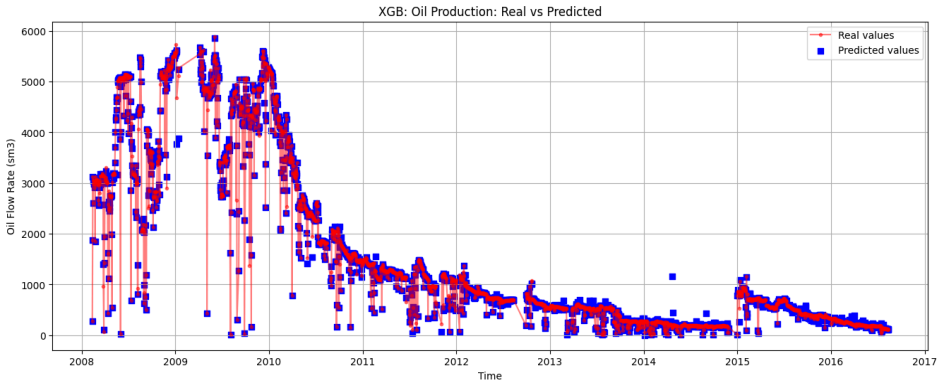

Figure 125. Test data (Real vs. Predicted) oil flow rate for Well-F-12 (XGB).

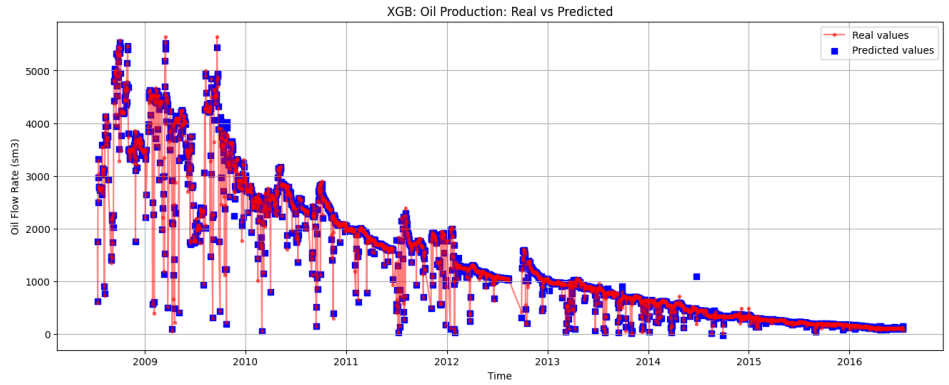

Figure 126. Test data (Real vs. Predicted) oil flow rate for Well-F-14 (XGB).

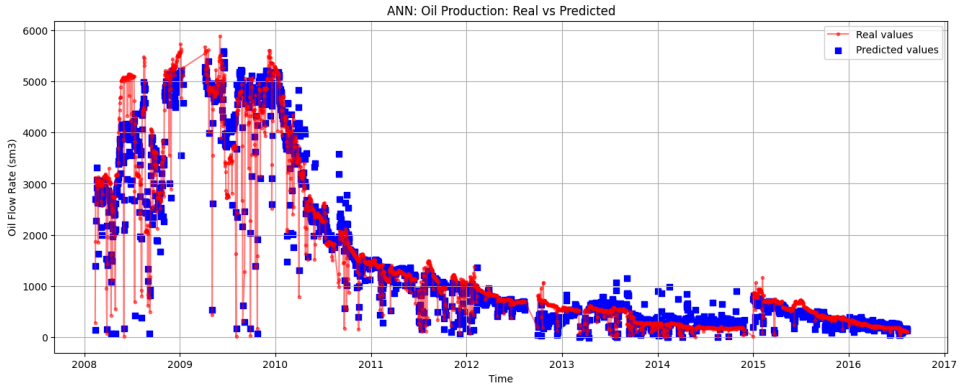

Figure 127. Test data (Real vs. Predicted) oil flow rate for Well-F-12 (ANN).

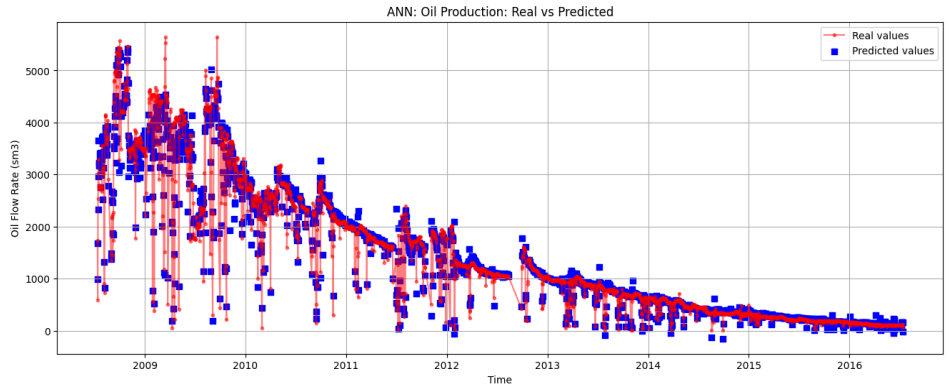

Figure 128. Test data (Real vs. Predicted) oil flow rate for Well-F-14 (ANN).

The comparative analysis of machine learning models for F-12 and F-14 oil and gas production shows that tree-based models, Random Forest Regressor, XGBoost and GBR, demonstrated the highest performance across training and testing phases. Despite that ANN showed not the best results, it is still competitive and has the least difference between train and test data. The training performance of the GBR-based model is practically excellent, while RF Regressor yielded the best outcome in the testing phase (almost perfect results for loss functions for F-12 oil prediction without overfitting). It also can be seen that the predictive performance of GBR and ANN (MLP) are slightly lower than others, since they did not show a close match of predicted data to actual data.

Time-based production data analysis through Python implementation gives significant insights. Periodic analysis of oil production together with Gas-Oil-Ratio and water-cut measurements from every production well was conducted throughout each month. Analysis of illustrations shows that oil production volumes decreased after 2010 along with decreasing water production volumes and may indicate the onset of water breakthrough.

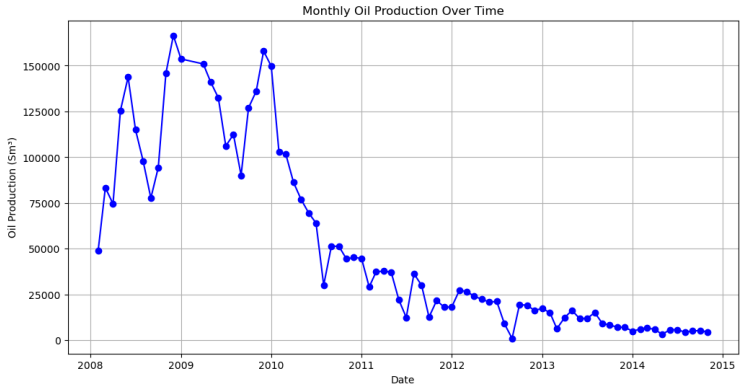

Figure 129. Monthly oil production.

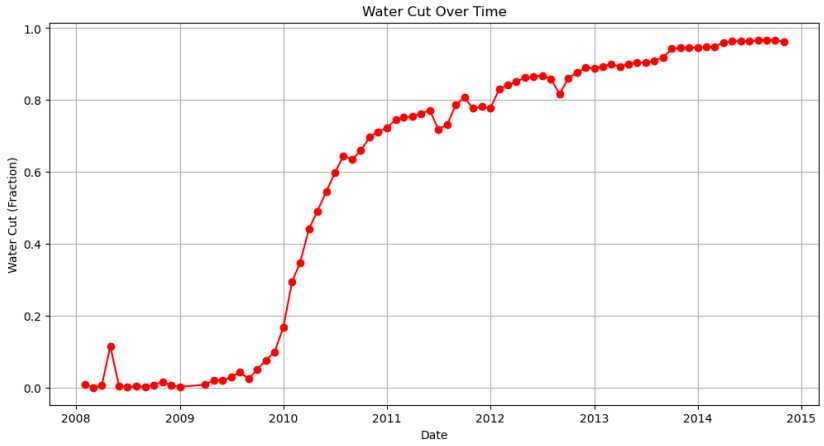

Figure 130. Monthly water cut.

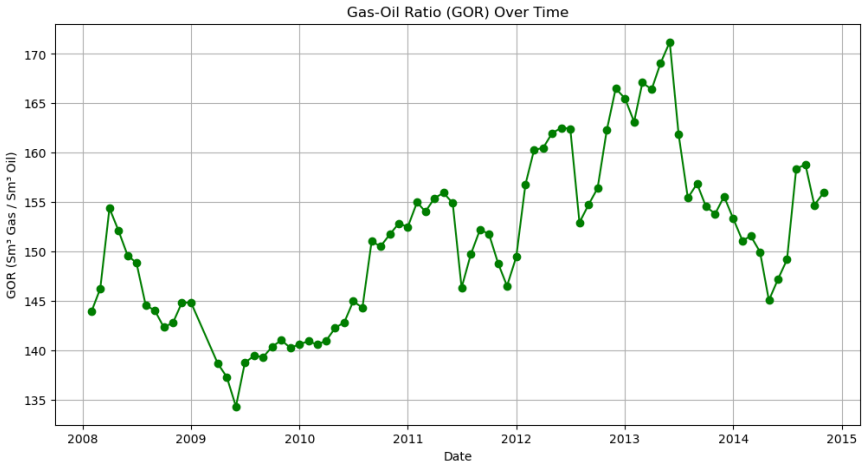

Figure 131. Monthly GOR.

Chapter VII

7.1. Economics

Economics is a crucial part of every project in the world. Companies start working if they are sure that they will get profit. Investors start investing in potentially profitable projects. All these factors are important in field development plan in the oil and gas industry. In the energetic segment prices of oil and gas are main factors which define project profitability. High prices will give high gains. Several factors are affecting oil prices to fluctuate. For instance, global crisis in 2008, pandemic of COVID-19 in 2020. They dropped oil prices, huge companies lost their income and millions of people were fired from their workplaces. It means that projects in industry are risky and need serious preparation. Another important factor is the cost of the project itself. Minimizing capital and operational costs of a project is a hard but needed operation. Minimal cost of the project will lead to a small payback period, if prices will be higher than average. These features of economics are important to make a field development of the Volve field.

The economic viability of the Volve field is assessed based on factors such as oil prices, production costs, and potential revenues. This low break-even point reflects the cost-conscious approach taken during development, including the decision to lease existing infrastructure, such as the Maersk Inspirer jack-up platform and the Navion Saga storage vessel, which helped reduce capital expenditure (CapEx).

7.1.1. Comparison between Kazakhstan and Norway taxation system

Kazakhstan:

The value of the tax base is determined by the value of crude oil, crude oil products, and gas condensate exported according to the valuation method used for the purposes of the Mineral Extraction Tax (MET). A tax rate at 7-32% is applied if global market prices for crude oil and its products reach more than $40 per barrel [13].

The tax rates are determined by the annual volume of production. The tax rates for oil are provided below:

Table 31. The tax rates for oil produced annually [13].

Annual production of oil, (thousand ton)	MET Rate (%)
Up to 250 (inclusive)	5
Up to 500 (inclusive)	7
Up to 1,000 (inclusive)	8
Up to 2,000 (inclusive)	9
Up to 3,000 (inclusive)	10
Up to 4,000 (inclusive)	11
Up to 5,000 (inclusive)	12
Up to 7,000 (inclusive)	13
Up to 10,000 (inclusive)	15
Over 10,000	18

Norway:

The Norwegian tax system is based on taxation of the entity rather than taxation of specific petroleum assets [14].

Direct taxes consists of:

- Corporate Incorporate Tax - 22%
- Special tax - 56%, which is applied on remaining of CIT.

As it is seen, the taxation system in Norway is strict, especially for the oil industry sector. For that case it is important to maximize profit by minimizing cost of the project.

7.1.2. Economical analysis

There are important formulas for calculating significant terms of economic analysis: Formula of gross profit (GP) (41) shows income from total revenue (TR), which already includes the cost of goods sold (COGS). Then it is important to know the earnings of the company before applying income tax depreciation (EBITDA) (42). To calculate EBITDA it is necessary to subtract total expense (TE) from gross profit. Formulas 43,44, 45 and 46 are closely related to each other. To obtain unlevered net income (UNI) it is needed to know depreciation (DE), or how much will the equipment lose in price during use in the project. Earnings before income tax

(EBIT) can be calculated by using formula 44. Then, it is necessary to use (45) calculate the income tax expense (ITE),where X is an EBIT at the appropriate period. By applying 22% of corporate income tax and 56% special tax regime, which is used in Norway. After making preparations it is possible to calculate the net income of the project by equation 6. Net working capital (NWC) is a reflection of the company to cover their short term obligations. Usually in the oil and gas industry NWC requires approximately 5%-10% of total revenue to cover expenses in a year. Change in NWC needed to calculate free cash flow (FCF) of the project. FCF (49) shows the amount of cash circulating in the project at the end of each year. Investors pay attention to the FCF values, because they are real and show the health of the company. Present value (PV) is the value of future money nowadays. Calculating PV includes risks and time. Formula (50) should be used to calculate PV, where r – discount rate in %, n – number of periods.

$$GP = TR - COGS \tag{41}$$

$$EBITDA = GP - TE \tag{42}$$

$$DE = \frac{Capital\ Expenditure}{years\ of\ project\ operation} \tag{43}$$

$$EBIT = EBITDA - DE \tag{44}$$

$$ITE = X * 22\% + (X - (X * 22\%)) * 56\% \tag{45}$$

$$UNI = EBIT - ITE \tag{46}$$

$$NWC = TR * 5\% \tag{47}$$

$$\Delta NWC = NWC_2 - NWC_1 \tag{48}$$

$$FCF = UNI + \Delta NWC + DE \tag{49}$$

$$PV = \frac{FCF*(1+g)}{r-g} \quad (50)$$

Net Present Value (NPV) is a sum of all present values minus initial investments. By applying NPV it is possible to see project potential: profitable or not;

NPV > 0, project is profitable;

NPV < 0, project is not profitable;

NPV = 0, break-even

IRR is an Internal Rate of Return, which indicates the average annual return a project is expected to generate over its lifespan.

IRR> r, project is profitable;

IRR< r, project is not profitable;

IRR= r, neutral, NPV=0;

Both values of NPV and IRR are easier to calculate in Excel software, to avoid unnecessary inaccuracies. This software is used to calculate other terms. All data was imported to Excel to conduct economic analysis. Plots are obtained by calculations in Excel software.

7.1.3. Volve field and CMG model economics

According to report data Volve field started operating in February 2008, however development and exploration of the field started in 2005. Till September 2016 Volve field was acting and operating, then in 2 years the company finished decommissioning the field. 6 wells operated for around 8 years, total amount of produced oil is estimated as 63 million barrels. Prices of oil were not constant during production. For instance, the maximum price for 1 barrel of oil during 2008-2016 (operation of Volve field) was 128,08 USD; it can also be seen in the simulation curves. It occurred in July 2008, during the global crisis. This price is a historical record of oil prices. However, in January 2009, Oil prices plummeted and reached $ 35 per barrel. One of the most productive years of the Volve field coincided with the period of falling oil prices. Approximately 17 million barrels of oil were produced in 2009. Tables 32-35 represent the information about production of wells, especially revenue for each year.

Table 32. Revenue for well P-F-12

P-F-12			
	Income from oil, million USD	**Income from gas, million USD**	**Total income per year, million USD**
2008	679.46	54.46	733.92
2009	537.82	30.33	568.14
2010	408.29	20.34	428.63
2011	204.03	7.45	211.49
2012	135.41	3.41	138.82
2013	83.71	2.93	86.64
2014	33.27	1.41	34.68
Total			2202.32

Table 33. Revenue for well P-F-14

P-F-14			
	Income from oil, million USD	**Income from gas, million USD**	**Total income per year, million USD**
2008	286.79	21.86	308.65
2009	406.15	22.95	429.09
2010	382.95	18.33	401.28
2011	305.14	11.19	316.33
2012	207.81	5.22	213.03
2013	159.26	5.38	164.65
2014	85.20	3.59	88.79
2015	22.08	1.10	23.18
2016	4.88	0.27	5.16
Total			1950.17

Table 34. Revenue for well P-F-15

P-F-15 D			
	Income from oil, million USD	**Income from gas, million USD**	**Total income per year, million USD**
2014	39.34	1.64	40.99
2015	15.14	0.76	15.90
2016	5.46	0.29	5.76

Total			62.64

Table 35. Revenue for wells P-F-5, P-F-9, P-F-11B

	P-F-11 B	P-F-5	15 9-F-9	
Year	**Revenue, million USD**	**Revenue, million USD**	**Revenue, million USD**	**Revenue, million USD**
2008	26.70	14.05	0.00	
2009	43.26	45.87	10.70	
2010	63.78	37.28	54.98	
2011	80.33	45.28	57.79	
2012	74.60	43.39	67.04	
2013	4.07	44.98	71.16	
2014	0.00	21.61	9.38	
Total	292.74	252.45	271.05	816.24

As it is seen, the most profitable years are 2008 and 2009. And the most productive well is 15/9-F-12.

Total revenue from all wells in 10 years is approximately 5030 million USD. 63 million barrels of oil were recovered. Due to fluctuations of prices and stoppage of some wells, revenue is not quite big. However, it is a good indicator, because field reserves are not huge and only primary recovery was implemented. And to analyse income of the campaign it is required to go through expenses of the company. After reviewing several resources and databases, the main expenditure list was obtained. There are capital expenditures (CapEx) from the beginning of the project and operational expenses (OpEx) of the platform. Tables 36 and 37 are representative of CapEx and OpEx of field life. Most expenses are related to rig. Drilling 1 rig takes approximately 7 million USD for equipment and needed materials. Overall, 85 million USD company spend on equipment for drilling, cementing, logging, fluid preparation and casings. Approximately 2 billion USD, company spend on operational actions such as drilling wells, rental platform, mobile underwater equipment, unforeseen cost, operation and maintenance, closing and plugging wells. Table 37 shows that the most expensive operation is a rental platform, 597 million USD company spend on it. Also it is important to pay attention to

additional costs such as logistics, CO2 taxes, chemicals and production organization. Additional spendings of the company indicated in Table 39.

Table 36. Capital expenditures

		Amount	Price per 1 unit, million USD	Total, million USD
Rig	Jack Up Rig	1	1	1
	Rig price for drilling 1 producer well	6	10	60
	Rig price for drilling 1 sidetracks	6	1.2	7.2
Cementing	Cement unit, materials, personnel for 1 sidetracks and 1 producer well	6	0.25	1.5
Fluid	Fluid materials, personnel and equipment	6	0.35	2.1
Logging	Logging for 8.5" sections (1 well), conventional	6	0.1	0.6
Completion	Completion 1 sidetracks and 1 producer well	6	0.075	0.45
Casing	Casing size 6 sections	6	1	6
Other	Costs include drill bits, completion services, wellhead equipment, casing hanger, personnel	6	1	6
				84.85

Table 37. Operational expenses.

	2005	2006	2007	2008	2009	2010	2011	2012	2013	2014	2015	Total, million USD
Wells, million USD	1.09	10.41	108.65	29.37								149.52

Mob., underwater equipment etc., million USD	24.24	101.9										126.11
Unforeseen cost, million USD		11.81										11.81
Rental platform/ FSU process facilities, million USD			59.93	94.05	91.41	90.32	85.66	79.71	55.67	40.49		597.23
Operation and Maintenance, million USD			18.39	38.85	40.55	42.42	43.20	41.64	42.73	37.91		305.69
Statoil operating cost & land support, million USD	0.78	4.97	16.41	25.64	25.95	25.95	26.10	26.10	26.88	25.64		204.42
Closing cost, million USD											9.48	9.48
Plugging of wells, million USD											17.09	17.09
Total cost, million USD	26.10	129.0	203.40	187.90	157.91	158.69	154.96	147.46	125.28	104.04	26.57	1463.9

Table 38. Additional expenses.

	Years	**Price per year, million USD**	**Total, million USD**
Logistics (helicopter, supply)	12	4.82	57.80
The operator's operating	10	5.75	57.49
Production organization	10	1.86	18.65
Chemicals (Well intervention)	10	4.20	41.95
CO2 tax	12	2.95	35.43
Various	12	4.51	54.07
Total			265.39

After preparing data for economic analysis of the original Volve field, it is important to make the same actions for the CMG model. In Tables 39-41 it is possible to see capital, operational and additional expenditures for the new case.

Table 39. CapEx for the CMG model.

		Amount	Price per 1 unit, million USD	Total, million USD
Rig	Jack Up Rig	1	1	1
	Rig price for drilling 1 producer well	4	10	40
	Rig price for drilling 1 sidetracks	4	1.2	4.8
Cementing	Cement unit, materials, personnel for 1 sidetracks and 1 producer well	4	0.25	1
Fluid	Fluid materials, personnel and equipment	4	0.35	1.4
Logging	Logging for 8.5" sections (1 well), conventional	4	0.1	0.4
Completion	Completion 1 sidetracks and 1 producer well	4	0.075	0.3
Casing	Casing size 6 sections	4	1	4
Other	Costs include drill bits, completion services, wellhead equipment, casing hanger, personnel	4	1	4
Total				56.9

Table 40. OpEx for the CMG model.

	2023	2024	2025	2026	2027	2028	2029	2030	2031	2032	2033	2034	2035	Total, million USD
Wells, million USD	11.40	130	30.60											172.00

Mob., underwater equipment etc., million USD	93.4													93.40
Unforeseen cost, million USD	8.00													8.00
Rental platform/ FSU process facilities, million USD			117	124.5	131.0	136.70	133.4	130.1	101.2	95.45	73.10	32	25.4	1097.5
Operation and Maintenance, million USD			53.9	55.55	57.42	58.20	56.64	57.73	52.91	42.35	33.02	31	26	524.67
Statoil operating cost & land support, million USD	5.40	8.10	32.7	32.50	31.95	30.10	33.10	33.88	32.64	31.71	29.80	28.9	29.56	353.79
Closing cost, million USD													21.00	21.00
Plugging of wells, million USD													34.80	34.80
Total cost, million USD	118	138.1	235	212.6	220.4	225	223.1	221.7	186.8	169.5	135.9	91.9	136.8	2362.4

Table 41. Additional expenses for the CMG model.

	Years	**Price per Year, million USD**	**Total, million USD**
Logistics (helicopter, supply)	13	5.44	70.72
The operator's operating	12	6.06	72.72
Production organization	12	2.64	31.68
Chemicals	13	4.2	54.6
EOR	5	51	255

Various	13	5.28	68.64
Total			553.92

According to Table 39 it can be seen that capital expenditure in the CMG model is less than in the original field. The difference between two cases occurred due to well numbers. 6 wells in the original case and 4 wells in the CMG model. However, this is the only case where the CMG model is cheaper. Here, spendings are larger than in the original case, because project lifespan is 14 years in the CMG model (original 10 years), inflation rate and using Enhanced Oil Recovery techniques to recover more oil. Even carbon dioxide taxes are equal to zero, because of the carbon storage approach. Revenue from 6 wells of the CMG model is reflected in Table 42. This revenue will be used in further analysis as a main source of the cash.

Table 42. Revenue for the CMG model.

Year	Revenue, million USD
2025	1009.46
2026	954.42
2027	1001.15
2028	953.20
2029	847.12
2030	750.18
2031	640.85
2032	534.52
2033	430.51
2034	326.33
2035	21.75

There is a history of oil price changing is presented in the below curve. Till 2008 prices increased. Growth of price was predictable, because consumption worldwide also showed an increasing trend. However due to the crisis in 2008 oil prices fluctuated not in years, but in months. In July 2008 there was a huge increase in oil price, However August and September showed a sharp drop in prices. Then prices were not constant. No significant trends which are

stable. Another drop of oil prices occured in 2020-2021. Due to the world pandemic of COVID-19. However, in this period Volve field was no longer operated. This data will be used in further calculations of economic values.

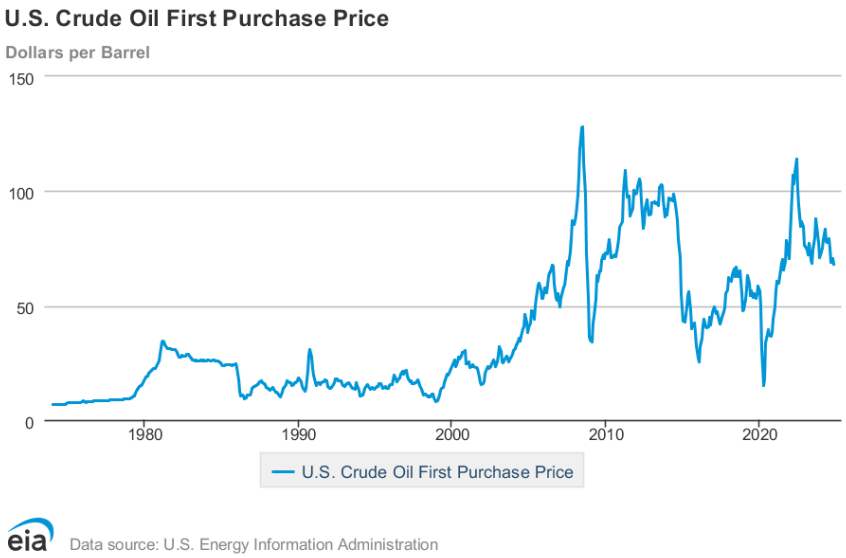

Figure 132. History of oil price changes [30].

7.1.4. Results of analysis

There are several plots which represent the behavior of cash movement in this project. All calculations for the original oil field used real oil prices from year 2005 to year 2016, which are shown above-provided curves. For the CMG model fixed oil price was used due to the impossibility of providing proper oil price forecasting for 10 years. This price is equal to 75 USD per barrel of oil. Plot 133 shows that in the first 2 years revenue is zero, because company only spend money for operational needs. Then, after starting production in 3rd year, revenue started rising. Such a trend is observed in the CMG model. After starting production, increased revenue, cash flow. Beginning of the production is a most profitable period, because during years, oil remaining in the reservoir started to decline. Daily and monthly production rates decreased. As a result, the trend of total revenue after the 4th year of production is decreasing. Similar trend is observed in Figure 134. Total revenue increased in the first years, however, after decreasing production rate, revenue also decreased.

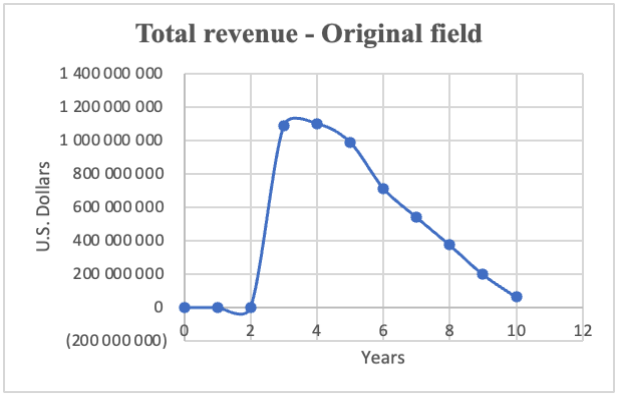

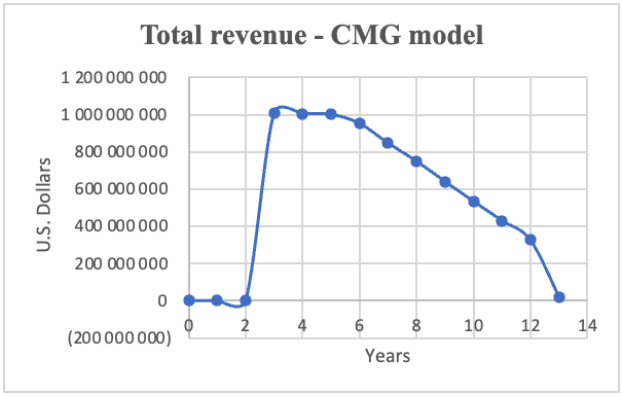

Figures 133-134. Total revenue.

Free cash flow is calculated by formula (9). First 2 years the company spent money therefore, there are negative values of cash flow. After receiving money from production, FCF values started increasing as seen in Figures 135 and 136. Both models have similar trends, the difference is in shape of the curve. The CMG model shows higher values of cash flow and more sharp decrease in flow of money. Also, it is important to notice that FCF values depend on production and revenue cause, change in production will lead to change in revenue and therefore free cash flow.

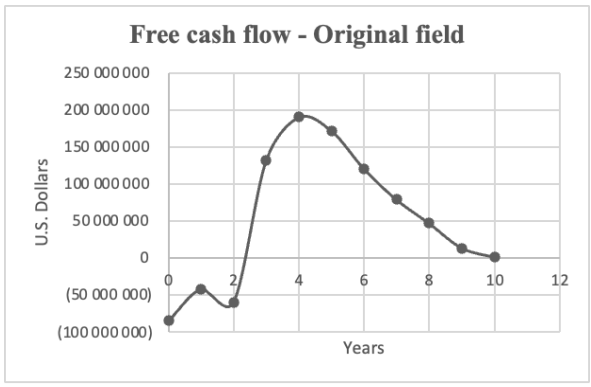

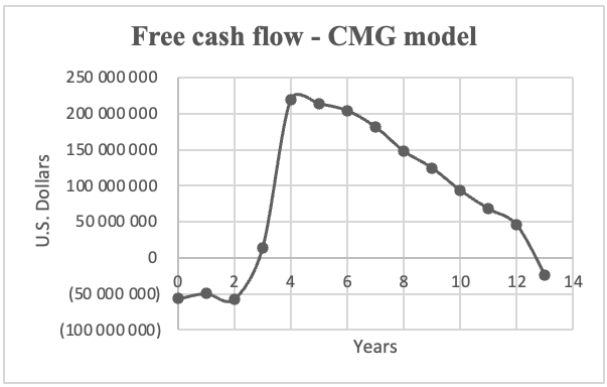

Figures 135-136. Free Cash Flow.

Expenses of the company have increased in the first years of the project. Spending by company increases in order to build a working platform, prepare equipment for operations and so on. After completion of preparation and starting production, expenses decrease because capital is needed for maintenance and operation, which is overall less than in the first 3 years. These trends and results are presented in Figure 137. Figure 138 represents the similar behavior, however there are some peaks in both cases, which are out of general trend. These peaks related to

spending money for drilling and production in the same year. For CMG model abandonment and closing wells are more expensive than in the original case.

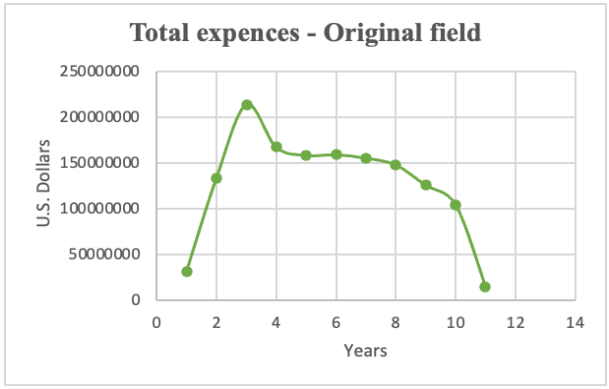

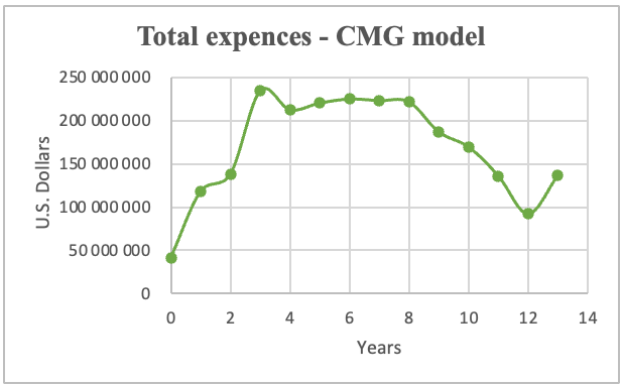

Figures 137-138. Total Expenses.

Another interesting part of the economic analysis is the net income of the company. After all spending, expenses and taxes, companies see some profit, this profit is called unlevered net income. Also, as in previous cases, there is no profit in the first 3 years, only spendings. Figure 139 indicates that the project has positive net income, even if the company spends huge amounts of money in the first years. For the CMG model in Figure 140, it is seen a sharp decrease of income, it is related to decrease in total revenue.

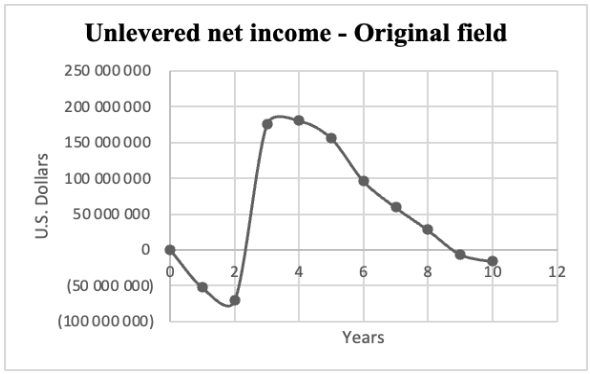

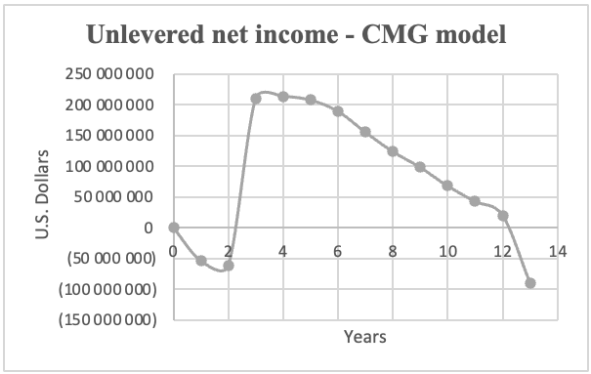

Figures 139-140. Unlevered net income.

Figures 141 and 142 illustrate the present value evolves from beginning of the project till the end. The CMG model suggests initial heavy investments, followed by significant value generation in the middle years, especially year 4. After the peak return on investment slows down but remains positive. The original field has a higher initial cost. It has higher short term gains, however long term returns are lower, as negative values appear in the 10th year.

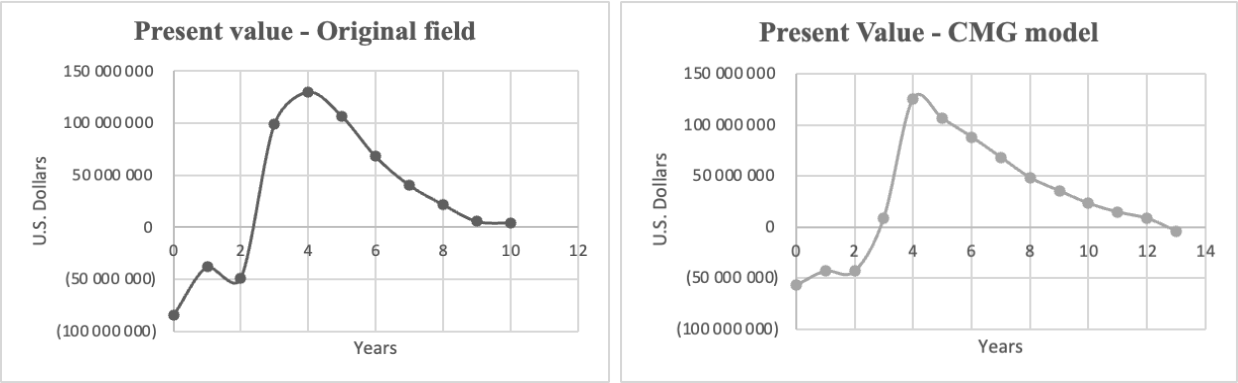

Figures 141-142. Present Value.

Payback period in Figures 143 and 144 indicates that CMG model has better long term value, higher returns and shorter payback period than original field. Payback period for the original case is 3.29 years, for the CMG model 3.12 years. This phenomena can be explained by the implementation of EOR techniques and the greater lifespan of the project with the CMG model.

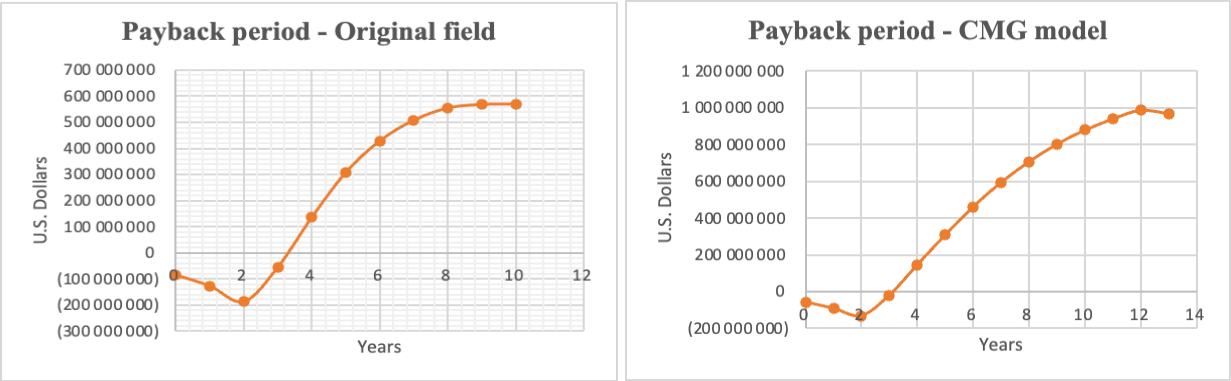

Figure 143-144. Payback period.

In both cases initial investments are equal to 350 million USD. That was made for fair comparison, both cases will start from the same point. NPV and IRR values for both cases are positive. For the original case field NPV is equal to 103.9 million USD, IRR is equal to 0.43. For the CMG model NPV is equal to 148.6 million USD, IRR is equal to 0.50. It can be seen that the CMG model is more profitable than the original Volve field. However, high IRR shows that this case is less risky. High IRR in CMG is because of the assumption of stable price of oil between 2025-2035 (75 USD/barrel), as forecasting of oil price for 10 years is highly impossible. Overall, both fields show good results in economical point, high NPV values, stable IRR. However, the

CMG model is more appropriate and represents better results, with high revenue, low risks, and lower payback period. Comparison of economical features presented in the Table 35 below:

Table 43. Comparison between original Volve field and CMG model.

Case	Total revenue	Capital expenditures	Operational expenditure	NPV	IRR	Payback period	Profit of the project
CMG model	7.469 billion USD	56.9 million USD	2.916 billion USD	148.6 million USD	0.50	3.12 years	970.9 million USD
Original Volve field	5.031 billion USD	84.85 million USD	1.728 billion USD	103.9 million USD	0.43	3.29 years	551.3 million USD

7.1.5. Gas lift and ESP approaches comparison

As it discussed in Chapter VI, gas lift and ESP techniques can be applicable in the field development plan of the Volve field. Both methods performed well and showed high results in production of oil. Now it is a moment to evaluate the effectiveness of such methods. Each new approach requires investments or planning, and how to manage money to use it. Such methods are not the cheapest techniques, due to complexity and required conditions they can cost more than they can bring by their implementation.

From Chapter VI, several data such as daily oil production, daily gas injection, horse power pumps were used as a main resource for economic estimation.

Table 44. Cost of gas lift, profit from the gas lift.

1 m^3	to	1 ft^3	Cost of 1000 ft^3/d, USD	9.24	Million USD/day	Million USD, annually	Oil produced by injected gas per day, bbl	Annual oil production by injected gas, bbl	Revenue from oil , million USD	Profit from gas lift, annually, million USD

1		35.31				0				
5000		176573	176.573		0.00163	1	5509	2010785	150.81	150
10000		353146	353.146		0.00326	1	6673	2435645	182.67	181
25000		882865	882.865		0.00816	3	8874	3239010	242.93	240
50000		1765730	1765.73		0.01632	6	11 084	4045660	303.42	297
75000		2648595	2648.595		0.02447	9	12 610	4602650	345.20	336
100000		3531460	3531.46		0.03263	12	13 760	5022400	376.68	365
150000		5297190	5297.19		0.04895	18	15 420	5628300	422.12	404
200000		7062920	7062.92		0.06526	24	16 516	6028340	452.13	428
250000		8828650	8828.65		0.08158	30	17 258	6299170	472.44	443
300000		10594380	10594.38		0.09789	36	17 771	6486415	486.48	451
350000		12360110	12360.11		0.11421	42	18 142	6621830	496.64	455
400000		14125840	14125.84		0.13052	48	18 379	6708335	503.13	455
450000		15891570	15891.57		0.14684	54	18 539	6766735	507.51	454
500000		17657300	17657.3		0.16315	60	18 634	6801410	510.11	451
550000		19423030	19423.03		0.17947	66	18 681	6818565	511.39	446
600000		21188760	21188.76		0.19578	71	18 702	6826230	511.97	441

Bright yellow row is an optimal gas injection rate, at which profit from recovered oil is maximum and equal to 455.5 million USD. Gas injection is 400 thousand cubic meters per day. Price of 1 cubic foot of gas is equal to 9.24 USD [29]. By conversion it was obtained that 400 thousand cubic meters of injected gas can push to recover 18379 barrels of oil. More detailed information was presented in table 35.

Figure 145 represents the relation between possible profit and injection rate.

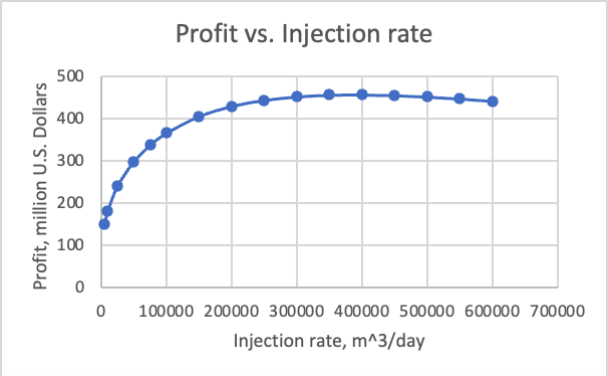

Figure 145. Profit vs. Injection rate curve.

The ESP way of analyzing is the same, however a different scenario is obtained. Cost of the pump is dependent on the power of the pump. Approximately 1000 USD per 1 horsepower. In Table 36 it is possible to see the relation of power of pump to its potential in terms of produced oil volumes. Optimal pump which gives the highest possible profit highlighted in bright yellow row.

Table 45. Identifying optimal ESP.

Power, HP	Oil volume, bbl/d	Cost of pump, million USD	Operation of the pump, million USD annually	Revenue per day, million USD	Annual profit, million USD
350	16425.42	0.35	0.225	1.23	449.07
450	18088.33	0.45	0.29	1.36	494.43
550	19526.17	0.55	0.354	1.46	533.62
650	20798.55	0.65	0.419	1.56	568.29
750	21944.76	0.75	0.484	1.65	599.50
850	22872.67	0.85	0.548	1.72	624.74
950	22872.67	0.95	0.612	1.72	624.58

There is a Figure 146 showing the relation of possible profit to pump power.

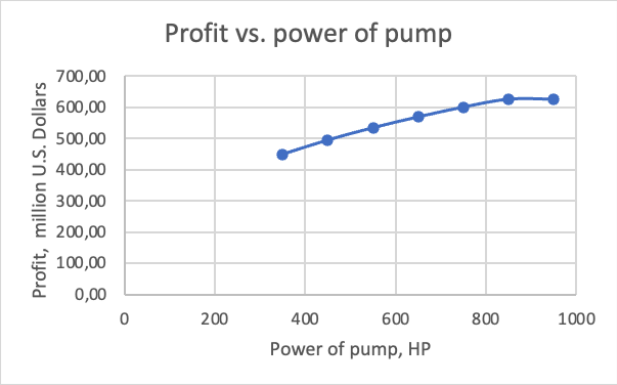

Figure 146. Profit vs. Power of pump.

Following Table 37 illustrates the comparison between best scenarios of gas lift method and ESP technique, to obtain the best option for the Volve field.

Table 46. Comparison of two techniques for oil production.

Technique	Produced oil volume for 1 year, million bbl	Cost of implementation for 1 year, million USD	Net profit for 1 year, million USD
ESP, with pump of 850 horsepowers	8.35	1.4	624.7
Gas lift, injection of $400*10^3\ m^3/d$ of gas	6.71	0.13	455.5

Oil price is stated as 75 USD per barrel. In this scenario, using ESP with a pump power of 850 horsepower is beneficial from an economic point of view.

Chapter VIII

8.1. Health, Safety, and Environment (HSE) Considerations

There should be a Safety Measurement System (SMS), before having the first group of people on the platform. SMS is needed to investigate each action, accident and incident. Main core of the SMS is a structure: Plan-Do-Check-Act. This structure includes:

Plan:

- Policy
- Planning

Do:

- Risk profiling
- Organizing
- Implementing Plans

Check:

- Measuring performances
- Investigating accidents / Incidents / Near misses

Act:

- Reviewing performance
- Learning lessons

Figure 147. Plan-Do-Check-Act.

This model of SMS is applicable for field development, due to its simplicity and transparency. Every member of the company, each person on the board should understand and need to follow such rules and regulations. This structure will provide sufficient, safe and constant workflow. Every step is controllable. Crew members will get support and control.

Development and operation of the Volve field were according to Equinor's internal HSE regulations, as well as requirements established by Norwegian authorities. The Equinor safety objective of the Volve project was to achieve "no harm" according to the requirements set by the authorities. In this regard, a dedicated organizational unit was formed in Equinor which is responsible for the HSE challenges of the project in close cooperation with operating organizations of Volve and Sleipner in order to implement similar safety behavior.

Rules and regulations are an important part of any project. Field development is crucial in planning and implementing innovations into projects, to get higher results. All staff should follow lifesaver rules in working, because such rules are a key strategy to successful working of the field. The illustration below represents the important rules needed to follow to every person on the board.

Figure 148. 11 crucial rules of the company needed to correct and accurately work on the board.

Description of Environmental Impact

The Volve project was developed to be built with a goal of zero environmentally harmful emissions. These plans align with the environmental goals of Equinor: reducing emissions, minimal change to marine ecosystems.

The water produced was reinjected into the reservoir structure to avoid disposal to the sea, thereby minimizing environmental hazard consequences. Besides, the usage of Utsira water for injection, along with ESPs was appropriate for reducing risks of deposits in formation and process equipment for smooth production with minimal environmental damage.

Decommissioning plans were also drawn up, including those required for regulatory arrangements for the safe, environmentally sound decommissioning of field infrastructure, such as pipelines and buoys, and well plugging to prevent leakage.

It is important to explore regions of the field. For instance, near the Volve field there are some cities and settlements. Aberdeen - 220 kilometers, Stavanger - 200 kilometers. Mostly, the economy of these cities are related to the oil industry, however it is important to consider such aspects as tourism, fishing and marine transport. Also, there are several Fjords on the coast. All these factors in some give high risk of environmental problems. If an oil spill occurs, the attention of the regional community will be focused on this issue.

Transport

Mainly, 2 transport systems are present in this project. Via ship and pipeline. The stabilized oil is stored in the Vessel "Navion Saga" FSO – (Floating Storage and Offloading Unit) & the oil is offloaded to tankers for transportation to the market. There may be oil spills as well as fires and explosions due to electrostatic current. The rich gas is piped to the Sleipner A Facility Platform, 8 kilometres to the south of Volve, for final processing and export. That means, we develop the Loading and unloading processes, and for that, an FSO protocol is required, (hose connection and disconnection), this can generate spills, fires, explosions due to static current, since there is fluid moving from point to another and there are frictions).

Platform

Volve field has a dual platform configuration and separation, which means that field development is based on production using the Inspirer self-lifting rig, which performs the functions of a drilling, processing and production platform. There is a set of two offshore construction platforms: a self-lifting drilling rig and a borehole casing. A self-lifting drilling rig is a drilling rig and an offshore production platform that contains all the necessary production equipment, wellheads, and onshore production equipment (test separator, pressure relief burner, metering equipment, etc.). The shaft body of a small structure is towed to an elevator and contains a helipad, offices and living quarters. They are separated from each other so that, for example, in the event of a fire in the building, there will be no problems with the evacuation of workers. The living quarters are located in two V-shaped blocks. There are many risk factors that will be analyzed later when determining the degree of danger. They can be affected by weather conditions, corrosion, fires and explosions, electric shock when moving workers, and other factors.

People on Board

No more than 120 people work on the platform. There will be 60 people on the board, who will work in 2 shifts.

Works by shifts: 12 hours of working per day/night.

Working time: duration of 1 shift is 28 days. Shifts are calculated in accordance with Offshore Working Time UK regulation.

The HSE aspect is at the core of the development and operation of the Volve field. Throughout the project life cycle, the operator Equinor (formerly Statoil) followed the strictest possible safety standards and environmental regulations. Maximum attention was targeted to choose suppliers and develop concepts concerning very high safety and environmental standards.

8.2. Risk Management

Offshore oil and gas development across the North Sea environment includes multiple serious operational hazards due to its sensitive location. Operating at Volve Field functions as an essential establishment that supplies vital services to the energy industry while enhancing regional safety measures. The sustainable operation of this field requires strategic risk management because it is located near Aberdeen (220 kilometers away) and Stavanger (200 kilometers away) and their maritime-based industries depend on this field.

8.2.1. Risk identification and assessment

The Volve field presents operational hazards that stem from three main areas: environmental hazards and technological risks along with socio-economic concerns. The environmental risks from Volve's operation consist of oil and gas leaks alongside water pollution with chemical reagents and atmospheric emissions. The nearby fjords make this area prone to marine ecosystem damage from such incidents that reduce both fishing opportunities and tourism potential of the region.

Human operations at the Volve field involve multiple dangers starting from equipment breakdowns to fuel explosions and extending to metal corrosion risks and human worker_interfaces. The North Sea demands special attention to its characteristic unpredictable

weather due to its prevalence. Nearby coastal settlements face both supply-chain disruption risk from oil and gas distribution along with economic damage from dangerous incidents at the site.

8.2.2. Risk Minimization Measures

Developing an extensive industrial safety management system with environmental protection measures represents the necessary solution to reduce these risks. A system requires implementation for regular technical equipment monitoring along with scheduled preventive maintenance of equipment. Technological systems that employ automatic leak detectors along with pressure sensors will monitor operations to identify threats before they occur.

The training program should involve following international protocols which cover personnel emergency procedures and building evacuation practices. Key measures to minimize potential incident consequences depend on the creation and ongoing development of oil spill and gas emission containment plans. Environmental monitoring demands special priority through regular water and bottom sediment collection as well as constant monitoring of marine fauna and flora states.

8.2.3. Risk response

A specific and coordinated response becomes essential when any risk situation occurs. Emergency responders need to stand prepared for instant emergency activations. Commercial fishing operations and tourist businesses need to use pre-established communication networks when receiving information from the platform operators.

The system must operate for direct communication with environmental authorities at national and international levels and perform clear reporting about incidents and response initiatives. The strengthened public confidence helps to prevent extensive long-term impacts.

Risk management at Volve field functions as an essential component for achieving sustainable operation of the field. A standardized risk management system must follow steps of analysis and prevention as well as preparation and rapid response. A complete strategic approach will guarantee platform personnel safety and protect coastal communities alongside marine ecosystem interests.

9. References

[1] Alom, M. Z., Taha, T. M., Yakopcic, C., Westberg, S., Siddique, P., Nasrin, M. S., Hasan, M., Van Essen, B. C., Awwal, A. A. S., & Asari, V. K. (2019). A state-of-the-art survey on deep learning theory and architectures. *Electronics, 8*(3), 292. https://doi.org/10.3390/electronics8030292

[2] Bagci, A. S., Kece, M., & Nava, J. (2010, June). Challenges of using electrical submersible pump (ESP) in high free gas applications. Paper presented at the International Oil and Gas Conference and Exhibition in China, Beijing, China. https://doi.org/10.2118/131760-MS

[3] Breiman, L. (2001). Random forests. *Machine Learning, 45*(1), 5–32. https://doi.org/10.1023/A:1010933404324

[4] Buduma, N., & Locascio, N. (2017). *Fundamentals of deep learning: Designing next-generation machine intelligence algorithms*.

[5] Chen, T., & Guestrin, C. (2016). XGBoost: A scalable tree boosting system. In *Proceedings of the 22nd ACM SIGKDD International Conference on Knowledge Discovery and Data Mining* (pp. 785–794). https://dl.acm.org/doi/10.1145/2939672.2939785

[6] Commonwealth Files. (2023, February). *FDP - Chapter 1* [PDF]. https://production-new-commonwealth-files.s3.eu-west-2.amazonaws.com/s3fs-public/2023-02/FDP%20-%20Ch%201.pdf?VersionId=a1VhZ826zbvbRyRBMgCyIlOk5NO07cEe

[7] Deloitte. (n.d.). *Norway oil and gas tax guide*. https://www2.deloitte.com/content/dam/Deloitte/global/Documents/Energy-and-Resources/gx-er-oil-and-gas-taxguide-norway.pdf

[8] EPConsult Energies. (n.d.). *Field development plan - Oil and gas*. https://www.epconsultenergies.com/services/field-development-planning/field-development-plans

[9] Equinor. (n.d.). *Volve data sharing*. https://www.equinor.com/energy/volve-data-sharing

[10] Ernst & Young. (2023). *Kazakhstan oil and gas tax guide 2023*. https://assets.ey.com/content/dam/ey-sites/ey-com/ru_kz/topics/oil-and-gas/ey-kz-oil-and-gas-tax-guide-2023.pdf

[11] Eurasian Research Institute. (2023). Current challenges for the Kashagan offshore oil field project. https://www.eurasian-research.org/publication/current-challenges-for-the-kashagan-offshore-oil-field-project/

[12] Friedman, J. H. (2001). Greedy function approximation: A gradient boosting machine. *Annals of Statistics, 29*(5), 1189–1232. https://projecteuclid.org/journals/annals-of-statistics/volume-29/issue-5/Greedy-function-approximation-A-gradient-boosting-machine/10.1214/aos/1013203451.full

[13] GeeksforGeeks. (2025, February 5). Multi-layer perceptron learning in TensorFlow. https://www.geeksforgeeks.org/multi-layer-perceptron-learning-in-tensorflow/

[14] Gharbi, R. B. C., & Mansoori, G. A. (2005). An introduction to artificial intelligence applications in petroleum exploration and production. *Journal of Petroleum Science and Engineering*. https://doi.org/10.1016/j.petrol.2005.09.001

[15] Hastie, T., Tibshirani, R., & Friedman, J. (2009). *The elements of statistical learning: Data mining, inference, and prediction*. Springer. https://www.sas.upenn.edu/~fdiebold/NoHesitations/BookAdvanced.pdf

[16] Institut Teknologi Sepuluh Nopember (ITS). (2024, February 23). *Kuliah tamu: Basic RE teknik geofisika*. https://www.its.ac.id/tgeofisika/wp-content/uploads/sites/33/2024/02/1.-KULIAH-TAMU_BASIC-RE_TEKNIK-GEOFISIKA-ITS_23-Feb-2024.pdf

[17] International Trade Administration. (2021). *Energy resource guide: Oil and gas - Kazakhstan*. https://www.trade.gov/energy-resource-guide-oil-and-gas-kazakhstan

[18] Jiratitipat, T. (2021). Mapping of fault system related to salt movement in Volve Field, offshore Norway, North Sea. *Bulletin of Earth Sciences of Thailand, 12*(2), 25–36. https://ph01.tci-thaijo.org/index.php/bestjournal/article/view/246792

[19] Karachaganak Petroleum Operating B.V. (n.d.). *About KPO*. https://www.kpo.kz/en/about-kpo

[20] Ke, G., Meng, Q., Finley, T., Wang, T., Chen, W., Ma, W., & Liu, T. Y. (2017). LightGBM: A highly efficient gradient boosting decision tree. *Advances in Neural Information Processing Systems, 30*, 3146–3154. https://proceedings.neurips.cc/paper_files/paper/2017/file/6449f44a102fde848669bdd9eb6b76fa-Paper.pdf

[21] MCC LLP. (n.d.). *Tengiz oil and gas field project*. https://mcc.kz/en/projects/kopiya-zavershennyie-proektyi/kopiya-neftegazovoe-mestorozhdenie-tengiz/

[22] Mehregan, M.-R., Mohaghar, A., & Esameili, A. (2016, February). Developing a mathematical model for optimizing oil production using gas-lift technology. https://www.researchgate.net/publication/297656449_Developing_a_mathematical_model_for_optimizing_oil_production_Using_Gas-Lift_Technology

[23] Norsk Petroleum. (n.d.). *Volve oil field*. https://www.norskpetroleum.no/en/facts/field/volve/

[24] Norwegian Petroleum Directorate. (n.d.). 4.1—Geology of the North Sea—The Norwegian Petroleum Directorate. https://www.npd.no/en/whats-new/publications/co2-atlases/co2-atlas-for-the-norwegian-continental-shelf/4-the-norwegian-north-sea/4.1-geology-of-the-north-sea/

[25] Offshore Technology. (n.d.). *Volve oil field, North Sea*. https://www.offshore-technology.com/projects/volve-oil-field-north-sea/

[26] Pelemo-Daniels, D., & Stewart, R. R. (2024). Petrophysical property prediction from seismic inversion attributes using rock physics and machine learning: Volve field, North Sea. *Applied Sciences, 14*(4), 1345. https://doi.org/10.3390/app14041345

[27] Pelemo-Daniels, D., & Stewart, R. R. (2024). Petrophysical property prediction from seismic inversion attributes using rock physics and machine learning: Volve field, North Sea. *Applied Sciences, 14*(4), 1345. https://doi.org/10.3390/app14041345

[28] Sun, Z., Garza, A., Salazar-Tio, R., Fager, A., & Crouse, B. (2021, June). A novel 3D mechanical earth modeling of the Volve Field and its application to fault stability analysis. Paper presented at the 55th U.S. Rock Mechanics/Geomechanics Symposium, Houston, TX. American Rock Mechanics Association. https://www.researchgate.net/publication/358040761_A_Novel_3D_Mechanical_Earth_Modeling_of_the_Volve_Field_and_Its_Application_to_Fault_Stability_Analysis

[29] Talinga, D., & Reine, C. (2021). Integrating pore pressure and lithology prediction from well and seismic data to characterize abnormal pressures in the compartmentalized Volve oil field, Central North Sea. *CSEG Recorder, 46*(2). https://csegrecorder.com/articles/view/integrating-pore-pressure-lithology-prediction-from-well-and-seismic-data

[30] U.S. Energy Information Administration. (2025, January 4). U.S. crude oil first purchase price (dollars per barrel). https://www.eia.gov/dnav/pet/hist/LeafHandler.ashx?n=pet&s=f000000__3&f=m

[31] Van Nguyen, T. (2021). Salt tectonics control on reservoir geometry, Volve field, North Sea. *Bulletin of Earth Sciences of Thailand, 11*(2), 68–79. https://ph01.tci-thaijo.org/index.php/bestjournal/article/view/246771

[32] Vapnik, V. N. (2013). *The nature of statistical learning theory*. Springer. https://doi.org/10.1007/978-1-4757-2440-0

[33] Wang, B., Sharma, J., Chen, J., & Persaud, P. (2021). Ensemble machine learning assisted reservoir characterization using field production data–an offshore field case study. *Energies, 14*, 1052. https://doi.org/10.3390/en14041052

[34] West Virginia University. (n.d.). *Dissertation VF* [PDF]. https://researchrepository.wvu.edu/cgi/viewcontent.cgi?params=/context/etd/article/12519/&path_info=Dissertation_VF.pdf